



**NTNU – Trondheim**  
Norwegian University of  
Science and Technology

# Numerical study of hydrogen adsorption

**Inger-Anne Rasmussen**

Master of Science in Product Design and Manufacturing

Submission date: June 2012

Supervisor: Erling Næss, EPT

Co-supervisor: Christian Schlemminger, EPT

Norwegian University of Science and Technology  
Department of Energy and Process Engineering



EPT-M-2012-74

**MASTER THESIS**

for

student Inger-Anne Rasmussen

Spring 2012

English title

**Numerical study of hydrogen adsorption***Numerisk analyse av hydrogenlagring***Background and objective**

Hydrogen can be an energy carrier for the future. The main challenges of the investigation in hydrogen technology are the potential disadvantages in handling. The present project work efforts are focused on hydrogen material properties for hydrogen storage technologies.

The most promising hydrogen storage methods are: gas compression, liquefaction, chemical storage via metal hydrides and gas adsorption via physisorption. Adsorption type storage systems are inexpensive alternatives that also have the potential to reach the goals for handling hydrogen in on-board storage systems. Sorption type materials, like e.g. metal organic frameworks (MOF) have been identified as a viable option. These are characterized by high porosity and specific surface area.

The transient processes during charging and discharging of a storage system play an important role in the utilization of the hydrogen adsorption storage systems.

The main objective of this work is to describe the transient thermodynamics during the physisorption of hydrogen gas. Therefore, a finite volume can be defined, and a commercial numerical software such as Comsol can be used.

**The following tasks are to be considered:**

1. Perform a literature survey on adsorption theories and models (e.g. Langmuir, Ono-Kondo) and thermodynamic assumptions (e.g. real gas approach, local thermal equilibrium) for use in numerical simulations for hydrogen storage. The models shall be presented, compared and discussed, and a recommendation for models to use for numerical calculations shall be made.
2. The recommended models shall be adapted for a selected adsorptive storage material and implemented into the chosen numerical software (e.g. Comsol Multiphysics).
3. Define a computational geometry in cooperation with the Department, and perform numerical transient calculations on the hydrogen adsorption behavior under different initial and boundary conditions. The results shall be presented and discussed. Where possible, the numerical results shall be compared to available experimental data.

4. Suggestions for further work shall be made.

Within 14 days of receiving the written text on the master thesis, the candidate shall submit a research plan for his project to the department.

When the thesis is evaluated, emphasis is put on processing of the results, and that they are presented in tabular and/or graphic form in a clear manner, and that they are analyzed carefully.

The thesis should be formulated as a research report with summary both in English and Norwegian, conclusion, literature references, table of contents etc. During the preparation of the text, the candidate should make an effort to produce a well-structured and easily readable report. In order to ease the evaluation of the thesis, it is important that the cross-references are correct. In the making of the report, strong emphasis should be placed on both a thorough discussion of the results and an orderly presentation.

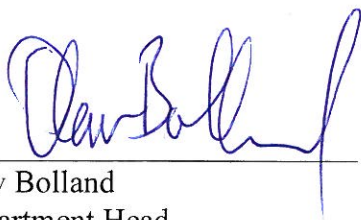
The candidate is requested to initiate and keep close contact with his/her academic supervisor(s) throughout the working period. The candidate must follow the rules and regulations of NTNU as well as passive directions given by the Department of Energy and Process Engineering.

Risk assessment of the candidate's work shall be carried out according to the department's procedures. The risk assessment must be documented and included as part of the final report. Events related to the candidate's work adversely affecting the health, safety or security, must be documented and included as part of the final report.

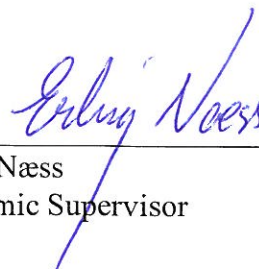
Pursuant to "Regulations concerning the supplementary provisions to the technology study program/Master of Science" at NTNU §20, the Department reserves the permission to utilize all the results and data for teaching and research purposes as well as in future publications.

The final report is to be submitted digitally in DAIM. An executive summary of the thesis including title, student's name, supervisor's name, year, department name, and NTNU's logo and name, shall be submitted to the department as a separate pdf file. Based on an agreement with the supervisor, the final report and other material and documents may be given to the supervisor in digital format.

Department of Energy and Process Engineering, 16. January 2012



Olav Bolland  
Department Head



Erling Næss  
Academic Supervisor

Research Advisor:

Ph.d.-student Christian Schlemminger, EPT

## Preface

---

This report is a result of my Master Thesis at The Norwegian University of Science and Technology at the Department of Energy and Process Engineering. Upon completion of the thesis, I would like to express my gratitude to the people who have helped me throughout the process.

First, I would like to thank my supervisor Professor Erling Næss for our weekly meetings and his constant monitoring. Several obstacles encountered during the past months have been overcome due to his help and patience.

Furthermore, I will like to give a special thanks to my co-supervisor Christian Schlemminger for his dedication, presence at every meeting and always providing me with good advice and important information. Also, his positive attitude and motivation speeches has been valuable in motivating me when my results obtained have shown to be wrong or when my simulation model has not worked properly.

I am also very grateful to Erlend Kristiansen at COMSOL Support who has always answered my e-mails and given me valuable advice throughout the simulation process.

Trondheim, June 8<sup>th</sup> 2012,

*Inger-Anne Rasmussen*

---

Inger-Anne Rasmussen



## Abstract

---

The main objective of this thesis is to describe the transient thermodynamics during physisorption of hydrogen gas using a commercial numerical software.

Simulations of thermal effects during adsorption are valuable tools for the efficient design of hydrogen adsorption storage systems. Transient mass and energy equations are used for describing the adsorption process. For this purpose, experimental adsorption data has to be presented analytically. Several models have been developed for this objective.

The thesis consists of two parts. In the first, a literature study on adsorption theories and thermodynamic assumptions for development of transient mass and energy balances is conducted. The models are discussed, and from this, the Langmuir approach is selected to be used for numerical calculations. The model is implemented into a lumped-parameter analysis describing an infinitesimal element within an adsorbent bed, allowing for neglecting heat leaks into the system as well as the structural steel mass.

The second part describes the simulations conducted in the study. The numerical software COMSOL Multiphysics 4.2.a is used for numerical calculations. Modules for implementation of the transient mass and energy balances are considered, before Heat Transfer in Porous Media and Brinkman Equations are applied, for heat transfer, pressure- and velocity calculations, respectively. The simulations are run for different initial and boundary conditions. The porous material is defined with Fe-btc properties. The simulation model is built step by step, and problems encountered are analyzed continuously in the process towards a complete model. After completion, the model geometry is adjusted and the porous material is changed to MOF-5 properties, to resemble a selected published paper.

Numerical results are compared and discussed. Modeling restrictions for the present study is accounted for, and all choices made when considering the assigned task are justified. The report is completed by listing the conclusions drawn from the present study, and concrete suggestions for further work are given.

Simulation results found in the present study differs slightly from the published research work. Instabilities in the solver results in a temperature dip in the simulated domain. This leads to an increased adsorption rate. Furthermore, it appears that mass is not conserved, which means that the inlet velocity of the feed gas does not change as expected when the adsorption is disabled from the model.





## Sammendrag

---

Formålet med den foreliggende avhandlingen er å beskrive transient termodynamikk for adsorpsjon av hydrogen, dette gjennomføres ved å benytte et numerisk analyseverktøy.

Oversikt over alle termiske effekter under adsorpsjon er avgjørende for effektiv design av lagringssystemer for adsorpsjon av hydrogen. I denne forbindelse er simuleringer i numeriske analyseverktøy verdifulle. For implementering av transiente masse- og energibalanser inn i disse, må eksperimentell adsorpsjonsdata presenteres analytisk. Flere ulike modeller er utviklet for denne konverteringen.

Avhandlingen består av to hoveddeler. Del 1 består av en litteraturstudie på adsorpsjonsteorier og modeller, samt termodynamiske antagelser for utvikling av masse- og energibalanser. Gjennom diskusjonen av de ulike modellene, velges Langmuir-modellen for videre implementering i en «lumped- parameter Analysis». Masse- og energibalansene i denne analysen beskriver et uendelig lite element i adsorpsjonstanken. Dette tillater neglisjering av varmetap, samt massen til konstruksjonsstålet i tanken.

Del 2 er en simuleringsdel. Her benyttes den numeriske programvaren COMSOL Multiphysics 4.2.a. Modulene Heat Transfer in Porous Media og Brinkman Equation's velges for henholdsvis varme overføringsberegninger og hastighet- og trykkberegninger. Det porøse materialet defineres med Fe-btc egenskaper. Simuleringsmodellen bygges opp trinnvis, og problemer samt oppdagede avvik analyseres kontinuerlig i prosessen mot en komplett modell. Etter ferdigstilling justeres modellens geometri. Videre omdefineres det porøse materialet til MOF-5 egenskaper, for å ligne tilfellene analysert i en utvalgt forskningsartikkel.

Numeriske resultater sammenlignes og diskuteres. Modelleringsrestriksjoner for oppbygging av modellen gjøres rede for. Valgene tatt underveis i prosessen mot en ferdigstilt avhandling begrunnes. Avslutningsvis listes konklusjonene fra arbeidet, og det gis konkrete forslag til videre arbeid.

Simuleringsresultatene fra modellen avviker noe fra det publiserte forskningsarbeidet. Det viser seg at ustabiliteter i løseren resulterer i en temperatursenkning i det simulerte domenet. Dette fører til en økt adsorpsjonsrate. Videre viser det seg at masse ikke er bevart. Dette medfører at innløpshastigheten ikke endrer seg som forventet når adsorpsjonsleddet i modellen er avslått.



## Contents

---

Preface.....	i
Abstract .....	iii
Sammendrag .....	v
List of Figures.....	ix
List of Tables.....	xi
Nomenclature.....	xiii
1. Introduction .....	1
1.1. Background .....	1
1.2. Objectives .....	1
1.3. Structure .....	1
2. Physisorption of hydrogen gas.....	3
2.1. Adsorption .....	3
2.1.1. Adsorption isotherms .....	5
2.1.2. Excess and absolute adsorption.....	5
3. Literature study on adsorption models and thermodynamic approaches.....	9
3.1. Adsorption models .....	9
3.1.1. Langmuir adsorption .....	9
3.1.2. Ono-Kondo .....	10
3.1.3. The Dubinin-Astakhov method.....	11
3.2. Comparison of adsorption model performance.....	13
3.2.1. A complete model for hydrogen adsorption .....	18
3.2.2. Discussion.....	20
3.3. Recommendation of model for further use .....	21
4. Proposed model.....	23
4.1. Governing equations .....	24
4.2. Implementation .....	30
4.2.1. Purpose of study .....	30
4.3. COMSOL model.....	30
4.3.1. Heat Transfer module .....	32
4.3.2. Mass Transfer module.....	33
4.3.3. Model inputs .....	34

5. Results and discussion .....	35
5.1. Simple model - Defined Inlet and outlet .....	36
5.2. Implementing Heat Source .....	43
Case 1 .....	43
Case 2 – imposing equal inlet and domain pressure .....	49
5.3. Implementing mass source.....	55
5.3.1. System analysis .....	55
5.3.2. Adsorption .....	59
5.4. Discussion .....	64
5.5. Modeling restrictions.....	78
6. Conclusions .....	81
Results from literature survey .....	81
Modeling results .....	81
7. Suggestions for further work .....	83
8. References .....	85
APPENDIX .....	I
APPENDIX A .....	III
Langmuir constants.....	III
Governing equations.....	III
APPENDIX B.....	VII
Velocity distribution.....	VII
Density distribution.....	VIII

## List of Figures

---

Figure 1: Large micro pore with adsorbed layer and hydrogen gas inside the pore [5].....	4
Figure 2: Adsorption on a porous surface [6] .....	4
Figure 3: Absolute and excess hydrogen adsorption [9].....	6
Figure 4: Maximum in excess adsorption isotherm curves [9] .....	7
Figure 5: a) Adsorption isotherms expressed as Langmuir plots, b) Langmuir plots of the three lowest temperatures [1].....	14
Figure 6: Ono-Kondo fit of the adsorption isotherms (lines) to the experimental data (points). The adsorption density is shown as a function of bulk gas density [1] .....	14
Figure 7 : Comparison of the low-temperature adsorption isotherms of hydrogen at 77 K for two different carbons (AX-21 powder and pellets.) [1] .....	15
Figure 8: Modified D-A model fit (solid lines) to experimental excess adsorption isotherms of hydrogen on activated carbon AX-21 [10] .....	16
Figure 9: Hydrogen excess adsorption isotherms on Maxsorb MSC-30, and AX-21 .....	17
Figure 10: Hydrogen excess adsorption isotherms on a) CNS-201 and b) Cu <sub>3</sub> (BTC) <sub>2</sub> .....	17
Figure 11: Langmuir fit (lines) for MOF-5 excess adsorption data (symbols) of Zohu et al. [13] .....	19
Figure 12: Cuboidal infinitesimal element within a cryo-adsorber bed [2] .....	23
Figure 13: COMSOL model of adsorption cell .....	30
Figure 14: Cut planes.....	35
Figure 15: Average outlet temperature for the Simple Model.....	37
Figure 16: Density profile for the Simple Model.....	37
Figure 17: Density at different temperatures at p=1.6 bar [16] .....	38
Figure 18: Pressure change at different outlet conditions at t=800.....	39
Figure 19: Velocity plot over the length of the domain, t=1-800 seconds .....	40
Figure 20: Inlet and outlet mass flow rate .....	41
Figure 21: Average outlet temperature, red line: with mass source, blue line: Simple Model .....	44
Figure 22: 2D temperature plot of the temperature profile at t=1300 seconds.....	44
Figure 23: Average outlet temperature with disabled heat source.....	45
Figure 24: Average outlet temperatures for different tolerances.....	47
Figure 25: 2D temperature plot at t=1300 tolerance=0.0001 .....	48
Figure 26: 2D temperature plot with new imposed $d(n_{ex})/dt$ .....	48
Figure 27: Average outlet temperature for Simple Model, Case 1 and Case 2 .....	49
Figure 28: Heat source term for Case 2 .....	50
Figure 29: Heat source Case 1 for t=1 to 1000 seconds.....	51
Figure 30: Heat source term Case2 for t=1320-1600 seconds.....	51
Figure 31: Outlet density evolution for Case 1 and Case 2 .....	52
Figure 32: Pressure change over the domain at t=0-1600.....	53
Figure 33: Velocity evolution over time for Case 2.....	53
Figure 34: Inlet an outlet mass flow rates.....	54

Figure 35: 2D temperature profile at t=1600 seconds.....	56
Figure 36: Average outlet temperatures for the complete system and Case 2.....	57
Figure 37: Pressure change over time.....	57
Figure 38: Pressure drop over the domain for t=0-1600 seconds.....	58
Figure 39: Average inlet velocity for the complete system and Case 2.....	59
Figure 40: Adsorbed gas over time in the bed.....	60
Figure 41: Temperature over time in the bed.....	61
Figure 42: Total and adsorbed hydrogen in the bed over time.....	61
Figure 43: Tank to be compared to [2].....	65
Figure 44: Pressure drop over the domain from present study for t=1-1000 seconds.....	66
Figure 45: 2D temperature plot of the bed at t=0.....	66
Figure 46: Temperature evolution in the axial flow bed [2].....	67
Figure 47: Temperature evolution in the bed for Model 2.....	67
Figure 48: Density evolution in the bed [2].....	69
Figure 49: Density evolution in the bed predicted by Model 2.....	70
Figure 50: Superficial gas velocity evolution in the bed [2].....	71
Figure 51: Velocity evolution predicted by Model 2.....	71
Figure 52: Mass flow evolution in the bed [2].....	73
Figure 53: Mass flow rate evolution predicted by Model 2.....	74
Figure 54 : Hydrogen capacity evolution predicted by the 0-D model and the 1-D axial isobaric model during the isobaric refueling period [2].....	75
Figure 55: Hydrogen load predicted by Model 2.....	76

## List of Tables

---

Table 1: Hydrogen uptake for selected porous materials [7] .....	5
Table 2: Literature survey .....	13
Table 3: Fe-btc and gas properties .....	31
Table 4: Comparison of equations used in COMSOL and by Kumar et al. [2].....	32
Table 5: Comparison of COMSOL equations and Equation 3.5.....	33
Table 6: Initial and boundary conditions for the Simple system .....	36
Table 7: Density at different temperatures at p=1.6 bar.....	38
Table 8: Boundary and initial conditions for Case 1 .....	43
Table 9: Initial and boundary conditions imposed in Case 2 .....	49
Table 10: Initial and boundary conditions for the Complete System .....	55
Table 11: Summary of predicted heat of adsorption.....	63
Table 12: Model properties.....	64
Table 13: Initial and boundary conditions imposed in Model 1 and Model 2.....	64
Table 14: Comparison of outlet temperatures .....	68
Table 15: Decrease in outlet density for Model 1 and Model 2 .....	69
Table 16: Comparison of outlet velocities .....	72
Table 17: Predicted mass flow rate for the two models.....	73
Table 18: Comparison of Hydrogen load predicted by Model 1 and Model 2 .....	76
Table 19: Summary of change in properties over time predicted by Model 1 and Model 2 ..	77





## Nomenclature

Symbol	Description	Unit
$T, P$	Temperature and pressure	K, bar
$m_s, V_b$	Mass and volume of the adsorbent bed	kg, m <sup>3</sup>
$Cp_s, Cp_g$	Specific heat capacity adsorbent and gas	J/(kg×K)
$H_g, H_{n_{ex}}, H_s$	Specific heat enthalpy of gas, adsorbate and adsorbent	J/kg
$\rho_s, \rho_p, \rho_b$	skeletal, pellet/particle and bed densities	kg/m <sup>3</sup>
$\rho_g, v_g$	Gas density and specific volume,	kg/m <sup>3</sup> , m <sup>3</sup> /kg
$\varepsilon_p, \varepsilon_b, \varepsilon_t$	Pellet, bed and total porosities,	m <sup>3</sup> /m <sup>3</sup>
$\theta$	Volume fraction MOF	
$n_{ex}, n_{ex}^*$	Excess adsorbate concentration and its equilibrium value	kg <sub>H2</sub> /kg <sub>adsorbent</sub>
$n_{max}, b$	The two Langmuir parameters	kg/kg, 1/bar
$\Delta H_a$	Heat of adsorption	J/kg <sub>H2adsorbed</sub>
$\alpha_{Pg}, \beta_{Tg}$	Isobaric thermal expansion coefficient and isothermal compressibility	1/K, 1/bar
$\mu_g$	Gas viscosity	Pa × s
$k_g, k_p$	Gas and particle thermal conductivity	W/(m×K)
$k_{eq}$	Total thermal conductivity of the adsorbent bed	W/(m×K)
$k_{eff}$	Effective thermal conductivity of the adsorbent bed	W/(m×K)
$\kappa$	Permeability	



# 1. Introduction

---

This chapter introduces the thesis by presenting the background for the assigned study. The objectives will be specified and an overview on how the assigned thesis is solved will be given by presenting the overall structure.

## 1.1. Background

Hydrogen is recognized as one of the most appealing energy carriers for the future due to a high heating value and its environmental friendly nature including clean combustion. However, storage of hydrogen at feasible temperatures and pressures has proven to be a challenge due to an unacceptably low volumetric energy density at ambient temperatures and pressures. For 2015, The US department of Energy (DOE) has set targets for on-board automobile storage systems to have gravimetric and volumetric densities of 7.5 wt% and 70 g H<sub>2</sub>/L, respectively [3]. As of today, the storage technologies fail to meet these targets. To make hydrogen powered vehicles competitive with internal combustion engines the storage capacities needs to increase at the same time as the operating conditions of pressure and temperature can be set to less extreme values (lower pressures and higher temperatures).

## 1.2. Objectives

The main objective of this work is to describe the transient thermodynamics during physisorption of gas. This can be done by imposing a selected adsorption model into transient mass and energy balances. A finite volume can be defined and the equations can be solved in a numerical software.

## 1.3. Structure

The complete thesis consists of 7 chapters, the present included. In Chapter 2 a brief introduction to physisorption of hydrogen gas will be given with the goals for the technology and the current status in reaching these goals. Then the concept of adsorption will be explained in detail, before three selected adsorption theories are presented in Chapter 3. A literature survey on the adsorption models, together with thermodynamic approaches in developing mass and energy balances to describe the adsorption process, will then be conducted. One of the adsorption models will be nominated for further use in the study. In Chapter 4, the selected model will be implemented into transient mass and energy balances. The equations will be derived in detail. In Chapter 5, the derived equations will be implemented into COMSOL. The implementation process will be conducted step by step and the reliability discussed by comparing the obtained results to available experimental data. In Chapter 6, an overall conclusion will be given, before the thesis is completed with Chapter 7. Suggestions for further work.



## 2. Physisorption of hydrogen gas

---

Hydrogen is believed to have the ability of becoming an important energy carrier for the future. It appears to be especially promising in connection with electricity generation in fuel cells in cars [4]. Possibilities for storage methods include gas compression, liquefaction, chemical storage via hydrides and gas adsorption via physisorption, where adsorption on porous materials are considered one of the most promising. The advantage of sorption based storage systems are fast kinetics and low operating pressures. In addition it is completely reversible. Furthermore, relatively high volumetric and gravimetric storage densities for hydrogen can be achieved when adsorbed in materials with high specific surface area and porosity. For instance, the same gravimetric and volumetric densities as for compression of gas to 70 MPa can be achieved via physisorption. Metal Organic Frameworks have been identified as a viable option for storage material and there seem still to be a potential in improvement in the storage properties [4]. For investigation of the storage systems, the transient processes during charging and discharging is to be handled carefully.

### 2.1. Adsorption

Physisorption in microporous adsorbents is used for a variety of applications such as gas storage, gas separation and in adsorption heat pumps, to mention some. During adsorption of hydrogen, the hydrogen molecules enter the pores of the adsorbent (porous material) and interact with the material surface via Van der Waals forces. This is a weak force that leads to a formation of an additional phase of the gas, namely the adsorbate (adsorbed gas). The strength of this interaction is expressed by the heat of adsorption. The heat of adsorption is the energy that is released when the gas molecules change from gas phase to adsorbed phase, typically in the range of 1 kJ/mol to 10 kJ/mol for hydrogen adsorption [5]. Only the hydrogen close to the inner surface of the pores is bound by the Van der Waals bindings due to the low interaction strength. At conditions well above the critical point, only a monolayer of hydrogen is adsorbed on microporous materials (pore size 1-10nm) and the adsorption capacity of a microporous material is proportional to its surface area. Most adsorbents have larger pores than double the kinetic diameter of the hydrogen molecule; this means that the remaining pore space can be filled with hydrogen gas. As a consequence, hydrogen will be present in two different phases with different densities. Furthermore, most storage tanks filled with MOF-powder will have inter-particle void space where additional hydrogen gas is present. Therefore the total capacity of an adsorbent is the sum of the adsorbed hydrogen, the hydrogen gas in the pores and the hydrogen gas in the inter-particle voids [5].

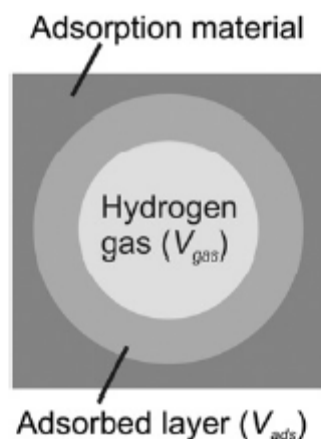


**Figure 1: Large micro pore with adsorbed layer and hydrogen gas inside the pore [5]**

Figure 1 shows the absolute uptake which is the amount of hydrogen in the adsorbed layer occupying,  $V_{ads}$ . The additional gas occupying the remaining void space,  $V_{gas}$ , together with the adsorbed layer is called the total uptake of an adsorbent particle.

Figure 2 illustrates the complexity of adsorption on a porous surface by displaying four possible incidents. Region 1 has low adsorption potential and can hold few molecules while Region 2 has the highest of the four and can hold a great number. Region 3 has a pore entrance smaller than the molecule and thus will not adsorb any particles. Region 4 illustrates a monolayer adsorption mechanism which is characteristic for supercritical gas adsorption on MOFs and Activated carbons. Here the adsorption potential is higher than for Region 1 and lower than for Region 2 [6].

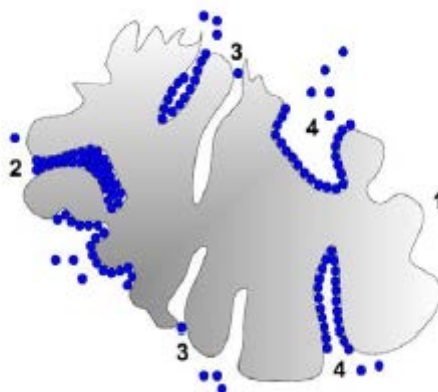


**Figure 2: Adsorption on a porous surface [6]**

A large variety of adsorbents have been investigated in the search for encountering the most suitable material for hydrogen storage via adsorption. Activated carbon (AC), carbon nanotubes and metal organic frameworks (MOF) are good candidates as these materials have a high specific surface area as well as pore sizes within the size range of nanometers. Thus, they seem to be well suited in that the adsorption enthalpies are lower in small pores compared to bigger pores [4]. In research literature, several MOFs are found to have good

hydrogen storage capacities. For the investigation of heat and mass transfer at NTNU, EPT, the following linked MOFs are of interest. (See Table 1 for the hydrogen uptake of these and other porous materials).

**Table 1: Hydrogen uptake for selected porous materials [7]**

MOF	%wt excess	%wt absolute	%wt total	T[K]	p[bar]
Fe-btc	1.68	1.83	2.37	77	25
Cu-btc	1.36	1.54	2.26	77	25
MOF-5	5.2	-	-	77	50
MOF-177	6.7	7.45	8.59	77	25
AC-Norit 8.0	-	-	2.9	77	20

### 2.1.1. Adsorption isotherms

Adsorption is usually described through isotherms. An isotherm gives the amount of adsorbate on the adsorbent as a function of pressure or concentration at constant temperature. The isotherm, depend on the phase of the adsorbate, gas or liquid, respectively, the gas components (if it is a mixture), and the solid material, and can be expressed as:

$$n_{ex} = (P, T, gas, solid) \quad (2.1) [8].$$

In this equation,  $n_{ex}$  is the excess amount adsorbed. (See Section 2.1.2. for detailed explanation).

To design adsorption processes over a wide range of temperatures and pressures above the critical point of the adsorbate, a characterization of the adsorption isotherm is required. The ability to predict the adsorption properties reduces the number of experiments required to evaluate the process performance. Hence, modeling is of key importance. Once a suitable model is adapted, only a small number of experiments are required to parameterize it. Furthermore, it enables all other isotherms within the range of validity of the model to be predicted. When a model is defined, the best operating parameters can be detected. Thus, the model helps select appropriate adsorbents by defining optimal operating temperature and pressure ranges, density of adsorbents and its specific surface. This is preferably done by simulations [1].

### 2.1.2. Excess and absolute adsorption

The adsorption models described in the previous section generally describe absolute adsorption,  $n_a$ . The absolute adsorption is, as mentioned in Section 2.1 defined as the quantity of gas contained in the adsorption volume  $V_a$  (the space where the density of the

adsorbate is higher than that of the bulk gas), and is in interaction with the adsorbent. Mathematically this can be written

$$n_a = \frac{n_{tot}}{m_s} - \rho_g(V_v - V_a) \quad (2.2)$$

where

$$n_{tot} = n_a + n_g = n_a + \rho_g V_g \quad (2.3)$$

Here  $n_{tot}$  is the total amount of adsorbate introduced in the measuring system containing the adsorbent,  $n_g$  is the homogenous bulk gas,  $m_s$  is the mass of adsorbent,  $\rho_g$  is the density of the bulk gas and  $V_v$  is the total void volume of the adsorption system per unit mass of adsorbent (including the pore volume of the adsorbent, the interstitial space, and any additional empty space). This is illustrated in Figure 3.

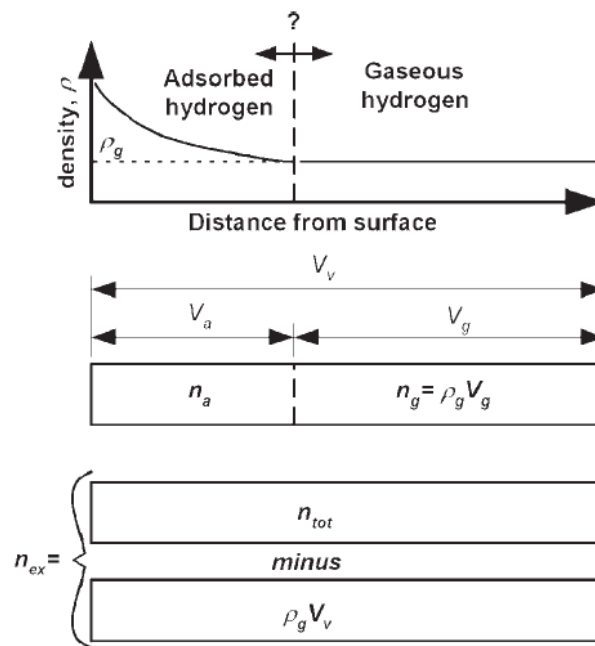


**Figure 3: Absolute and excess hydrogen adsorption [9]**

The total void volume can be measured by helium probing, however, the adsorption volume cannot be measured separately [10]. Due to this, it is common practice to measure the excess adsorption which gives the additional amount of gas present in the total void volume.

To measure the excess adsorption, the amount of hydrogen in a sample cell with an adsorbent is compared to the amount of hydrogen in the sample cell filled with a non-adsorbing reference sample. As hydrogen is adsorbed, the adsorbed layer displaces some of the hydrogen gas from the pores. When the layer is saturated, the only way to increase the



amount of hydrogen is by compression. There will be less space available in the saturated adsorbent than in the reference sample; this means that the compressed gas contribution has a smaller inclination than the reference sample gas [5]. The excess adsorption can be found from:

$$n_{ex} = \frac{n_{tot}}{m_s} - \rho_g V_{v,syst} \quad (2.4)$$

By assuming a density of the adsorbed layer, its volume,  $V_a$ , can be calculated and the excess uptake can be corrected to give the absolute adsorption. The excess adsorption given in terms of absolute adsorption can thus be written as:

$$n_{ex} = n_a - \rho_g V_a = n_a \left[ 1 - \frac{\rho_g}{\rho_a} \right] \quad (2.5)$$

where  $\rho_a$  is the average adsorbed density [10].

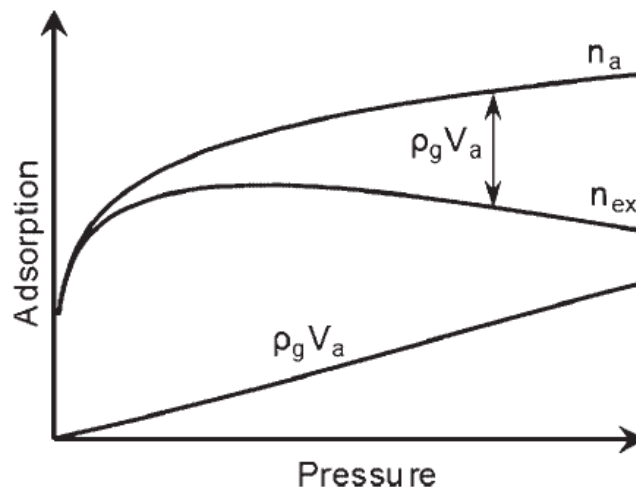


Figure 4: Maximum in excess adsorption isotherm curves [9]

As illustrated in Figure 4, the excess uptake usually has a maximum at a given pressure and for higher pressures it will monotonously decrease until the excess adsorption reaches zero for the pressure where the bulk and pore densities are the same. When the porous adsorbent reaches saturation, the absolute adsorption,  $n_a$ , reaches a maximum value. However, the density of the gas increases monotonically and hence; the excess adsorption,  $n_{ex}$ , will increase to a maximum before it decreases (that is if the hydrogen gas is compressed to the same density as the adsorbed layer). The differences in the excess and the absolute adsorption may be ignored in the very low-pressure subcritical region and in the sub-atmospheric supercritical region [11].

As seen from Figure 4, the absolute adsorption,  $n_a$  increases with pressure and then saturates. The amount of bulk gas that would have been in the micro pores in the absence of adsorption forces increases with pressure according to the ideal gas law, this is seen as the term  $\rho_g V_a$ . The excess adsorption is given as the difference between these two, and has a maximum near the saturation point typically at high pressure and low temperature. If the temperature is decreased the maximum is shifted to lower pressure due to the fact that  $n_a$  saturates at lower densities and  $\rho_g V_a$  increases faster with pressure [9]. Beyond this point, the amount of stored hydrogen will be higher than a compressed gas under similar thermodynamic conditions, and even though to a lesser extent than at lower pressures, the adsorption forces are still beneficial.

### 3. Literature study on adsorption models and thermodynamic approaches

---

The model equations for adsorption storage are widely reported in literature. This chapter comprises of three parts. First, three different adsorption models will be introduced. Then, a literature survey on adsorption theories and models as well as thermodynamic assumptions will be presented. In the last section, a discussion will be carried out and a recommendation for a model to use in numerical calculations will be given.

#### 3.1. Adsorption models

As mentioned in Section 2.1.1, all theoretically derived adsorption models assume parameters that need to be adapted to fit the experimental isotherms. A general procedure for determining these parameters includes calculations of the model parameters based on assumptions before fitting the isotherms to experimental data. When this is done the models with the fitted parameters are used to calculate the quantity of adsorbed hydrogen at a given pressure and temperature. A wide range of adsorption models have been suggested and investigated, among them are the Langmuir model, the Ono Kondo model and the Dubinin-Astakhov model. These will be presented in Sections 3.1.1, 3.1.2, and 3.1.3, respectively.

##### 3.1.1. Langmuir adsorption

The Langmuir adsorption model is the most basic theory in adsorption. It gives the amount of adsorbate adsorbed on an adsorbent as a function of partial pressure or concentration at a given temperature. This model is the most commonly used assuming ideal gas and an idealized adsorbent surface. It is used for monolayer adsorption only and neglects the interactions between adsorbate molecules; hence, the model is mostly useful at low pressures and high temperatures. The Langmuir model provides a simple description of the filling of a monolayer and is based on kinetic adsorption theory, that is the rate of adsorption is equal to the rate of desorption from the surface [1], [12].

Assumptions:

- The adsorbent surface is perfectly homogenous, flat and plane with no corrugations.
- The adsorbing gas adsorbs into an immobile state.
- All sites are equivalent.
- Each site can hold one molecule at most.
- There are no interactions between adsorbate molecules on adjacent sites.

The Langmuir isotherm in terms of fractional loading [12]:

$$\theta = \frac{bP}{1 + bP} \quad (3.1)$$

In terms of amount adsorbed [12]:

$$n_{ex} = n_{max} \frac{bP}{1 + bP} \quad (3.2)$$

where [12]:

$$b = b_0 \exp\left(\frac{Q}{R_g T}\right) \quad (3.3)$$

Here  $n_{max}$  is the maximum adsorbed concentration corresponding to complete monolayer coverage,  $P$  is the pressure,  $Q$  is the heat of adsorption and  $R_g$  is the universal gas constant.

The amount adsorbed increases linearly with pressure. For a sufficiently high pressure, the amount adsorbed reaches a saturation capacity and hence, all adsorption sites are covered with adsorbate molecules ( $\theta \rightarrow 1$ ). An increase in temperature will decrease the amount adsorbed at a given pressure due to the great energy acquired to evaporate an adsorbed molecule. Contrarily, the amount of adsorbed gas increases when the heat of adsorption increases due to the higher energy barrier that the adsorbed molecules have to overcome to evaporate back to the gas phase. The heat of adsorption is constant and independent of loading.

### *Improved Langmuir models*

An improved Langmuir model is the Brunauer-Emmet-Teller model (BET). By taking the adsorbate-adsorbate interactions into account, it allows for multilayer adsorption [1].

Another improvement of the Langmuir approach is the Sips model, also known as the Langmuir-Freundlich model. This model is based on the energy distribution approach. It is purely empirical and assumes a heterogeneous surface.

### **3.1.2. Ono-Kondo**

The Ono-Kondo equations are a set of coupled self-consistent nonlinear equations describing the density profile of successive layers of adsorbed molecules. In this approach the adsorption takes place on a discrete lattice with a symmetry reflecting the periodic arrangement of the adsorption sites. One particle can be adsorbed on an adsorption site at most [1].

The excess adsorption is given by [1]:

$$n_{ex} = C \sum_{i=1}^M (x_i - x_b) \quad (3.4)$$

Where,  $x_i$ , is the molecular fraction per adsorption site on the  $i$ -th layer and is related to the molar density  $\rho_i$  by the expression

$$x_i = \frac{\rho_i}{\rho_{mc}} \quad (3.5)$$

Where  $\rho_i$  is the molar density at the  $i$ -th layer,  $\rho_{mc}$  is the density at maximum capacity,  $\rho_b$  is the bulk molar density of the adsorbate,  $M$  is maximum number of layers and  $C$  is a prefactor that takes the density of the active pores and other structural properties of the adsorbent into account. The model fails when the bulk density of the adsorbate nears the saturation density of the adsorbent (when  $x_b$  reaches 1)

The prefactor  $C$  has been found to be temperature dependent and can be fitted by a third-order polynomial

$$C = C_0 + C_1T + C_2T^2 + C_3T^3 \quad (3.6)$$

The Ono Kondo equations are [1]:

$$\ln\left(\frac{x_k(1-x_b)}{x_b(1-x_k)}\right) + \frac{z_0E}{kT}(x_k - x_b) + \frac{z_2E}{kT}(x_{k+1} - 2x_k + x_{k-1}) = 0 \quad (3.7)$$

boundary conditions:

$$x_1 = x_N \quad (3.8)$$

$$\ln\left(\frac{x_k(1-x_b)}{x_b(1-x_k)}\right) + \frac{E}{kT}(z_1x_1 + z_2x_2 + z_0x_b) + \frac{E_A}{kT} = 0 \quad (3.9)$$

Here  $E$  describes the interactions between adsorbate molecules (limited to nearest neighbor sites of the lattice), and can be viewed as an average interaction energy between co-planar and inter-planar neighboring adsorbate molecules.  $E_A$  is the on-site adsorption potential which parameterizes the interaction between the adsorbate particles and the adsorbent surface. Equations 3.7 - 3.9 are a set of nonlinear equations and needs to be solved self-consistently [1].

### 3.1.3. The Dubinin-Astakhov method

Another important adsorption mechanism applicable for microporous solids is the micropore filling. The adsorption mechanism in micropore filling is very different from that on a surface of a large pore where the adsorption occurs by layering processes. In the micropores the adsorption force field covers the entire volume. This leads to a higher heat of adsorption for the micropore compared to that on a surface [12]. This method is developed to describe

subcritical adsorption which means that the saturation pressure is undefined for temperatures over the critical state and another standard state has to be chosen. The excess adsorption data can be converted into absolute adsorption by determining either the adsorbed phase density or the adsorption volume [10].

The degree of filling is [12]:

$$\theta = \frac{n_a}{n_{max}} \quad (3.10)$$

Where,  $n_a$ , is the absolute adsorbate in the micropore and,  $n_{max}$ , is the maximum absolute adsorption. The adsorption equation is

$$\theta = \exp \left[ - \left( \frac{A}{E} \right)^n \right] \quad (3.11)$$

Where the adsorption potential, A is given by

$$A = R_g T \ln \left( \frac{P_0}{P} \right) \quad (3.12)$$

$E$  is the characteristic energy and  $n$  describes the surface heterogeneity and is usually equal to 2 for most activated carbons [10].

By setting (3.10) equal to (3.11) we have

$$n_a = n_{max} \exp \left[ - \left( \frac{A}{E} \right)^n \right] \quad (3.13)$$

Here  $E$  is a measure of the strength of interaction between adsorbate and adsorbent. This is different for the interaction energy,  $b$ , in the Langmuir equation. In the Langmuir equation the interaction energy is a measure on the interaction between an adsorbate molecule and surface atoms, in the case of micropore filling the interaction is between the adsorbent and the volume of adsorbate.

### *A modified D-A model*

In the modified model the characteristic free energy of adsorption,  $E$ , is replaced by[10]:

$$E = \alpha + \beta T \quad (3.14)$$

Where  $\alpha$  [J/mol] is related to the enthalpic contribution of the characteristic free energy of adsorption and  $\beta$  [J/×K] is related to the entropic contribution. The modification allows for a reduction in the standard error fitting in supercritical regions for a wide range of

temperatures and pressures. It is also possible to fit the model parameters using only two measured isotherms at 77 K and 298 K without significantly reducing the quality of the fit.

### 3.2. Comparison of adsorption model performance

Difficulties can be encountered when comparing theory and experiment due to the fact that the thermodynamic theories and molecular simulations of adsorption of gases on porous solids are formulated as absolute variables while the experimental measurements are reported as excess variables. However, as showed in Section 2.1.2, there are ways to convert the theoretical absolute variables into the corresponding excess variables using thermodynamics. In this section, a literature survey on adsorption model performance is conducted by considering three published works representing each model presented in the previous section. The table below lists the published works considered.

**Table 2: Literature survey**

Published work	Adsorption model	Temperature range	Pressure Range	Adsorbent material	Numerical approach
Bénard et al.[1]	Ono Kondo	77-298 K	Up to 6MPa	AX-21	Standard volumetric approach
Richard et al.[10]	Dubinin-Astakhov	30-298 K	Up to 6MPa	AX-21	Solution thermodynamics
Richard et al.[9]	Modified D-A	60-298 K	Up to 35MPa	Maxsorb MSC-30 (AX-21)	Solution thermodynamics
V.Senthil Kumar[13]	Langmuir	60-125 K	1-3MPa	MOF-5	Lumped parameter

P. Bénard and R. Chahine [1], compared experimental adsorption measurements of hydrogen on activated carbon AX-21 with excess adsorption isotherms predicted by the Langmuir and the Ono-Kondo lattice model. The experiments were conducted for the temperature and pressure ranges of 77-273 K and 0-6 MPa (0-60bar), respectively.

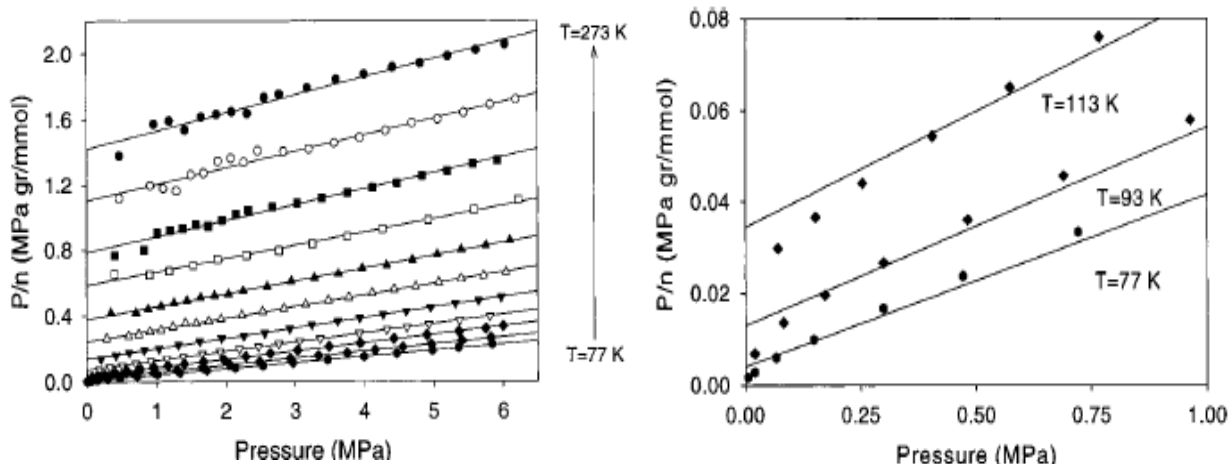


Figure 5: a) Adsorption isotherms expressed as Langmuir plots, b) Langmuir plots of the three lowest temperatures [1]

Figure 5 a) illustrates adsorption isotherms expressed as Langmuir plots. As seen, was good agreement obtained at high temperatures ( $T>133$ K). In Figure 5 b) the Langmuir plots for the lowest temperatures are given with the best linear fit from the whole pressure range. Deviations from the linearity are seen in the experimental results. This is due to the presence of the excess adsorption maximum which cannot be predicted by the Langmuir model.

In contrast, the Ono-Kondo equations proved to fit well over the whole temperature and pressure range and especially in the low-temperature region when fitted to the experimental data. This is seen from Figure 6 below.

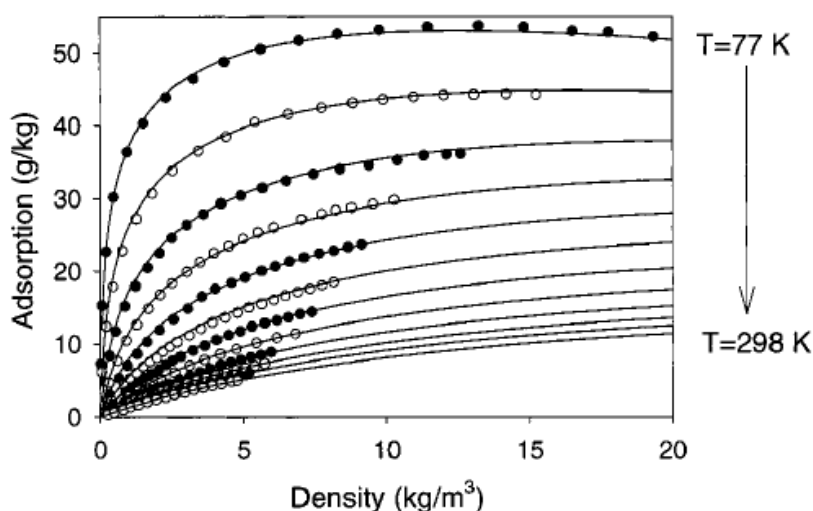
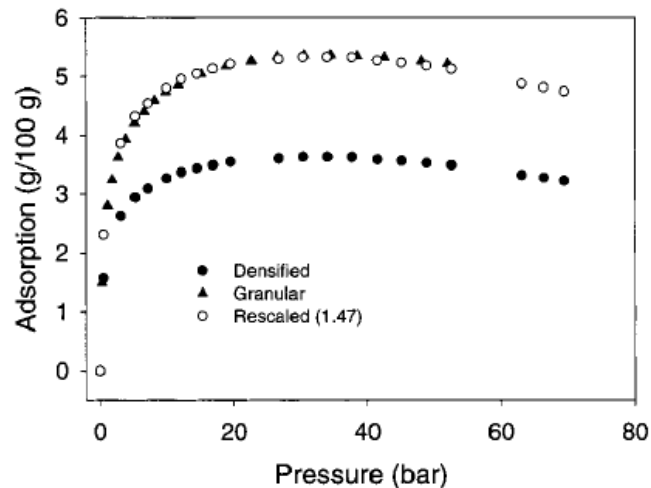


Figure 6: Ono-Kondo fit of the adsorption isotherms (lines) to the experimental data (points). The adsorption density is shown as a function of bulk gas density [1]



Hydrogen was also fitted to a pelletized carbon and it was found that the adsorption data of the two carbons had a constant ratio over the whole pressure range as seen from Figure 7. This proved that the Ono-Kondo parameterization already obtained could be applied to other carbons with similar porous structure, provided that the change in specific area was taken into account.



**Figure 7 : Comparison of the low-temperature adsorption isotherms of hydrogen at 77 K for two different carbons (AX-21 powder and pellets.) [1]**

It was concluded that the Ono-Kondo model is more useful than the Langmuir model in the temperature and pressure ranges of interest to storage applications.

M.-A. Richard [10] investigated the gas adsorption process in activated carbon over wide temperature and pressure ranges above the critical point. The study comprises of two parts, where in the first, the Dubinin-Astakhov (D-A) model was adapted to model hydrogen, methane and nitrogen adsorption isotherms on the activated carbon AX-21 at high pressures and supercritical temperatures. The excess adsorption is not feasible to use as it reaches a maximum at high pressures and low temperatures, thus a constant microporous adsorption volume  $V_a$  (microporous volume of the adsorbent) was defined by fitting experimental data to the modeled excess isotherm and the excess adsorption was converted to absolute adsorption. The objective was to find a model that was simple enough to allow for analytical derivation of the adsorbed phase terms of the mass rate and energy rate balance equations. Several different interpretations of the D-A parameters were evaluated along with the Langmuir model and the quality of these different fitted parameters was analyzed using the standard error of the estimate. In addition, a parameterization performed only at 77K and 298K (but with the error estimate calculated using the whole range of experimental data) was included. The modified D-A model showed to fit the experimental data over the whole range (30-293 K, 0-6 MPa for hydrogen) with a very good overall quality. This can be seen from Figure 9 below.

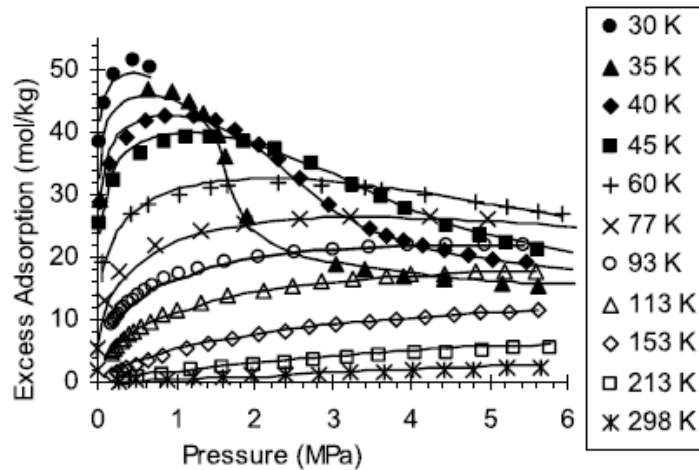


**Figure 8: Modified D-A model fit (solid lines) to experimental excess adsorption isotherms of hydrogen on activated carbon AX-21 [10]**

The model specific excess adsorption standard error of estimate was found to be 0.79 mol/kg for the D-A model, compared to 3.33 mol/kg for the Langmuir model. They found that when using only two hydrogen adsorption isotherms (at 77 K and 298 K) the quality of the fit was not significantly affected (error of 1.19 mol/kg). This is of high practical interest as it suggests that less experimental data is required

As was seen from the Ono-Kondo fits [1], the D-A modeled isotherms also follows the experimental results well. It was concluded that the modified D-A model provided a significantly better fit for the hydrogen adsorption when taking the enthalpic and entropic contributions into account for the characteristic free energy of adsorption (see Equation 3.14)

In a later study, Marc-André Richard [9] evaluated the feasibility of an adsorption based hydrogen storage system for a fuel cell vehicle system by determination of the net storage capacity of the system in the temperature range 60–298 K and for pressures up to 35 MPa. The adsorbent used was activated carbon Maxsorb MSC-30. The modified D-A model developed in [10] was used with values previously obtained to describe the absolute adsorption. In addition, volumetric and gravimetric adsorption experiments were performed to ascertain the validity of the parameters in the range of higher pressures (up to 23 MPa). Good consistency was seen and it was concluded that the parameters determined for pressures up to 6 MPa are still valid at 23 MPa and thus these values were used further in the study.

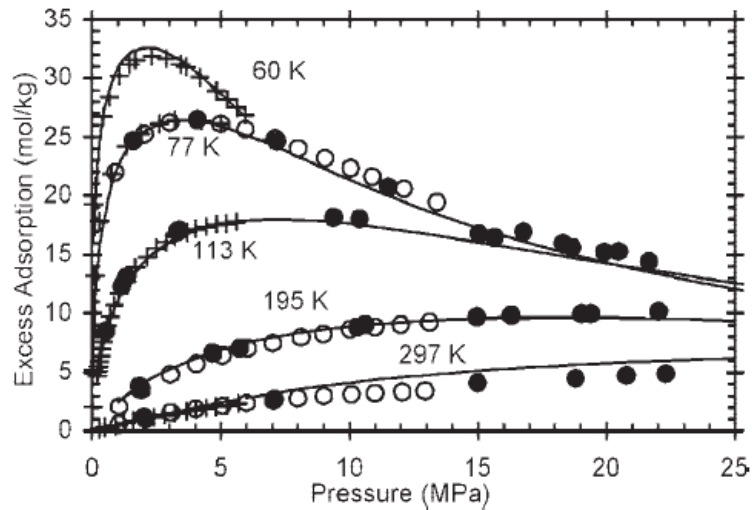


**Figure 9: Hydrogen excess adsorption isotherms on Maxsorb MSC-30, and AX-21**

Figure 9 presents the excess adsorption of hydrogen where the solid line is the Modified D-A model, the crosses, clear dots and black dots are the 0-6 MPa AX-21 adsorption data, high pressure Maxsorb MSC -30 adsorption data (gravimetric method) and high pressure Maxsorb adsorption data(volumetric method), respectively. As can be seen from the figure, the results showed good agreement with the experiments, only a slight deviation occurs at 297 K for pressures over 10 MPa; here most of the hydrogen is stored in gaseous state.

Furthermore, it was found that the modified D-A model could represent the hydrogen adsorption on the activated carbon CNS-201(prepared by physical activation) and the Metal-organic framework  $\text{Cu}_3(\text{BTC})_2$ . These results are presented in Figure 10 below.

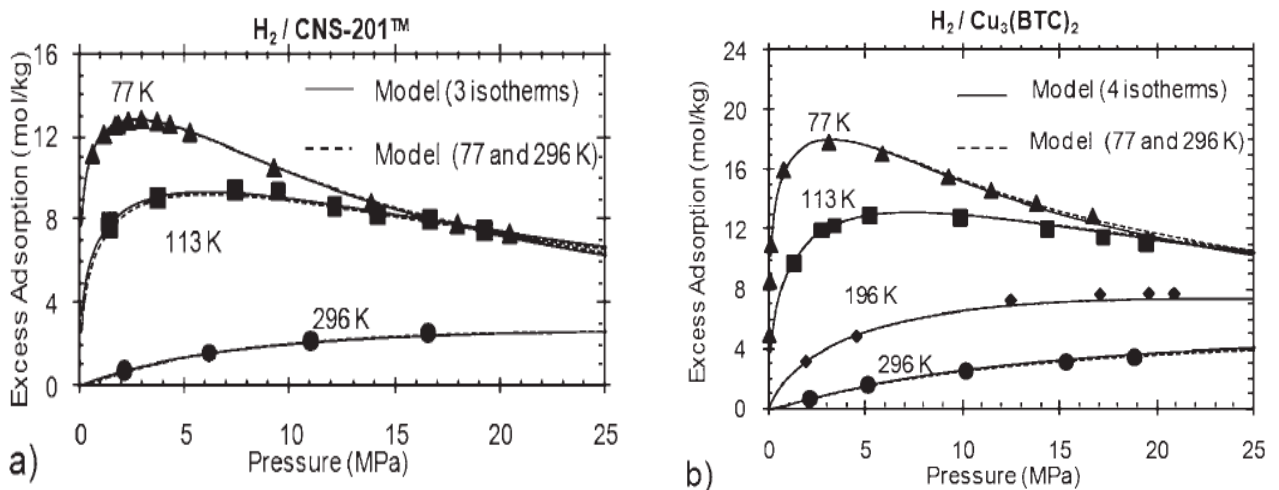


**Figure 10: Hydrogen excess adsorption isotherms on a) CNS-201 and b)  $\text{Cu}_3(\text{BTC})_2$**

The results found from Figure 9 and Figure 10, were compared to other published works and found to be in good agreement.

### 3.2.1. A complete model for hydrogen adsorption

In the previous section a selection of studies done on the Langmuir, Ono-Kondo and Dubinin-Astakhov models were presented. To describe the complete adsorption process, these models are implemented into transient mass and energy balances. In the present section, three thermodynamical approaches will be presented by giving the assumptions and theories applied. However, the actual equations developed will only be derived for the one selected for further implementation into COMSOL Multiphysics. Details regarding the derived equations from the remaining two articles can be found in the respective references cited.

V. Senthil Kumar et al. [13] described a quasi-static lumped parameter model for a cryo-adsorber fuel tank. The four fuel tank processes occur over different time scales: refueling over a few minutes, discharge over a few hours, dormancy over a few days and venting over a few weeks. The slower processes like discharge, dormancy and venting are expected to have negligible temperature gradients within the bed and are thus amenable to a lumped-parameter analysis. The lumped parameter model involves intra-pellet lumping and across the bed lumping of temperature, pressure and solid phase concentration fields. The intra-pellet lumping of temperature and concentration was justified by a Biot number analysis, and the pressure lumping by an Ergun equation analysis.

A quasi-static approach implies local thermal and mass equilibrium at any time which means that the transient system passes through a series of equilibrium states. This implies that there are negligible temperature differences between gas and solid (Equation 3.15) at any location within the bed. This allows for a single energy balance describing both gas and solid phases.

$$T_s(\vec{r}, t) \approx T_g(\vec{r}, t) \equiv T(\vec{r}, t) \quad (3.15)$$

$$n_{ex}(\vec{r}, t) \approx n_{ex}^*[T(\vec{r}, t), P(\vec{r}, t)] \quad (3.16)$$

Also, the adsorbate loading  $n_{ex}$  can be described by its equilibrium value  $n_{ex}^*$  (Equation 3.16). Furthermore, when the fuel tank processes are quasi-static, only adsorption isotherms and heat capacity of the adsorbent needs to be measured at different temperatures for the ability to design or simulate the fuel tank.

All steel components in the inner thermal masses were accounted for as a steel wall with one total mass. The average heat of adsorption was assumed to be constant and the thermal expansion of the material to be negligible.

The Langmuir model was used to describe the adsorbed phase. To verify that this was an appropriate model, excess adsorption data earlier reported on MOF-5 powder was fitted to a Langmuir isotherm in the temperature and pressure ranges of 60-125 K and 1- 30 bar, respectively.

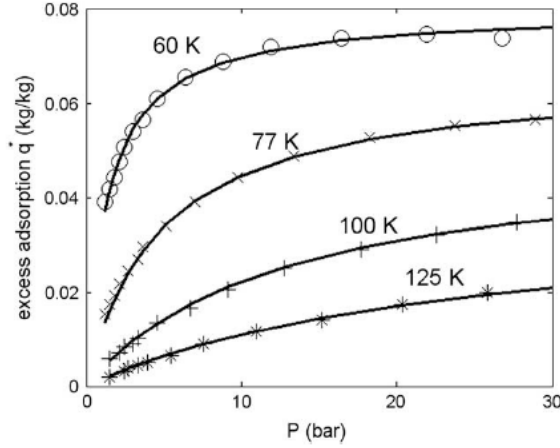


**Figure 11: Langmuir fit (lines) for MOF-5 excess adsorption data (symbols) of Zohu et al. [13]**

As seen from the figure above, the Langmuir isotherms were found to fit well to the adsorption data. However, as reported in the previous section, P. Bénard and R. Chahine[1] did not, find the Langmuir model to fit the plots for low temperatures. This might be explained from the correlations used for the maximum adsorption in Equation 3.2:

$$n_{max} = \frac{n_{max0}}{f(t)} \quad (3.17)$$

where Kumar et al. set  $f(t) = 1 + AT^2$ , while in [1] it was set to:  $f(t) = 1 + AT$ . In addition, the homogeneity of the surface is essential for the validity of the Langmuir approach discussed in Section 3.1.1.

As Kumar et al. found the Langmuir model to give satisfactory results; it was incorporated into the mass and energy balances of the adsorption system.

In a later work V. Senthil Kumar et al. [2] presented a set of 3-D model equations for a cryo-adsorption hydrogen storage tank. The model was reduced to a 1-D isobaric system and the isobaric refueling time studied. The 3-D transient mass and energy balances were developed considering an infinitesimal element of the adsorbent bed and using a lumped parameter analysis. Constant bed density and total porosity was assumed. Quasi-static approximations were used, and hence the gas and the adsorbate are in local equilibrium. This implies that any change in property of gas or adsorbate is due to temperature and pressure change at that location, also the adsorbate concentration was approximated to the equilibrium adsorbate concentration ( $n_{ex}^*$ ) at that location by the Langmuir adsorption isotherm. Furthermore a constant heat of adsorption was assumed. The heat leak that should be considered for the structural steel domain was neglected as the equations are based on an element inside the adsorbent bed. This is due to the fact that for the system considered, the heat effects due to adsorption or desorption will be significantly larger than the heat leak into the tank during refueling and discharge. However, for the slow processes (venting and dormancy) the heat leak drives the tank system. This was taken into account in [13] where

the lumped parameter analysis used a single energy balance where the heat leak term was represented.

Marc-André Richard [14] developed mass and energy balance equations for hydrogen, nitrogen and methane adsorption on activated carbon valid over a large pressure and temperature range in the supercritical region. The adsorbed phase contribution in the balance equations was obtained from an isotherm expressing the adsorbed gas as a function of temperature and pressure using the modified Dubinin-Astakhov model. In contrast to the work of Kumar et al., the isosteric heat of adsorption was not considered constant, but given as

$$\Delta \bar{h}_a = -ZRT^2 \left[ \frac{\partial \ln P}{\partial T} \right]_{n_a} \quad (3.18)$$

If the compressibility factor  $Z$  is set equal to 1, perfect gas is assumed. Solution thermodynamics was applied to the condensed phase (adsorbent and adsorbed gas), the adsorption volume was assumed constant and the reference was to the perfect gas enthalpy. The adsorbent was assumed to be rigid with a fixed mass. For the mass conservation, it was assumed that the molar flux in and out of a volume element is composed of gas only. The volumes of bulk and adsorbed gas were assumed constant and the densities are functions of pressure and temperature. For the Energy balance the adsorbent, the adsorbed gas and the gas phase are assumed to be in thermal equilibrium in the control volume and there is no external work. The mass and energy balances were solved using COMSOL and compared to nitrogen desorption experiments, these showed to be in agreement with the experiments.

### 3.2.2. Discussion

In the previous sections three adsorption models were introduced before reported data on the models fitted to experimental measurements was presented. In addition, a literature study on different thermodynamic assumptions, used for developing mass and energy equations intended to describe the hydrogen adsorption, was conducted.

P. Bénard and R. Chahine [1], and M.-A. Richard [14] compared the Ono-Kondo equations and the Modified D-A model, respectively, to the Langmuir model. Both concluded that the Langmuir model was the poorer choice due to its restricted validity range. The Ono-Kondo equation improves on the Langmuir model by including the interactions between neighboring adsorbate molecules. In addition, it directly provides the excess adsorbate isotherm [1]. The D-A Model proved to have a precision more than four times better than the Langmuir equation. However, the Langmuir approach is a lot simpler, and therefore also easier to parameterize and implement into transient mass and energy balances. In addition, it can be used with satisfactory results within more restricted regions.

### 3.3. Recommendation of model for further use

The purpose of this study is to perform numerical transient calculations on the hydrogen adsorption behavior using a numerical software. Hence, the motivation for recommending a model for further use is based on the assumed ability of succeeding in doing so. The Langmuir approach has proven to be suitable for modeling over a limited pressure and temperature range. Yet, it is well known that there are models more accurate and better suited when it comes to cryogenic adsorption. Nevertheless, the Langmuir model was chosen in this study due to its simplicity, allowing for an easier detection of possible errors and numerical instabilities.

The generalized model developed by V. Senthil Kumar [2] is a good starting point for the purpose of this study as it considers an infinitesimal element within a cryo-adsorber bed. Hence, heat leakage and the mass of structural steel are neglected. The study is profound, yet it assumes constant heat of adsorption (ideal gas law) and uses quasi-static approximations, which will facilitate the implementation in a numerical software.

When the model is built and transient calculations on the hydrogen adsorption behavior under different initial and boundary conditions are carried out, the model can be extended and more exact adsorption theories can be used. However, this will not be a priority in the present study.





## 4. Proposed model

In the coming sections, the model equations developed by V. Senthil Kumar et al. [2], will be presented in more detail. Then, the transient mass and energy balances are implemented into the numerical software COMSOL Multiphysics 4.2.a. Here, the effects of heat and mass transfer are analyzed. In addition, different initial and boundary conditions are implemented to yield a better understanding of the effects of temperature, pressure and velocity, on the adsorption process.

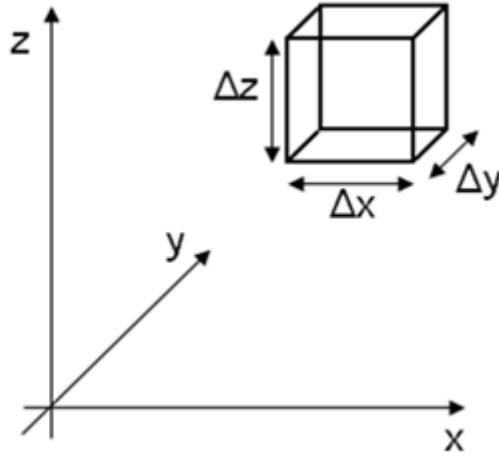


Figure 12: Cuboidal infinitesimal element within a cryo-adsorber bed [2]

The mass and energy balances are developed considering an infinitesimal element of the adsorbent bed, as seen in Figure 12.

To estimate the adsorbate concentration, the Langmuir adsorption isotherm presented in 3.1.1 is used. The following formulas visualize the nomenclature used. In addition, Equations 4.3 and 4.4 shows the used approach to describe the temperature dependence of the maximum uptake. Hereby,  $n_{max0}$ , is the maximum uptake at the reference temperature and  $A$  is an empirical coefficient.

$$n_{ex}^*(T, P) = n_{max} \frac{bP}{1 + bP} \quad (4.1)$$

$$b = b_0 \exp\left(\frac{B}{T}\right) \quad (4.2)$$

$$n_{max} = \frac{n_{max0}}{f(T)} \quad (4.3)$$

$$f(T) = 1 + AT^2 \quad (4.4)$$

## 4.1. Governing equations

The governing equations are presented by listing the most important ones. A complete derivation of the transient mass and energy balances are given in the Appendix.

### Mass balance

The mass balance describes the flow rate or velocity changes due to adsorption.

The transient mass balance for the element is:

$$\left( \begin{array}{c} \text{rate of change of total} \\ \text{hydrogen content} \end{array} \right) = \left( \begin{array}{c} \text{convective mass} \\ \text{inflow} \end{array} \right) - \left( \begin{array}{c} \text{convective mass} \\ \text{outflow} \end{array} \right) \quad (4.5)$$

The adsorbate diffusion is often negligible compared to the convective component, and is typically neglected in literature [2]. The expressions for the terms in the mass balance are listed below:

$$\text{Mass of adsorbent in the element:} \quad \Delta x \Delta y \Delta z \rho_b \quad (4.6)$$

$$\text{Mass of hydrogen adsorbed in the element:} \quad \Delta x \Delta y \Delta z \rho_b n_{ex} \quad (4.7)$$

$$\text{Total void volume of the element:} \quad \Delta x \Delta y \Delta z \varepsilon_t \quad (4.8)$$

$$\text{Mass of gaseous hydrogen in the element:} \quad \Delta x \Delta y \Delta z \varepsilon_t \rho_g \quad (4.9)$$

$$\text{Total hydrogen content of the element:} \quad \Delta x \Delta y \Delta z (\rho_b n_{ex} + \varepsilon_t \rho_g) \quad (4.10)$$

$$\text{Rate of change of total hydrogen content:} \quad \Delta x \Delta y \Delta z \frac{\partial}{\partial t} (\rho_b n_{ex} + \varepsilon_t \rho_g) \quad (4.11)$$

$$\text{Convective mass flow rate into the face at } x: \quad \Delta y \Delta z (U_x \rho_g)_x \quad (4.12)$$

$$\text{Convective mass flow rate out of face at } x + \Delta x: \quad \Delta y \Delta z (U_x \rho_g)_{x+\Delta x} \quad (4.13)$$

substituting these expressions into (3.5) and dividing by  $\Delta x \Delta y \Delta z$  and taking the limits  $\Delta x, \Delta y, \Delta z \rightarrow 0$ , gives

$$\frac{\partial}{\partial t} (\rho_b n_{ex} + \varepsilon_t \rho_g) = \frac{\partial (U_x \rho_g)}{\partial x} - \frac{\partial (U_y \rho_g)}{\partial y} - \frac{\partial (U_z \rho_g)}{\partial z} \quad (4.14)$$

which equals

$$\frac{\partial}{\partial t}(\rho_b n_{ex} + \varepsilon_t \rho_g) + \vec{\nabla} \cdot (\vec{U} \rho_g) = 0 \quad (4.15)$$

Assuming constant bed density and total porosity, the general form of mass balance is:

$$\rho_b \frac{\partial n_{ex}}{\partial t} + \varepsilon_t \frac{\partial \rho_g}{\partial t} + \vec{\nabla} \cdot (\vec{U} \rho_g) = 0 \quad (4.16)$$

Expanding the gradient term gives

$$\rho_b \frac{\partial n_{ex}}{\partial t} + \varepsilon_t \frac{\partial \rho_g}{\partial t} \vec{U} \cdot \vec{\nabla} \rho_g + \rho_g (\vec{\nabla} \cdot \vec{U}) = 0 \quad (4.17)$$

The assumption of gas and adsorbate being in local equilibrium is introduced. This is a quasi-static behavior which implies local thermal and mass equilibrium at any time. Hence, at any location within the bed, there are negligible temperature differences between the solid and the gas[2].

Assuming that the gas phase is in equilibrium at the corresponding temperature and pressure gives

$$\rho_g(\vec{r}, t) = \rho_g[T(\vec{r}, t), P(\vec{r}, t)] \quad (4.18)$$

then

$$\frac{\partial \rho_g}{\partial t} = \left( \frac{\partial \rho_g}{\partial T} \right)_P \frac{\partial T}{\partial t} + \left( \frac{\partial \rho_g}{\partial P} \right)_T \frac{\partial P}{\partial t} \quad (4.19)$$

Applying thermodynamic relations (See Appendix) into (4.19) gives:

$$\frac{\partial \rho_g}{\partial t} = -\rho_g \alpha_{p_g} \frac{\partial T}{\partial t} + \rho_g K_{T_g} \frac{\partial P}{\partial t} \quad (4.20)$$

Similarly the adsorbate concentration at any location is approximated to the equilibrium adsorbate concentration at that location

$$n_{ex}(\vec{r}, t) \approx n_{ex}^*[T(\vec{r}, t), P(\vec{r}, t)] \quad (4.21)$$

$$\frac{\partial n_{ex}}{\partial t} \approx \frac{\partial n_{ex}^*}{\partial t} \quad (4.22)$$

$$\frac{\partial n_{ex}^*}{\partial t} = \left( \frac{\partial n_{ex}^*}{\partial T} \right)_P \frac{\partial T}{\partial t} + \left( \frac{\partial n_{ex}^*}{\partial P} \right)_T \frac{\partial P}{\partial t} \quad (4.23)$$

$$\frac{\partial n_{ex}^*}{\partial t} = -n_{ex}^* \left[ \frac{f'(T)}{f(T)} + \frac{B}{(1+bP)T^2} \right] \frac{\partial T}{\partial t} + \left[ \frac{n_{ex}^*}{(1+bP)P} \right] \frac{\partial P}{\partial t} \quad (4.24)$$

Using these expressions in the mass balance gives

$$a_{11} \frac{\partial T}{\partial t} + a_{12} \frac{\partial P}{\partial t} - \rho_g \alpha_{Pg} \vec{U} \cdot \vec{\nabla} T + \rho_g \kappa_{Tg} \vec{U} \cdot \vec{\nabla} P + \rho_g (\vec{\nabla} \cdot \vec{U}) = 0 \quad (4.25)$$

where

$$a_{11} = -\rho_b n_{ex}^* \left[ \frac{f'(T)}{f(T)} + \frac{B}{(1+bP)T^2} \right] - \rho_g \alpha_{Pg} \varepsilon_t \quad (4.26)$$

and

$$a_{12} = \left[ \frac{\rho_g n_{ex}^*}{(1+bP)P} \right] + \rho_g \kappa_{Tg} \varepsilon_t \quad (4.27)$$

### Energy balance

The energy balance describes the temperature change due to the heat released on adsorption.

$$\begin{aligned}
 & \left( \begin{array}{l} \text{rate of change} \\ \text{total enthalpy} \end{array} \right) \\
 &= \left( \begin{array}{l} \text{rate of enthalpy} \\ \text{in flow by} \\ \text{convection} \end{array} \right) - \left( \begin{array}{l} \text{rate of enthalpy} \\ \text{out of flow by} \\ \text{convection} \end{array} \right) + \left( \begin{array}{l} \text{rate of enthalpy} \\ \text{in flow by} \\ \text{conduction} \end{array} \right) \\
 & - \left( \begin{array}{l} \text{rate of enthalpy} \\ \text{out flow by} \\ \text{conduction} \end{array} \right) + \left( \begin{array}{l} \text{rate of enthalpy} \\ \text{change due to} \\ \text{pressure changes} \end{array} \right) \quad (4.28)
 \end{aligned}$$

The expressions of the terms listed in the energy balance are listed below:

$$\text{Enthalpy of adsorbent in the element:} \quad \Delta x \Delta y \Delta z \rho_b H_s \quad (4.29)$$

$$\text{Enthalpy of adsorbate in the element:} \quad \Delta x \Delta y \Delta z \rho_b n_{ex} H_{n_{ex}} \quad (4.30)$$

$$\text{Enthalpy of gas in the element:} \quad \Delta x \Delta y \Delta z \varepsilon_t \rho_g H_g \quad (4.31)$$

$$\text{Total enthalpy in the element:} \quad \Delta x \Delta y \Delta z (\varepsilon_t \rho_g H_g + \rho_b n_{ex} H_{n_{ex}} + \rho_b H_s) \quad (4.32)$$

$$\text{Rate of change of total enthalpy of the element:} \quad \Delta x \Delta y \Delta z \frac{\partial}{\partial t} (\varepsilon_t \rho_g H_g + \rho_b n_{ex} H_{n_{ex}} + \rho_b H_s) \quad (4.33)$$

$$\text{Convective enthalpy flow rate into the face at } x: \quad \Delta y \Delta z (U_x \rho_g H_g)_x \quad (4.34)$$

$$\text{Convective enthalpy flow rate out of face at } x + \Delta x: \quad \Delta y \Delta z (U_x \rho_g H_g)_{x+\Delta x} \quad (4.35)$$

$$\text{Conductive enthalpy flow rate into the face at } x: \quad \Delta y \Delta z \left( -k_{eff} \frac{\partial T}{\partial x} \right)_x \quad (4.36)$$

$$\text{Conductive enthalpy flow rate out of the face at } x + \Delta x: \quad \Delta y \Delta z \left( -k_{eff} \frac{\partial T}{\partial x} \right)_{x+\Delta x} \quad (4.37)$$

$$\text{Rate of enthalpy change due to pressure changes.} \quad \Delta x \Delta y \Delta z \varepsilon_t \frac{\partial P}{\partial t} \quad (4.38)$$

Using these expressions in Equation 4.28 , dividing by  $\Delta x\Delta y\Delta z$  and taking the limits

$\Delta x\Delta y\Delta z \rightarrow 0$  gives

$$\frac{\partial}{\partial t}(\varepsilon_t \rho_g H_g + \rho_b n_{ex} H_{n_{ex}} + \rho_b H_s) - \varepsilon_t \frac{\partial P}{\partial t} + \vec{\nabla} \cdot (\vec{U} \rho_g H_g) + \vec{\nabla} \cdot (-k_{eff} \vec{\nabla} T) = 0 \quad (4.39)$$

Assuming constant bed density and total porosity and expanding the equation

$$\varepsilon_t \rho_g \frac{\partial H_g}{\partial t} + \varepsilon_t H_g \frac{\partial \rho_g}{\partial t} + \rho_b n_{ex} \frac{\partial H_{n_{ex}}}{\partial t} + \rho_b H_{n_{ex}} \frac{\partial n_{ex}}{\partial t} + \rho_b \frac{\partial H_s}{\partial t} - \varepsilon_t \frac{\partial P}{\partial t} + \rho_g \vec{U} \cdot \vec{\nabla} H_g + H_g \vec{\nabla} \cdot (\vec{U} \rho_g) + \vec{\nabla} \cdot (-k_{eff} \vec{\nabla} T) = 0 \quad (4.40)$$

The heat of adsorption is defined as

$$H_{n_{ex}} = H_g + \Delta H_a \quad (4.41)$$

The average heat of adsorption,  $\Delta H_a$ , is assumed constant. Hence,

$$\frac{\partial H_{n_{ex}}}{\partial t} \approx \frac{\partial H_g}{\partial t} \quad (4.42)$$

Using this result it follows

$$\varepsilon_t \rho_g \frac{\partial H_g}{\partial t} + \varepsilon_t H_g \frac{\partial \rho_g}{\partial t} + \rho_b n_{ex} \frac{\partial H_g}{\partial t} + \rho_b (H_g + \Delta H_a) \frac{\partial n_{ex}}{\partial t} + \rho_b \frac{\partial H_s}{\partial t} - \varepsilon_t \frac{\partial P}{\partial t} + \rho_g \vec{U} \cdot \vec{\nabla} H_g + H_g \vec{\nabla} \cdot (\vec{U} \rho_g) + \vec{\nabla} \cdot (-k_{eff} \vec{\nabla} T) = 0 \quad (4.43)$$

Rearranging

$$\varepsilon_t \rho_g \frac{\partial H_g}{\partial t} + \rho_b n_{ex} \frac{\partial H_g}{\partial t} + \rho_b \frac{\partial H_s}{\partial t} + \rho_b \Delta H_a \frac{\partial n_{ex}}{\partial t} - \varepsilon_t \frac{\partial P}{\partial t} + \rho_g \vec{U} \cdot \vec{\nabla} H_g + \vec{\nabla} \cdot (-k_{eff} \vec{\nabla} T) + H_g \left[ \rho_b \frac{\partial n_{ex}}{\partial t} + \varepsilon_t \frac{\partial \rho_g}{\partial t} + \vec{\nabla} \cdot (\vec{U} \rho_g) \right] = 0 \quad (4.44)$$

From the mass balance (4.16);

$$H_g \left[ \rho_b \frac{\partial n_{ex}}{\partial t} + \varepsilon_t \frac{\partial \rho_g}{\partial t} + \vec{\nabla} \cdot (\vec{U} \rho_g) \right] = 0$$

Hence,

$$\begin{aligned} (\varepsilon_t \rho_g + \rho_b n_{ex}) \frac{\partial H_g}{\partial t} + \rho_b \frac{\partial H_s}{\partial t} + \rho_b \Delta H_a \frac{\partial n_{ex}}{\partial t} - \varepsilon_t \frac{\partial P}{\partial t} + \rho_g \vec{U} \cdot \vec{\nabla} H_g + \vec{\nabla} \cdot (-k_{eff} \vec{\nabla} T) \\ = 0 \end{aligned} \quad (4.45)$$

Now the quasi-static approximation is introduced, assuming local equilibrium

$$H_x(\vec{r}, t) = H_x[T(\vec{r}, t), P(\vec{r}, t)] \quad (4.46)$$

The time derivative of  $H_g(T, P)$  is expanded as

$$\frac{\partial H_g}{\partial t} = \left( \frac{\partial H_g}{\partial T} \right)_P \frac{\partial T}{\partial t} + \left( \frac{\partial H_g}{\partial P} \right)_T \frac{\partial P}{\partial t} \quad (4.47)$$

Introducing thermodynamic relations to gas and adsorbate enthalpy and using the results (See Appendix) in the energy equations give

$$a_{21} \frac{\partial T}{\partial t} + a_{22} \frac{\partial P}{\partial t} + \rho_g C_{p_g} \vec{U} \cdot \vec{\nabla} T + (1 - \alpha_{p_g} T) \vec{U} \cdot \vec{\nabla} P + \vec{\nabla} \cdot (-\lambda_{eff} \vec{\nabla} T) = 0 \quad (4.48)$$

where

$$a_{21} = (\varepsilon_t \rho_g + \rho_b n_{ex}^*) C_{p_g} + \rho_b C_{p_s} - n_{ex}^* \rho_b \Delta H_a \left[ \frac{f'(T)}{f(T)} + \frac{B}{(1 + bP)T^2} \right] \quad (4.49)$$

$$a_{22} = (\varepsilon_t + \rho_b v_g n_{ex}^*) (1 - \alpha_{p_g} T) + (1 - 2\varepsilon_t) + \left[ \frac{q^* \rho_b \Delta H_a}{(1 + bP)P} \right] \quad (4.50)$$

The mass and energy balances are solved for the variables  $(\vec{U}, T, P)$ . If solved manually, they are coupled with Ergun equation (See the paper of Kumar et al. [2] for general solution procedure). In the present work, the equations are solely solved in COMSOL, and hence, the Ergun equation will not be presented.

## 4.2. Implementation

The equations derived in the previous section will now be implemented into COMSOL 4.2.a, and numerical calculations will be run for different boundary and initial conditions. The results obtained will be discussed and compared to experimental data.

### 4.2.1. Purpose of study

As mentioned in Section 2.1.1, a reliable adsorption model will facilitate the research process when investigating the quality of the adsorbents and also reduce the number of experiments required to evaluate the process performance. The transfer processes are unsteady and depend on spatial coordinates; therefore the chosen model is represented by a set of non-stationary differential equations. These equations can be solved in a numerical software. The goal of this study is to implement the transient mass and energy balances into a numerical software and perform transient calculations on the hydrogen adsorption behavior under different initial and boundary conditions.

## 4.3. COMSOL model

The main objective of the model to be developed is its functionality; and hence focus has been put on the implementation of correct modules and not the appearance of the modeled tank. The geometry of the adsorption cell is a simple 2D rectangle with height 100mm and width 10mm, as seen from Figure 13 below.

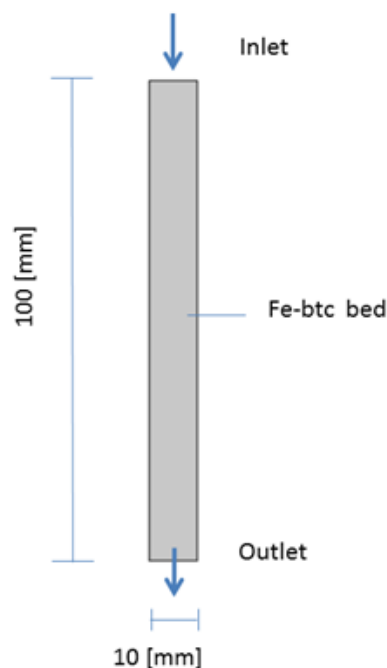


Figure 13: COMSOL model of adsorption cell



The domain is filled with a user-defined porous material and the hydrogen is added to the model as a built-in fluid. The porous matrix is defined as an immobile solid with the Fe-btc properties listed in Table 3.

Hydrogen gas will be inserted at the inlet at  $t=0$  and flow downwards due to pressure and velocity changes imposed as initial and boundary conditions. The adsorption process is affected by heat and mass transfer so suitable physical modules are to be selected. For simulation of heat transfer the module Heat Transfer in Porous Media (*ht*) will be used. For simulation of mass transfer there are two options, Darcy's law (*dl*) and Brinkman Equations (*br*). These will both be tested and one will be selected for further simulation.

**Table 3: Fe-btc and gas properties<sup>1</sup>**

Fe-btc Properties	Built-in hydrogen properties
Solid density, $\rho_s=1812 \text{ kg/m}^3$	Density, $\rho_g$ , varies with temperature in the range 0.323-0.486 $\text{kg/m}^3$
Particle density, $\rho_p=1085.388 \text{ kg/m}^3$	Heat capacity, $Cp_g= 11600 \text{ J/(kg}\times\text{K)}$
Bed density, $\rho_{bed}= 640 \text{ kg/m}^3$	Thermal conductivity, 0.22952 $\text{W/(m}\times\text{K)}$
Particle porosity, $\varepsilon_{particle}=0.401$	Ratio of specific heats, 1.41
Bed porosity, $\varepsilon_{bed}=0.41$	Dynamic viscosity, $\mu= 6.84319 \text{ e-6 Pa s}$
Fe-btc volume fraction, $\theta =0.59$	
Specific heat capacity, $Cp_p= 420 \text{ J/(kg}\times\text{K)}$	
Particle thermal conductivity, $k=0.3\text{W/(m}\times\text{K)}$	
Permeability: $\kappa_{br}= 1.1\text{e-10}$	

The densities and volume fraction are found from the equations below

$$\text{Bed density:} \quad \rho_{bed} = \rho_{particle}(1 - \varepsilon_{bed}) \quad (4.51)$$

$$\text{Volume fraction solid:} \quad \theta = 1 - \varepsilon_{bed} \quad (4.52)$$

$$\text{Particle density:} \quad \rho_{particle} = \rho_{solid}(1 - \varepsilon_{particle}) \quad (4.53)$$

<sup>1</sup> The table properties are provided by NTNU.

### 4.3.1. Heat Transfer module

The heat transfer module provides the capabilities to model heat transfer via convection, conduction and radiation. All material properties are functions of temperature, and thus, a thermal model can be coupled to any other physical model. Furthermore, heat generation from any other physics can be included into the thermal model.

The Heat Transfer in Porous Media (*ht*) module operates with temperature,  $T$ , as dependent variable. The time dependent governing equation for this module is:

$$(\rho_g C p_g)_{eq} \frac{\partial T}{\partial t} + \rho_g C p_g u \cdot \nabla T = \nabla \cdot (k_{eq} \nabla T) + Q \quad (4.54)$$

where

$$k_{eq} = \theta k_p + (1 - \theta) k_g \quad (4.55)$$

and

$$(\rho_g C p_g)_{eq} = \theta \rho_p C p_s + (1 - \theta) \rho_g C p_g \quad (4.56)$$

Here the subscript  $p$  and  $g$  is for solid material and gas, respectively and  $k_{eq}$  from (4.55) merely gives the bed thermal conductivity.

The heat source term,  $Q$ , calculates the heat release and is zero if not specified differently. This is where the energy equation (4.45) is implemented into the model, thus  $Q$  will give the heat released due to adsorption predicted by the Langmuir model at any time.

**Table 4: Comparison of equations used in COMSOL and by Kumar et al. [2]**

	Convection	Conduction	Heat source	Enthalpy of gas and solid in tank
COMSOL	$\rho_g C p_g u \cdot \nabla T$	$\nabla \cdot (k_{eq} \nabla T)$	$Q$	$(\rho C p)_{eq} =$ $(\varepsilon_t \rho_g C p_g + \rho_b C p_s) \frac{\partial T}{\partial t}$
[2]	$\rho_g \vec{U} \cdot \vec{\nabla} H_g$	$\vec{\nabla} \cdot (k_{eff} \vec{\nabla} T)$	$\rho_b \Delta H_a \frac{\partial n_{ex}}{\partial t}$	$(\varepsilon_t \rho_g + \rho_b n_{ex}) \frac{\partial H_g}{\partial t} + \rho_b \frac{\partial H_s}{\partial t}$  $= ((\varepsilon_t \rho_g + \rho_b n_{ex}) C p_g + \rho_b C p_s) \frac{\partial T}{\partial t}$

Table 4 is presented to verify that the Heat Transfer Module equations correspond well with Equation 4.45. As the module does not take the adsorbed hydrogen into account this is implemented into the Heat Source term to complete the energy balance with adsorption predicted by the Langmuir model.

### 4.3.2. Mass Transfer module

Darcy's law is the most basic form of describing a fluid flow through a porous media and is widely used due to its simplicity. The Brinkman Equations are an expanded version of Darcy's law and has proven to give less divergence and boundary condition problems[15]. Both modules are briefly presented before one is chosen for further simulations.

#### Darcy's law

The Darcy's law module operates with the equation with  $p$  as the dependent variable:

$$\frac{\partial}{\partial t}(\rho_g \varepsilon_t) + \nabla \cdot (\mathbf{u} \rho_g) = Q_m \quad (4.57)$$

where

$$\mathbf{u} = -\frac{\kappa}{\mu} \nabla p \quad (4.58)$$

The mass source term,  $Q_m$ , like the heat source term, is zero if not specified differently. This is where the adsorption of mass from the transient mass balance (4.16) will be implemented. The heat source term will then give the content of adsorbed hydrogen predicted by the Langmuir model at any time. The model equations are compared in with Equation 4.16 in Table 5 below.

**Table 5: Comparison of COMSOL equations and Equation 3.5**

	Convective flow	mass	Gas in the tank	Mass source
COMSOL	$\nabla \cdot (\mathbf{u} \rho_g)$		$\frac{\partial}{\partial t}(\rho_g \varepsilon_t)$	$Q_m$
[2]	$\vec{\nabla} \cdot (\vec{U} \rho_g)$		$\varepsilon_t \frac{\partial \rho_g}{\partial t}$	$\rho_b \frac{\partial n_{ex}}{\partial t}$

#### Brinkman Equations

The Brinkman Equation module operates with pressure,  $p$ , and velocity,  $\mathbf{u}$ , as dependent variables:

$$\frac{\rho_g}{\varepsilon_p} \frac{\partial \vec{u}}{\partial t} = \nabla \left[ -p 2 \vec{I} + \frac{\mu}{\varepsilon_p} (\nabla \vec{u} + (\nabla \vec{u})^T) - \frac{2\mu}{3\varepsilon_p} (\nabla \cdot \vec{u}) \vec{I} \right] - \left( \frac{\mu}{\kappa} + \beta_F |\vec{u}| + Q_b \vec{u} + \vec{F} \right) \quad (4.59)$$

Where the variables listed below are selected separately if needed

- $\vec{F}$ : Gravity/ other forces
- $F_F = \beta_F |\vec{u}| \vec{u}$  : The Forchheimer drag
- $Q_b$ : Mass Source
- $\vec{F}$ : Volume force

Hence, The Brinkman equation for this study will be:

$$\frac{\rho}{\varepsilon_p} \frac{\partial \vec{u}}{\partial t} = \nabla \left[ -p 2 \vec{I} + \frac{\mu}{\varepsilon_p} (\nabla \vec{u} + (\nabla \vec{u})^T) - \frac{2\mu}{3\varepsilon_p} (\nabla \cdot \vec{u}) \vec{I} \right] - \left( \frac{\mu}{\kappa} + Q_b \vec{u} \right) \quad (4.60)$$

Where the mass source term will be set to:  $Q_b = \rho_b \frac{\partial n_{ex}}{\partial t}$

### **Determining Mass Transfer module**

Darcy's model was tested first as this is the simplest model as well as the most commonly used. An inlet and outlet was imposed and simulations run. As Darcy's model does not take the compressibility of hydrogen into account, a Storage model was added. However, Darcy's law proved to be a poor choice of module when having an outflow in the model. When imposing Brinkman it was seen that the system was more stable and after recommendations from COMSOL Support it was decided that Brinkman Equations would be a better suited model to use for this study.

### **4.3.3. Model inputs**

The simulations will be run using absolute pressure to prevent numerical problems in the solver. The total pressure is  $P_{absolute} = p_{ref} + p$ , where  $p_{ref}$  is set to  $10^5$  Pa throughout the study. COMSOL uses  $p$  (the gauge pressure) as a variable in the pressure calculations and this will be the operating point for the pressure in the model. Hence,  $p$  is the pressure that is set as initial values for the domain and boundary conditions at the inlet and outlet so to get the actual value  $p$  needs to be added up with  $10^5$  Pa. This pressure setting will also be used in the Heat Transfer module.

The Langmuir model needs to be implemented into the two chosen modules. Equations 4.1-4.4 with its respective parameters are added to Global parameters and Global variables before implemented as customized equations in the two modules ( $Q$  and  $Q_b$ ). These terms will be activated by turn for analytical purposes as it facilitates the detection of possible errors in the model and enhances the understanding of how COMSOL 4.2.a operates.

The pressure settings used throughout the model needs to be taken into account in the Langmuir equations when implemented. The parameters used for the Langmuir equations are equal to those used in [2] and can be found in the appendix.

## 5. Results and discussion

---

As mentioned in the previous section, the model will be built and analyzed step by step. First, a simple system with thermal insulation imposed on the vertical boundaries will be analyzed to see how the temperature, velocity and pressure changes with time in the tank without external disturbances. Secondly, the heat source will be implemented to see how much heat is released as the gas is adsorbed (however the actual adsorption will not commence before the mass source is turned on), and finally a mass source will be implemented to see how much hydrogen is adsorbed and thus completing the model.

Several cut planes are imposed for the ability to see how the temperature varies with time at the inlet, outlet and a cross the domain. Figure 14 shows the four cut planes used throughout this study to extract the results required.

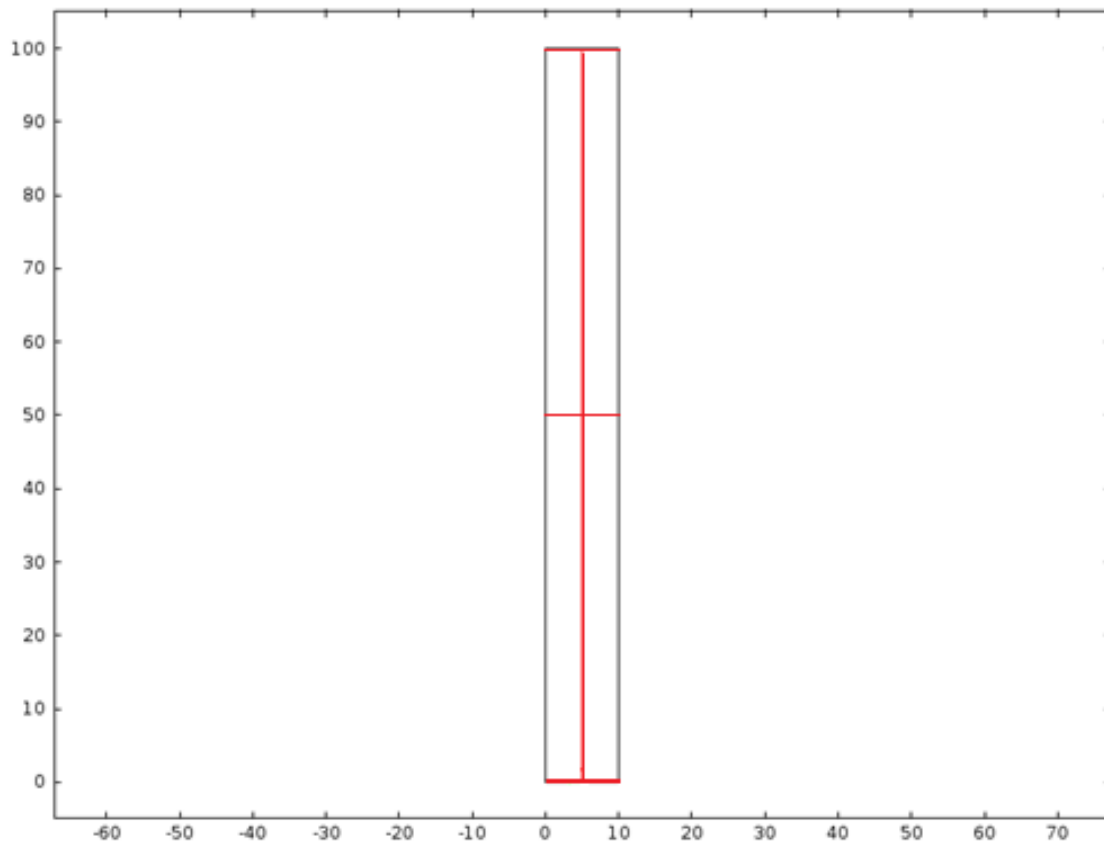


Figure 14: Cut planes

## 5.1. Simple model - Defined Inlet and outlet

The evaluation of the system will be divided into temperature, density, velocity and pressure analyzes to better compare the results for each step toward a complete model. For the Simple model an outlet velocity is defined in the brinkman module. The additional heat losses due to mass transport are to be taken into account by defining an Outlet in the heat transfer module.

It is of interest to see what boundary conditions and time ranges are required to cool down the entire domain to 80 K. When this information is obtained, the energy required to cool the entire domain can be calculated as a step towards finding the complete heat balance:

$$Q_3 = Q_2 - Q_1 - Q_{gas} \quad (5.1)$$

Where  $Q_3$  is the heat released due to adsorption and will be calculated when the system is completed,  $Q_2$  is the heat released due to adsorption and cooling of the domain and will be calculated as the heat source is enabled and  $Q_1$  is the energy required to cool the domain for the Simple model without adsorption and will be calculated in the present section.  $Q_{gas}$  is the energy required to cool the stored gas in the additional void space in the MOF and will be found in the section for the completed model.

**Table 6: Initial and boundary conditions for the Simple system**

Initial Conditions		Boundary Conditions		
T[K]	P[Pa]	$T_{0in}$ [K]	$p_{0in}$ [Pa]	$u_{out}$ [m/s]
120	1	80	$6 \times 10^4$	0.045

The initial and boundary conditions imposed in the first simulation are listed in Table 6. In addition, smaller outlet velocities (0.0025 m/s) and larger inlet pressures ( $7 \times 10^4$  Pa) as well as smaller time-ranges were implemented for comparison. The results will be commented on, however not presented in its full.

### Temperature

The temperature in the domain should reach 80 K at a given time. In finding this time-range, a Line Average and Line Integration were imposed on the outlet boundary to calculate the average outlet temperature at each time step. The Line Integration gives the temperature times length, while the Line Average gives solely the temperature; they were both calculated for comparison in accuracy. It was seen that the results were consistent, so for simplicity only the Line Average will be presented here and used further in this study. The Line Average plot of the outlet temperature is seen in Figure 15 on the next page.

It was found that the outlet temperature reaches 80.01 K after 288 seconds; however it does not reach 80.00 K before  $t = 574$  seconds. In addition, it was found that for the present

settings, the time-dependent solver in COMSOL will not be able to converge for a time range smaller than (0, 1, 800) due to numerical reasons.

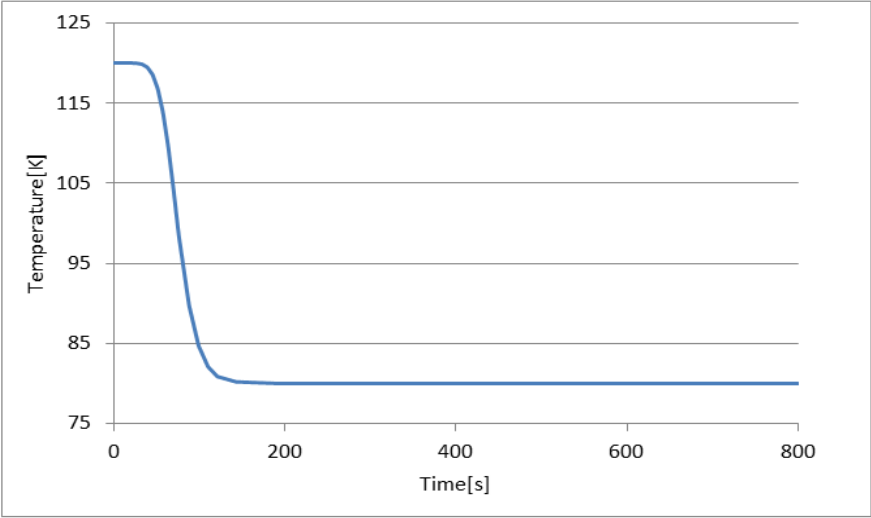


Figure 15: Average outlet temperature for the Simple Model

When imposing an outlet velocity with  $u=0.0025$  m/s it was seen, as expected, that the domain would not cool properly for the same time-range as the whole process slows down. However the tendencies were the same. Imposing an inlet pressure of  $7 \times 10^4$  Pa proved not to affect the cooling process.

**Density**

The density is inversely proportional to the temperature,  $\rho \sim \frac{1}{T}$ , and is expected to increase with the same factor as the temperature decreases. The temperature is decreased by 33 % as the domain cools from 120 K to 80 K and the density increases from  $0.323 \text{ kg/m}^3$  to  $0.484 \text{ kg/m}^3$ , this constitutes 33 %, showing that the temperature dependence of the thermodynamic properties should be correctly accounted for in the model.

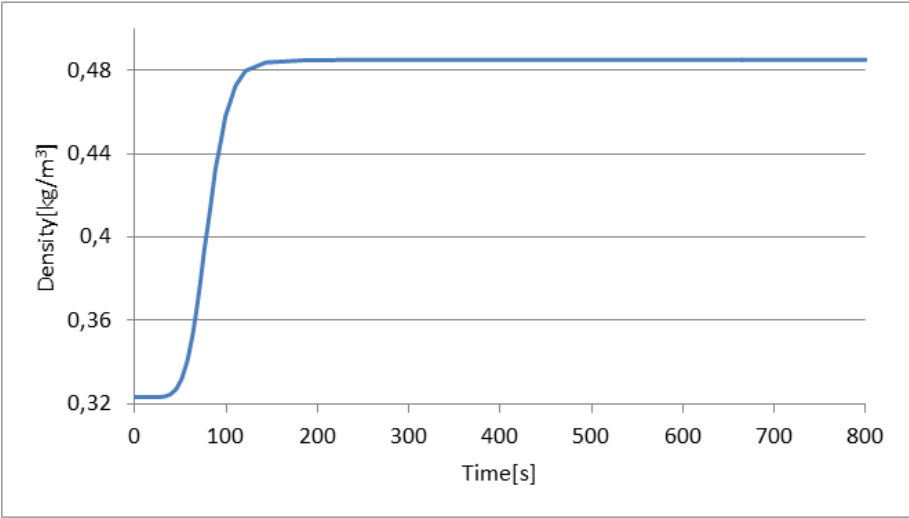
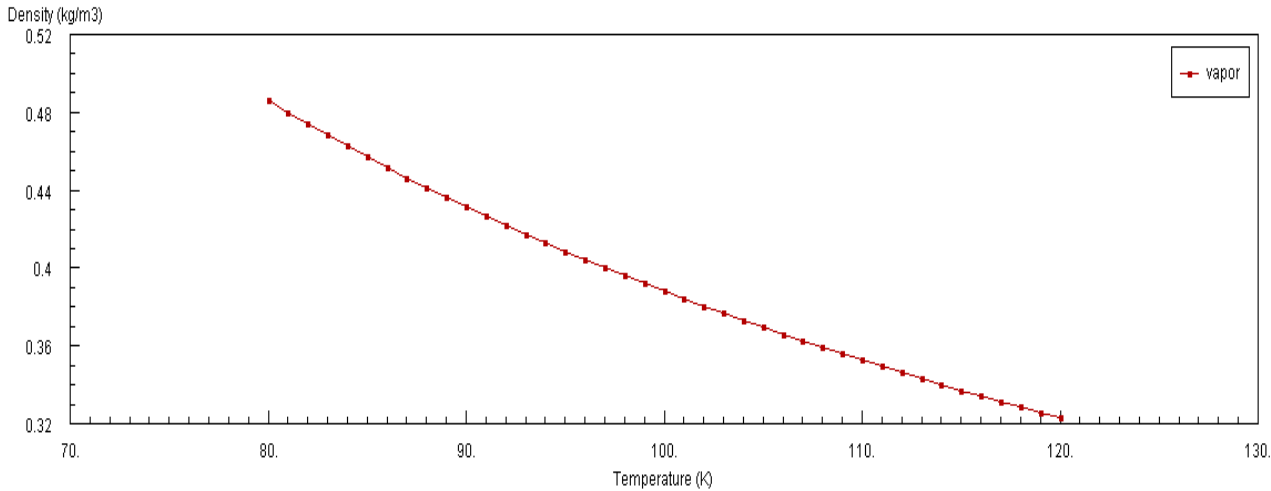


Figure 16: Density profile for the Simple Model

In addition, the density values were compared to the ones given by NIST web book[16] for a constant pressure of 1.6 bar in the temperature range 80 K to 120 K. As seen from Figure 17 and Table 7 below, the values fit well with the ones predicted by COMSOL for the Simple Model.

**Table 7: Density at different temperatures at p=1.6 bar**

Temperature[K]	Density[kg/m <sup>3</sup> ][16]	Density[kg/m <sup>3</sup> ] Simple Model
80	0.4860	0.484
100	0.3881	0.3867
120	0.3231	0.3233



**Figure 17: Density at different temperatures at p=1.6 bar [16]**



## Pressure

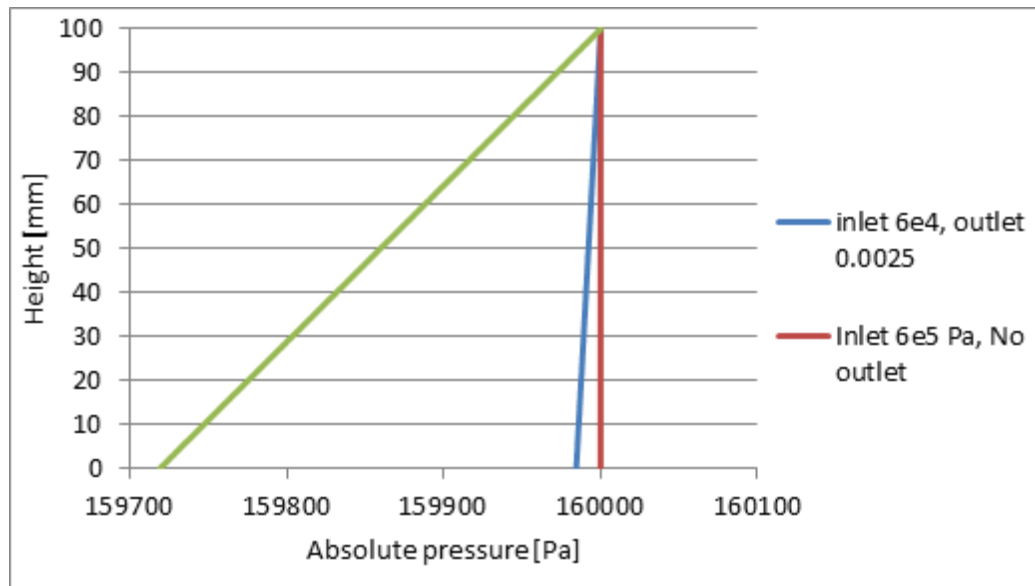


Figure 18: Pressure change at different outlet conditions at t=800

Figure 18 shows the pressure through the domain over the whole time range. To compare the effect of the outlet velocity on the pressure change, a smaller velocity of 0.0025 m/s as well as  $u=0$  m/s was imposed as outlet conditions. As seen from the figure above the outlet velocity will have a great effect on the pressure change in the domain. For the outlet condition  $u=0.0025$  m/s the pressure drop is

$$\begin{aligned}\Delta p &= 1.6 * 10^5 [Pa] - 1.59984 * 10^5 [Pa] \\ &= 15.4717 \text{ Pa (0.0097\%)}\end{aligned}$$

While a pressure drop for  $u=0.045$  m/s is

$$\begin{aligned}\Delta p &= 1.6 * 10^5 [Pa] - 1.5972 * 10^5 [Pa] \\ &= 280 [Pa]\end{aligned}$$

Which is 0.175% of the inlet pressure; hence the pressure drop increases a little more than 16 % when doubling the outlet velocity.

## Velocity

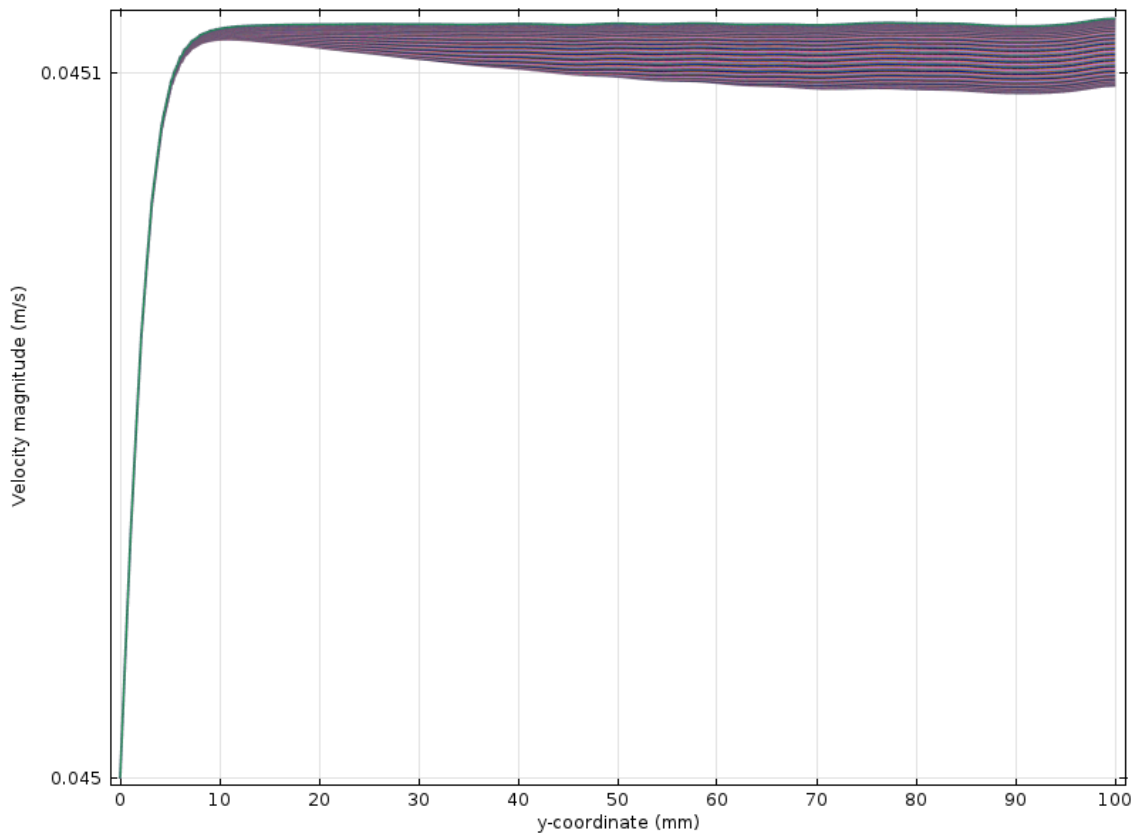


**Figure 19: Velocity plot over the length of the domain, t=1-800 seconds**

The figure above shows the velocity profile over the domain. It is seen that it is almost constant only increasing slightly at the inlet over time. However, as for the pressure the velocity changes are negligible. This result is unexpected as there is no adsorption and hence, inlet mass flow rate should be equal to outlet mass flow rate. As the area, inlet density and outlet velocity is fixed, while the outlet density varies, the inlet velocity should vary proportionally with the outlet density.

The mass flow rate is: 
$$\dot{m} = \rho u A \quad (5.2)$$

From conservation of mass: 
$$\rho_1 u_1 A_1 = \rho_2 u_2 A_2 \quad (5.3)$$

For present initial and boundary conditions: 
$$\rho_1 u_1(t) A_1 = \rho_2(t) u_2 A_2 \quad (5.4)$$

where subscript 1 and 2 describes the inlet and outlet, respectively.

As the outlet density increases by 33 %, the inlet velocity should increase by 33 %. The expected starting value would be 0,030m/s. An increase proportional to the density should

be seen until the outlet temperature reaches 80 K for which equilibrium is reached and the temperature, density and velocity is constant.

However, as seen from the figure below, this is not found from the simulation. The inlet mass flow rate is constant due to the negligible velocity changes, and thus mass is not conserved.

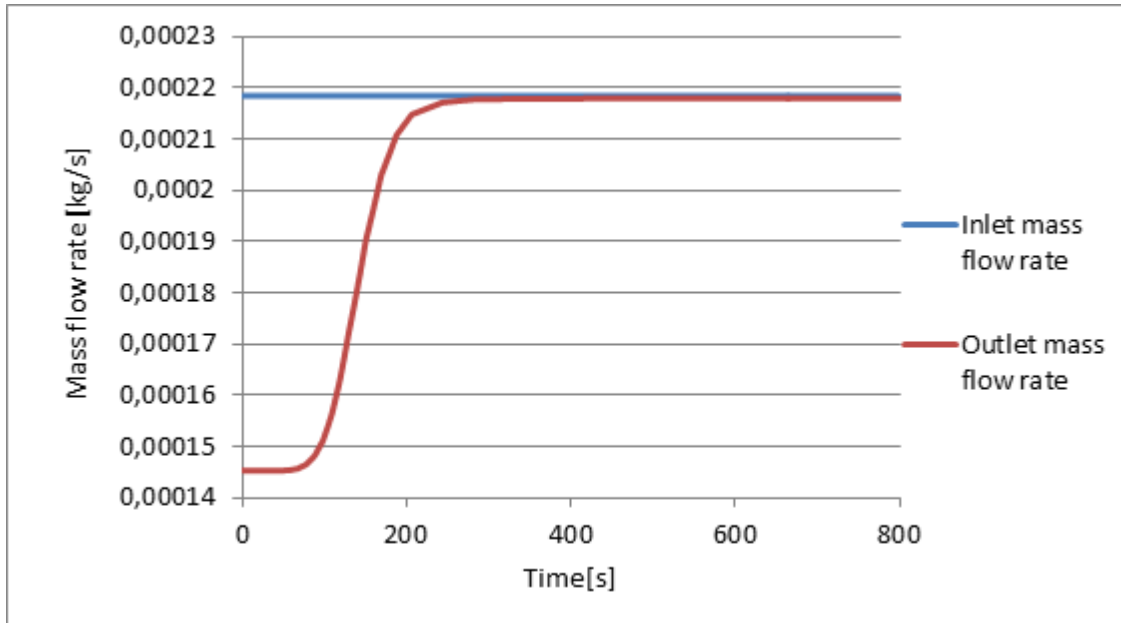


Figure 20: Inlet and outlet mass flow rate

The ideal plot of the inlet and outlet mass flow rate would give two lines close together meeting at the top when the bed is saturated. The only gap in between representing the stored hydrogen which is negligible compared to the total gas feed. The great area between the curves is still to be explained. Several tries in investigating this behavior has been conducted, among them reversing the inlet and outlet conditions. Furthermore, it was suspected that the values for the velocity magnitude could have been erroneously retrieved from COMSOL, resulting in deceptive values. As mentioned earlier in this section, a Line Average has been imposed at the inlet to obtain the values for each time-step. To test this theory, several 2D Cut Points were inserted at the following coordinates: (1,100), (5,100), (9,100), (1,99), (5,99) and (9,99) respectively (coordinates represented as (x,y) - for clarity in geometry see Section 4.3). The velocities were seen to be consistent with the ones predicted from the Line average plots, and thus, the suggestion of erroneous data collection was discarded. Another reason for the velocities seen could be a result of rounding errors; however, this was not tested in the present work.

In addition, as gas is inserted continuously throughout the simulation, some of the gas will not have reached the outlet as the simulation is ended. The throughput time is 2.22 seconds. Estimating the enclosed mass using the density for 100 K, this constitutes 0.0004 kg.

However, the mass not reaching the outlet is 0.011kg, and hence, cannot be explained by the throughput time of the gas.

Ideally, the energy required to reach equilibrium would be calculated from the equations:

$$Q_1 = \left[ \int_0^{800} \rho u A C_p T dt \right]_{out} - [\rho u A C_p T t]_{in} + \Delta Q_{stored} \quad (5.5)$$

Where

$$\Delta Q_{stored} = [\rho C_p V T]_{in} - [\rho C_p V T]_{out} \quad (5.6)$$

However, as the velocity does not change as expected, Equation 5.5 will not provide with the correct answer. Due to this, an approximation was done by calculating the energy based on the outlet mass flow rate of the system and the gas stored.

$$Q_1 = \sum_{t=0}^{800} \left( \dot{m}_{H_2out} C_p (T(t) - 80) \right) + \Delta Q_{stored} \quad (5.7)$$

where

$$\Delta Q_{stored} = [\rho C_p T V]_{out} - [\rho C_p T V]_{in} \quad (5.8)$$

$$\Delta Q_{stored} = 0.3342 \text{ J}$$

$$Q_1 = \underline{9704 \text{ J}}$$

To validate the value obtained from the equation above, the energy required to cool the MOF is calculated. This value should be the same as the energy calculated above:

$$Q_1 = m_{MOF} C_p (120 - T(t)) \quad (5.9)$$

$$m_{MOF} = \rho_{bed} V_{bed} \quad (5.10)$$

$$m_{MOF} = 640.38 [\text{kg/m}^3] * 0.001 [\text{m}^3] = 0.6404 \text{ kg}$$

$$\begin{aligned} Q_1 &= 0.6404 [\text{kg}] * 420 \left[ \frac{\text{J}}{\text{kgK}} \right] * (120 - T(t)) [\text{K}] \\ &= \underline{9728 \text{ J}} \end{aligned}$$

This is 0.24% higher than what was estimated for in Equation 5.7, and is a satisfying result. However, at present; it has not succeeded to overcome the problems encountered. Never the less, as the solver converges and provides with results amenable for evaluation, it has been decided to continue the modeling process towards a complete model. Thus, the present analysis will be conducted as assigned for in the thesis, and results found to be deviating will be analyzed. This is believed to have great value for further work in developing a transient model for numerical simulations.

## 5.2. Implementing Heat Source

In the previous section it was proved that the thermodynamic properties depending on temperature and pressure in the model are only partly accounted for. Never the less, the heat required to cool the tank was estimated and the system analyzed. In this section the model will be developed further by enabling the heat source term. The system will be investigated and the energy released due to adsorption will be calculated.

### Case 1

The same initial and boundary conditions imposed for the Simple Model will be used in Case 1, these are listed in the table below.

**Table 8: Boundary and initial conditions for Case 1**

Initial Conditions		Boundary Conditions		
T [K]	P[Pa]	T <sub>0in</sub> [K]	p <sub>0in</sub> [Pa]	u <sub>out</sub> [m/s]
120	1	80	6×10 <sup>4</sup>	0.045

### Temperature

As the Heat Source is turned on, the tank is heated from an initial temperature of 120K to 123.54K due to the heat released during adsorption. The cooling process will take longer as the temperature difference is larger, so the time-range of the simulations is increased to 1300 seconds. Figure 21 shows the average outlet temperature with and without the heat source for the same boundary conditions. At t=1300 the temperature has reached 80.37 K and thus, equilibrium has not been reached. Due to this, the time range should be increased and the simulations should be run for longer. However, when looking at the 2D model in Figure 22 a small region with a dip in temperature is detected. This should not be possible for the implied boundary an initial conditions as there is no temperature defined smaller than 80 K. Due to this unexpected behavior the heat source was disabled once again and a simulation run for the same initial and boundary conditions over the same time range (1300 seconds) to see if an instability could be detected in the temperature profile here as well.

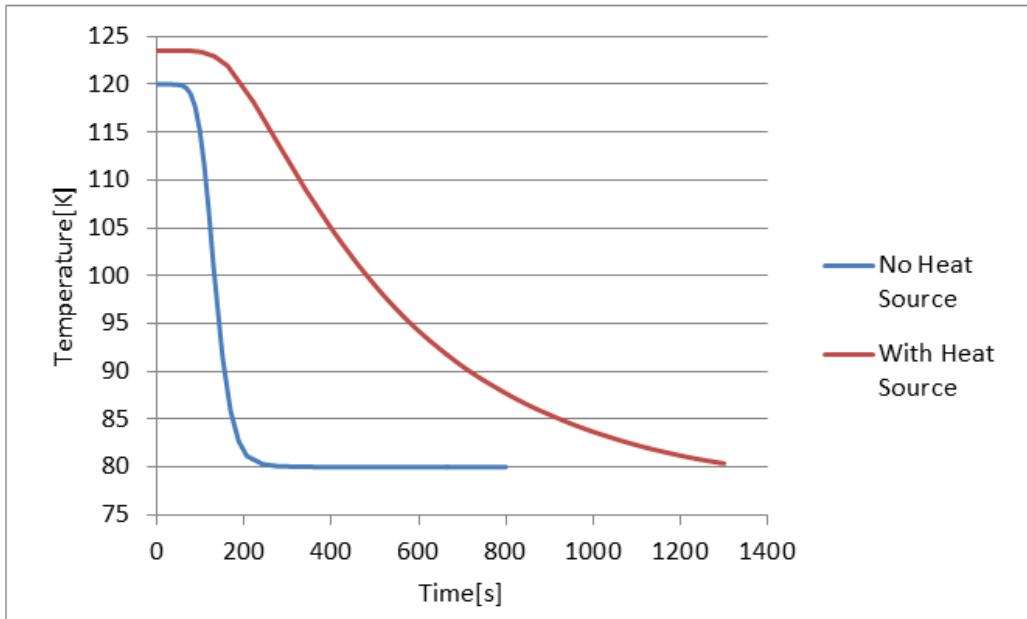


Figure 21: Average outlet temperature, red line: with mass source, blue line: Simple Model

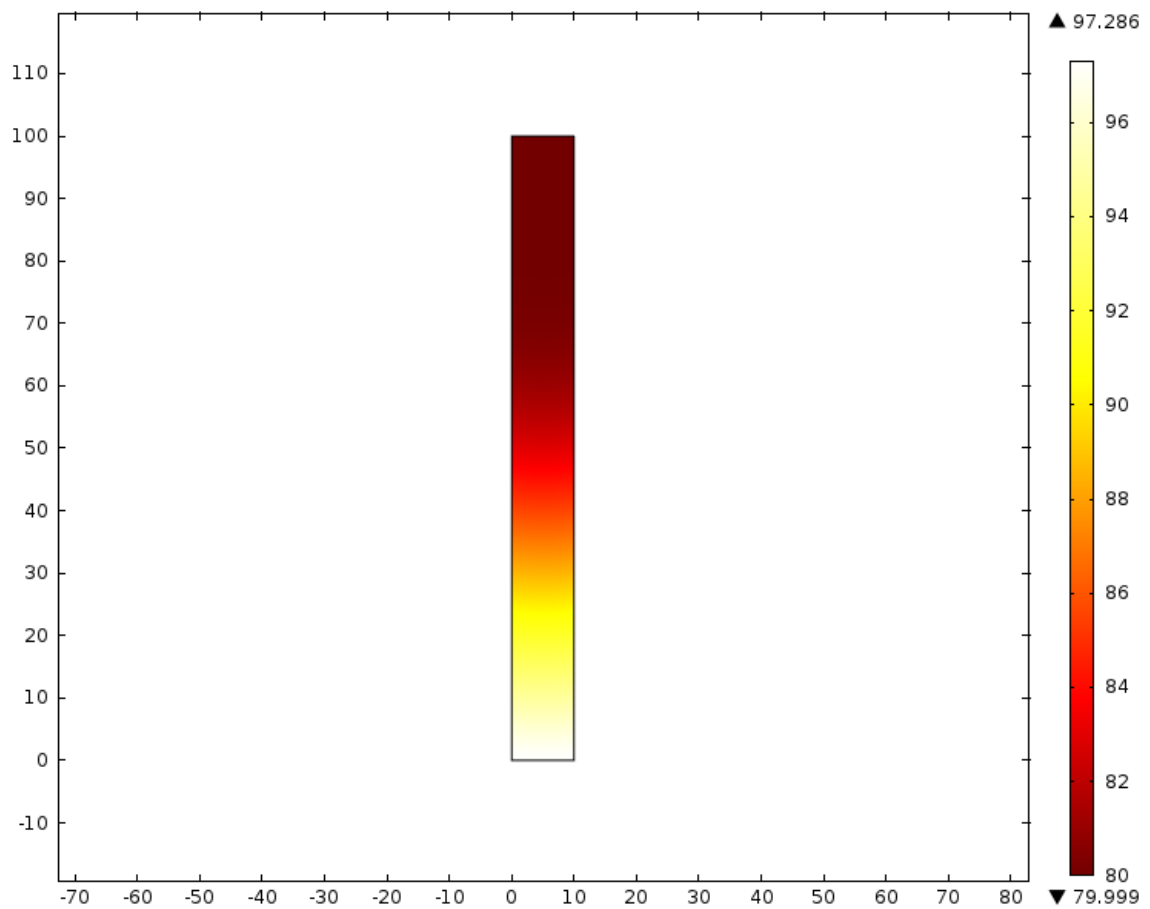
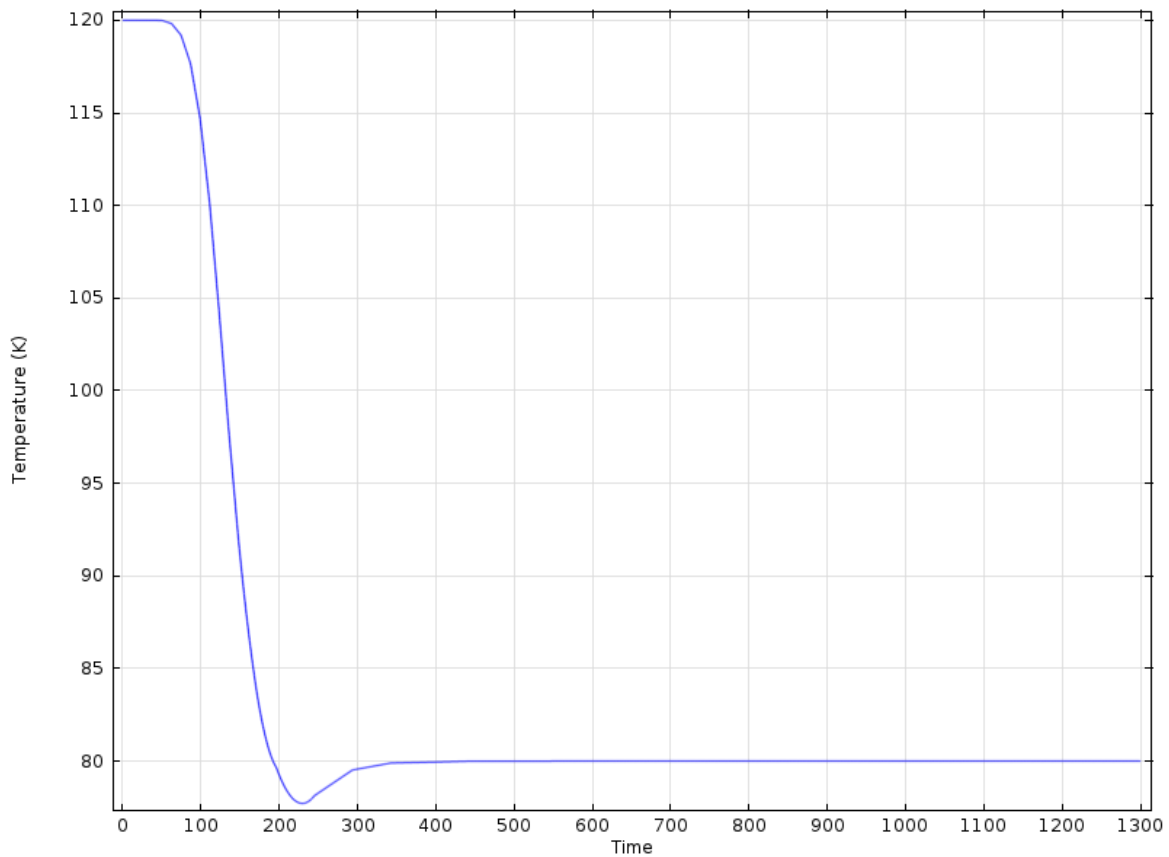


Figure 22: 2D temperature plot of the temperature profile at t=1300 seconds



**Figure 23: Average outlet temperature with disabled heat source**

From Figure 23, a peculiarity at the temperature profile can be seen at  $t=200$  seconds where the temperature continues to decrease from 80K. This was not detected previously as the simulations were run for a smaller time-range in Section 5.1. The figure shows the average outlet temperature when the heat source is disabled. It behaves unexpectedly by decreasing below 80 K over a small time range before increasing back up again and stabilizing at  $T=80$  K.

Before calculating the heat released due to adsorption, an analysis of the unexpected behavior of the temperatures needs to be carried out. Also, a large jump was seen in the pressure and velocity plots at  $t=0$  due to the large gap from inlet pressure to the initial pressure. When implementing the mass source term the solver will not be able to converge for a large pressure drop in the beginning and hence, new boundary conditions for the inlet pressure will be implemented as a Case 2 after the temperature deviations are investigated.

### *Investigating temperature deviations*

The unexpected temperature behavior can occur for several reasons. If to be explained thermodynamically it can be the result of a sharp reduction in temperature in the domain leading to adsorption of gas. Adsorption is an exothermic process and hence, heat will be released. As the domain is heated desorption might occur, and as this is an endothermic process the domain will be cooled. However, the explanation to the temperature dip is believed to be unphysical as the most likely explanation can be found in the numerical solver

due to the decrease in temperature around 200 seconds seen for the simple model where there is no adsorption.

The negative overshoot is most likely a result of the fact that the numerical accuracy in the time dependent solver for the given settings is not able to follow the sharp temperature gradient that is seen at around 90 seconds (See Figure 23). This accuracy generally depends on relative and absolute tolerance as well as the time integration method (the time-step method) used. In COMSOL, BDF is the standard integration method with several parameters that can be adjusted. The BDF solver uses backward differentiation formulas with order of accuracy varying from one to five. The methods are known for being stable; however, at lower order methods they can have severe damping effects, as the Backward Euler damps any high frequencies. This might result in a very smooth solution even when sharp gradients are expected.

The main objective is that the local tolerance is controlled. The local tolerance is affected by

- the total simulation length ( affects how small time-steps the time integration starts with and how fast it tries to increase based on estimated local errors)
- density of the stored solution times (depending on the setting “Steps taken by solver” the solver will compute the values internally at certain points and then interpolate the values in between to provide the solutions to the fixed points.
- Range (start, time-step, end)
- Relative tolerance (determines the local accuracy of each calculated internal time step)

Thus, to avoid the overshoot, the value of the relative tolerance can be decreased and possibly, the parameters that ultimately affect the local accuracy can be adjusted (as listed above)

The first try in overcoming the problem was to decrease the relative tolerance. As seen from the figure below this proved to be an efficient way to reduce the temperature dip although not eliminating it completely.

Figure 24 gives the average outlet temperatures for the relative tolerances 0.01(standard), 0.001, 0.0001 and  $10^{-6}$ . From 0.01 to 0.001 a great improvement was obtained, however adjusting it further did not seem to be very effective. The simulations will take longer for smaller relative tolerances and as the difference from 0.0001 to  $10^{-6}$  is negligible, the tolerance will be set to 0.0001 throughout the study. In addition it was found that as the tolerance is decreased the mesh did not affect the overall results and thus will be set to Fine.



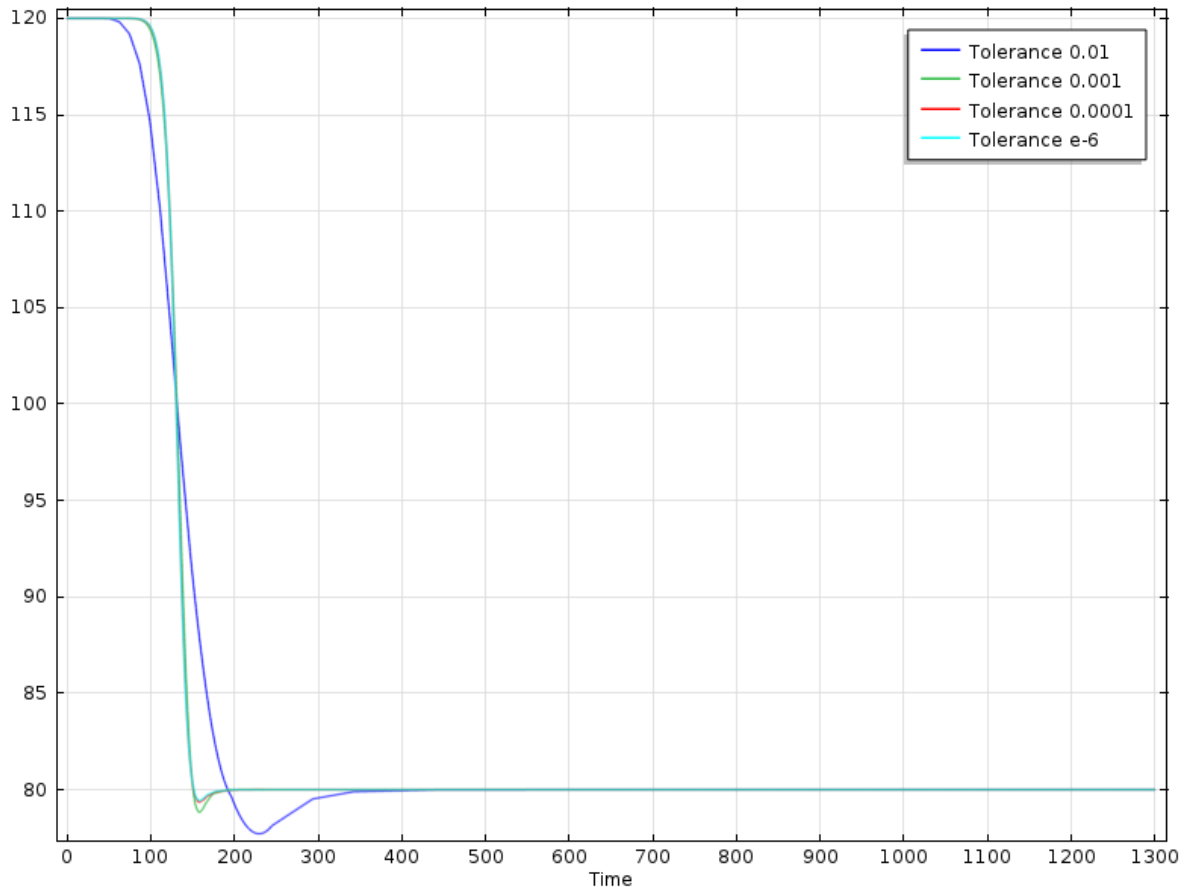


**Figure 24: Average outlet temperatures for different tolerances**

In addition, it is believed that the numerical problems encountered can have an effect on the velocity distribution. However, the tolerance adjustments did not affect the velocity. Thus, for now, the lack of conservation of mass remains unexplained.

As the fluctuations did not cease it was suspected that the implemented Langmuir equations could be a contributing factor to the instability in the system. The derived adsorption isotherm,  $\frac{\partial n_{ex}^*}{\partial t}$ , was implemented directly from Equation 4.24 into Global variables. The 2D temperature in Figure 25 shows the temperature profile in the domain at t=1300 seconds for Case 2 (see initial conditions in Table 9) with an enabled heat source. With the newly imposed tolerance of 0.0001 the entire domain is not properly cooled to 80K, however, small regions with temperatures below 80 K are detected. Due to this,  $\frac{\partial n_{ex}^*}{\partial t}$  was re-imposed, now by writing the commands for COMSOL derive the adsorption isotherm,  $n_{ex}^*$ , from Equation 4.23. This proved, as seen from Figure 26 to give a more stable temperature profile. There is no region with a temperature below 80 K seen from the 2D plot, and the domain is cooled better (note that the color scaling is numbered differently for the two figures). However, there might still be fluctuations in the outlet temperature although not showing from the 2D plots. Due to the improvement found, the isotherm derived by COMSOL will be used further in the study.

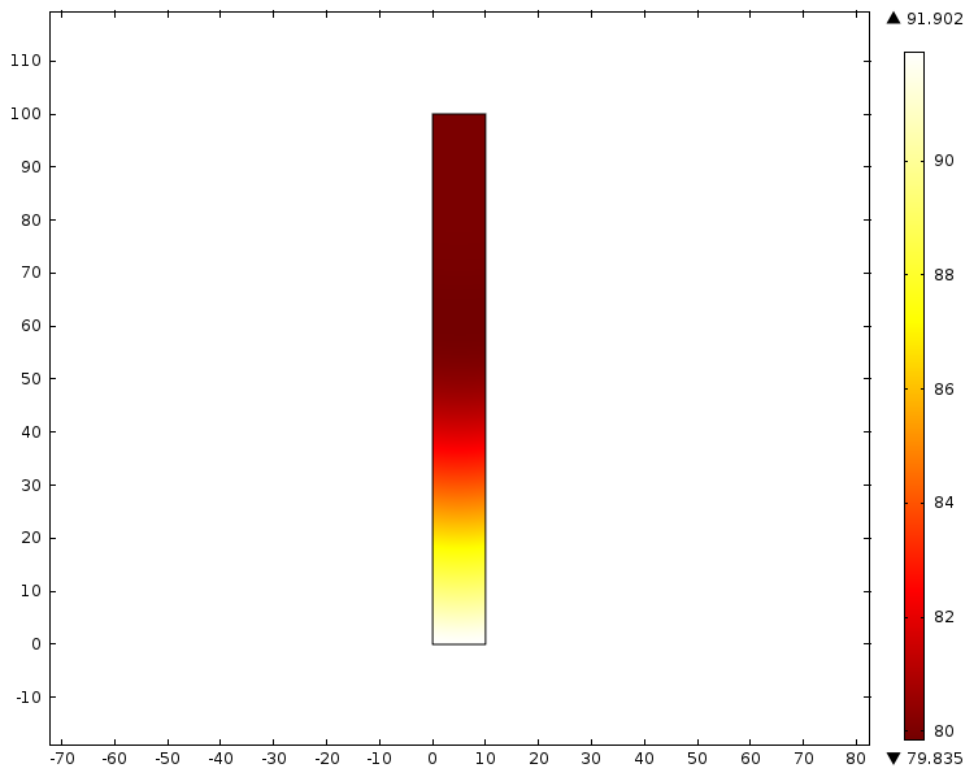


Figure 25: 2D temperature plot at t=1300 tolerance=0.0001

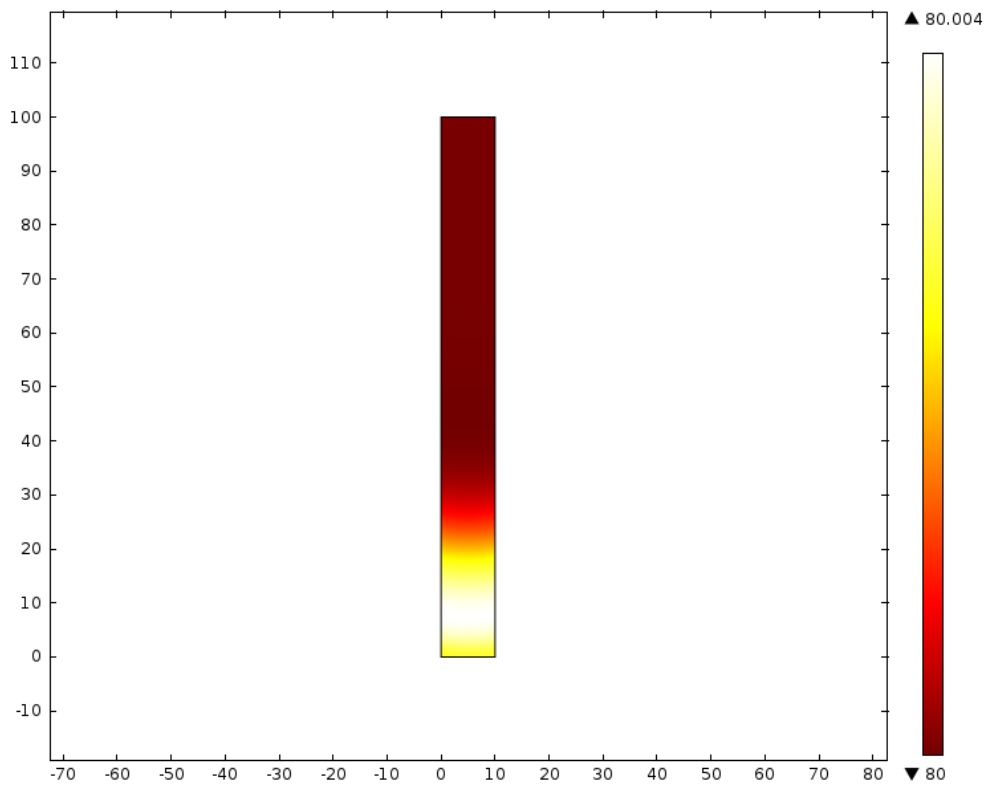


Figure 26: 2D temperature plot with new imposed  $d(nex)/dt$

## Case 2 – imposing equal inlet and domain pressure

To smooth out the great jump in pressure and velocity at  $t=0$ , a new boundary condition for the inlet pressure is imposed. The initial value is set equal to the boundary condition of 1.6 bar (which is the absolute pressure for the system when letting  $p=6 \times 10^4$  Pa). For the previous initial condition, the feed gas would flow directly into the domain as the simulations were initiated. For the case where inlet and domain pressures are consistent, the flow pattern will be somewhat different. Now, the mass flow will commence by flowing out of the domain. This creates a pressure change allowing for further feed in to the domain. However, this will happen over a very small time range. The simulations will be run for 1600 seconds to assure that the domain reaches a state of equilibrium.

**Table 9: Initial and boundary conditions imposed in Case 2**

Initial Conditions		Boundary Conditions		
T [K]	P [Pa]	$T_{0in}$ [K]	$p_{0in}$ [Pa]	$u_{out}$ [m/s]
120	$6 \times 10^4$	80	$6 \times 10^4$	0.045

### Temperature

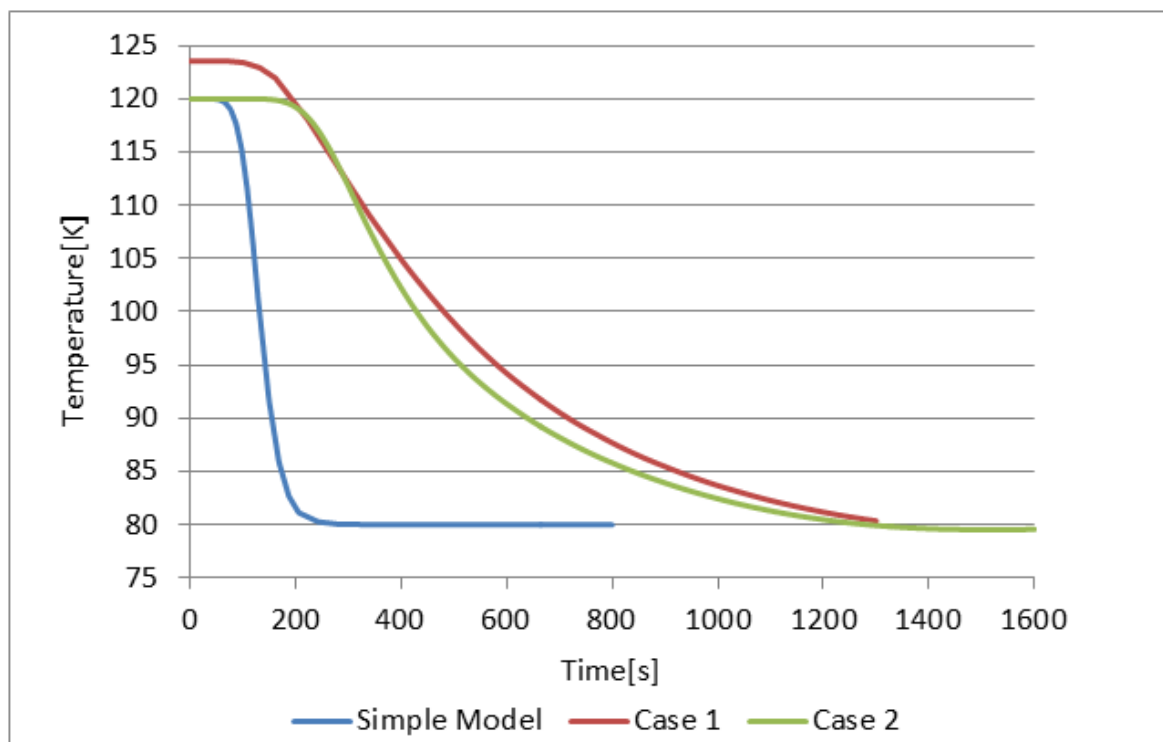


**Figure 27: Average outlet temperature for Simple Model, Case 1 and Case 2**

Figure 27 gives the average outlet temperatures for the Simple Model, Case 1 and Case 2. It is seen that as the initial and inlet pressures are set to be equal, the released heat due to adsorption will not heat the domain as before. However, as the cooling of the domain is clearly taking longer for Case 2 than for the Simple Model the heat source should be active. Furthermore, as the hydrogen gas start to cool down the domain, a steeper gradient is seen

for Case 2 than Case 1, this is explained by the newly imposed heat source term which proved to cool the domain faster than the one imposed for Case 1(see Figures 25 and 26). Also, it is seen that the temperature dip still remains even though the tolerance is decreased, at t= 1600 seconds the outlet temperature is 79.6 K having increased from the turning point with 79.55K at t=1518.

Never the less, it has been decided that the simulations will be run with the present system as the objective of this study is to implement mass and energy balances into COMSOL. To explain the initial temperature difference between Case1 and Case2 the Heat Source term  $\rho_b \Delta H_a \frac{\partial q}{\partial t}$  was plotted over the time range of the simulation to confirm the belief that it is still active.

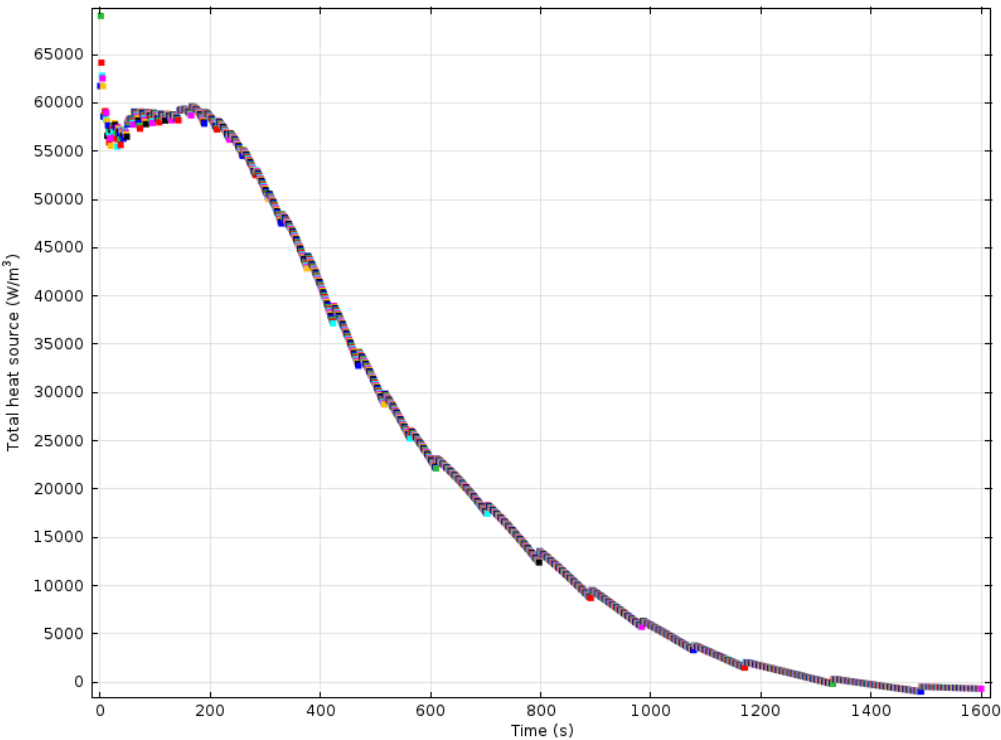


**Figure 28: Heat source term for Case 2**

Figure 28 shows the heat source plotted at the Cut Plane vertically cutting the domain (See Figure 15), it is seen to be active, so to understand the differences in the temperature profiles from Case 1 to Case 2, a plot of the heat source for Case 1 is added in Figure 29 below. The simulation is only run for 1000 seconds due to the fact that it is solely plotted to find the value at t=0, as well as making sure the evolution over time is similar for the two cases.

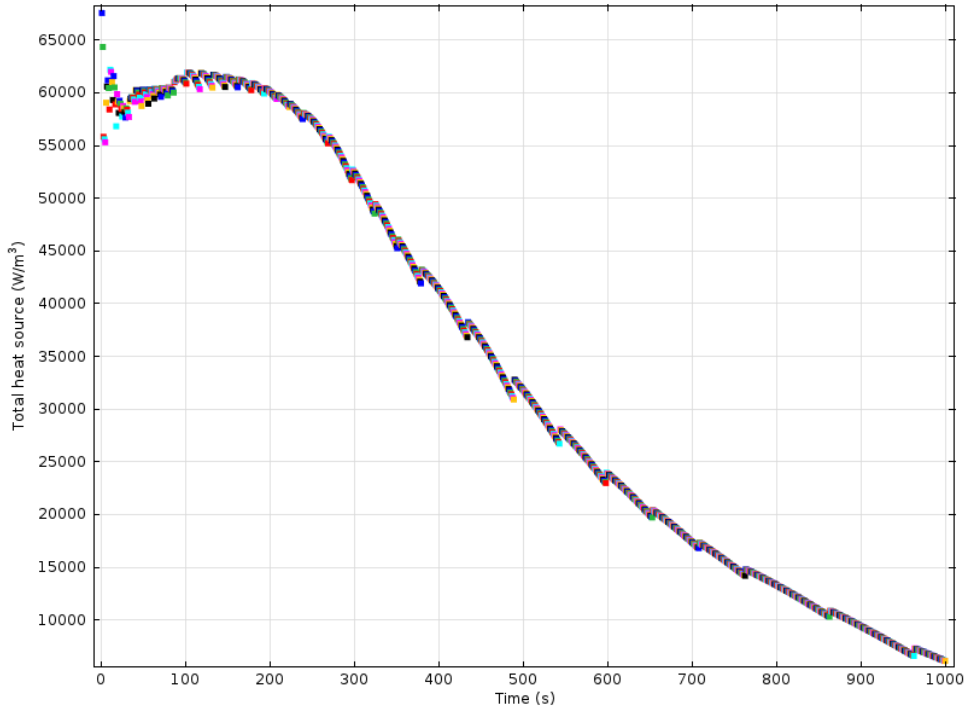


Figure 29: Heat source Case 1 for t=1 to 1000 seconds

It was seen that the great pressure jump at t=0 for Case1 results in a great jump in the heat source term with a value of  $4.5049 \times 10^8$  [W/m<sup>3</sup>]. Due to this the plot above is taken from t=1, to easier compare with the values from Case 2. When comparing Figures 28 and 29 it can be seen that the values are quite similar ranging from a value of 67565.5 [W/m<sup>3</sup>] to zero

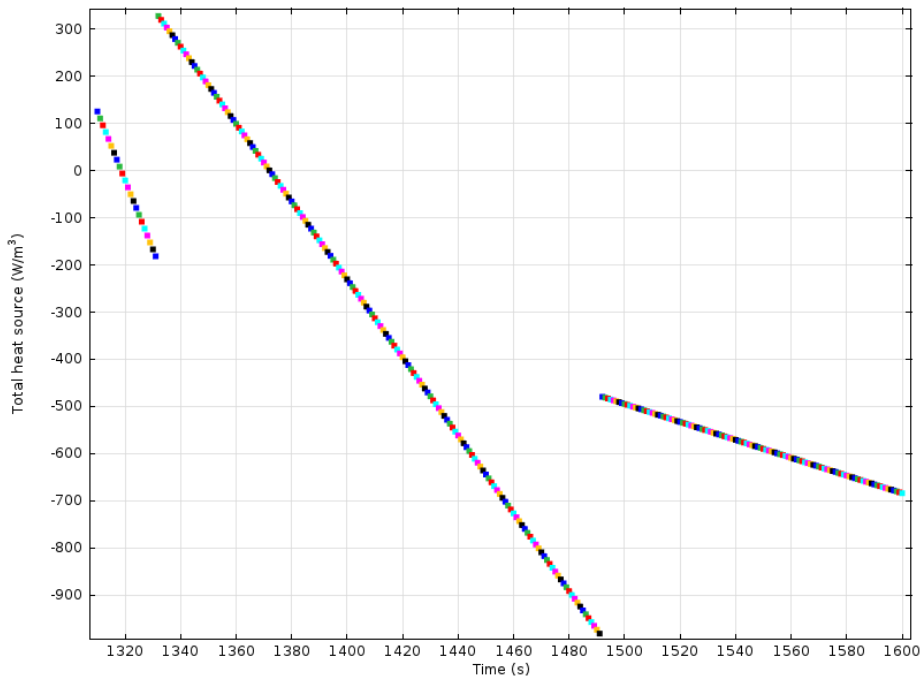
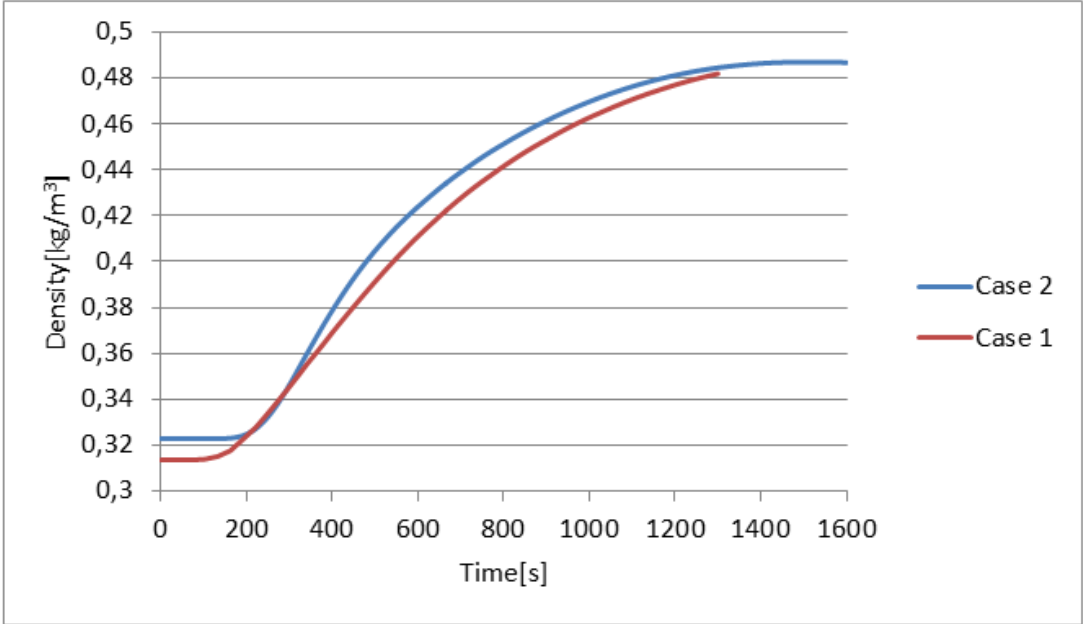


Figure 30: Heat source term Case2 for t=1320-1600 seconds

From Figure 30 it can be seen that at  $t=1320$  s, the heat source turns negative decreasing linearly to  $-110$   $[W/m^3]$ , then a jump to  $320$   $[W/m^3]$  is seen before it decreases linearly again to  $-1000$   $[W/m^3]$ , and for the last interval it is completely negative. From Figure 27 it was seen that at  $t=1320$  s, the temperature has decreased below from  $80K$  resulting in the negative heat source values.

**Density**



**Figure 31: Outlet density evolution for Case 1 and Case 2**

The density is plotted to confirm that it still is accounted correctly for with the newly imposed initial conditions. After 1200 seconds the temperature change is calculated to be 32.91 % which matches exactly with the density change and hence it can be concluded that the density function behaves as expected.

## Pressure and velocity

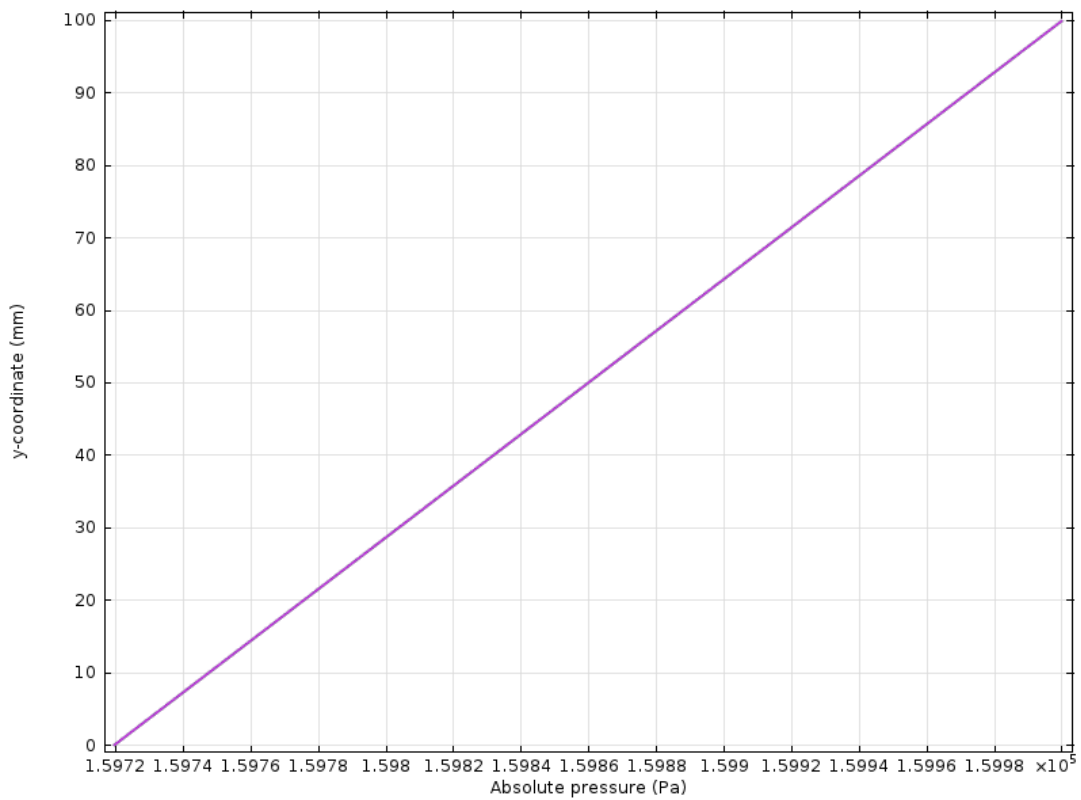


Figure 32: Pressure change over the domain at t=0-1600

Figure 32 gives the pressure drop over the length of the bed at all times where  $y=100$  mm is at the inlet. As expected the pressure drop does not change over time and is still 0.175 % as seen from the Simple Model.

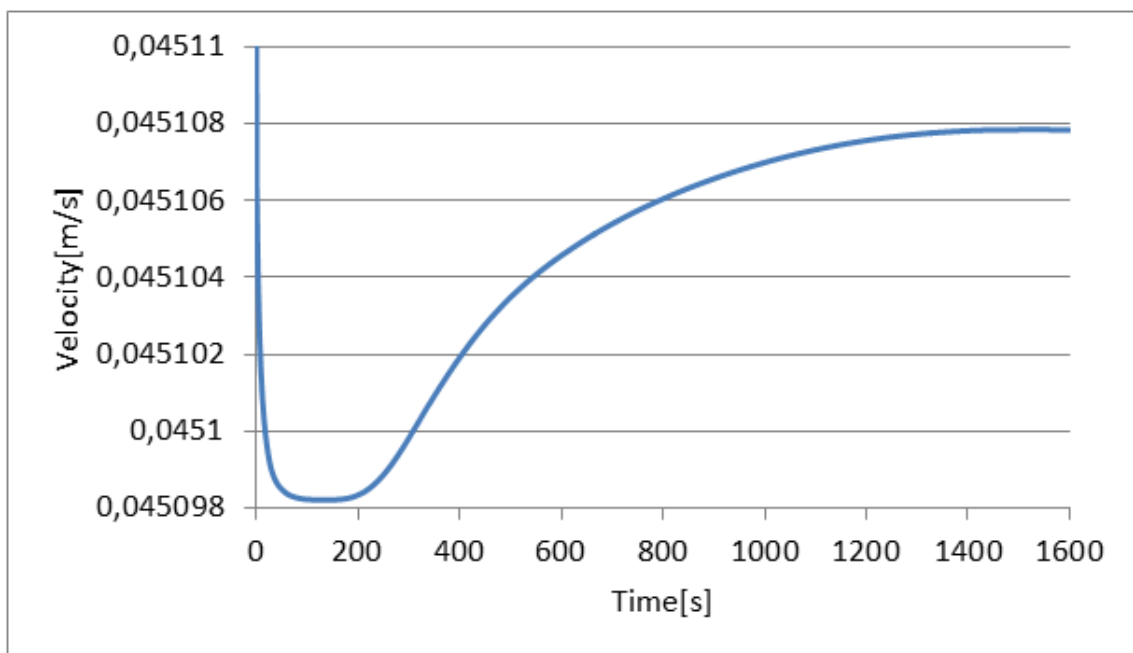


Figure 33: Velocity evolution over time for Case 2

The inlet velocity evolution over time is plotted in Figure 33. Noting the vertical axis values, the changes in velocity are negligible, as seen for the Simple system. This means that the problems encountered in the previous section withstands and are not affected by the adjustments in relative tolerance. However, when comparing the outlet mass flow rate from Figure 34 with the inlet velocity from Figure 33, it is clearly seen that they behave similarly. Thus, the inlet velocity trend seems to be correct, however, the magnitude of the change is insufficient for the inlet mass flow rate to match the outlet mass flow rate.

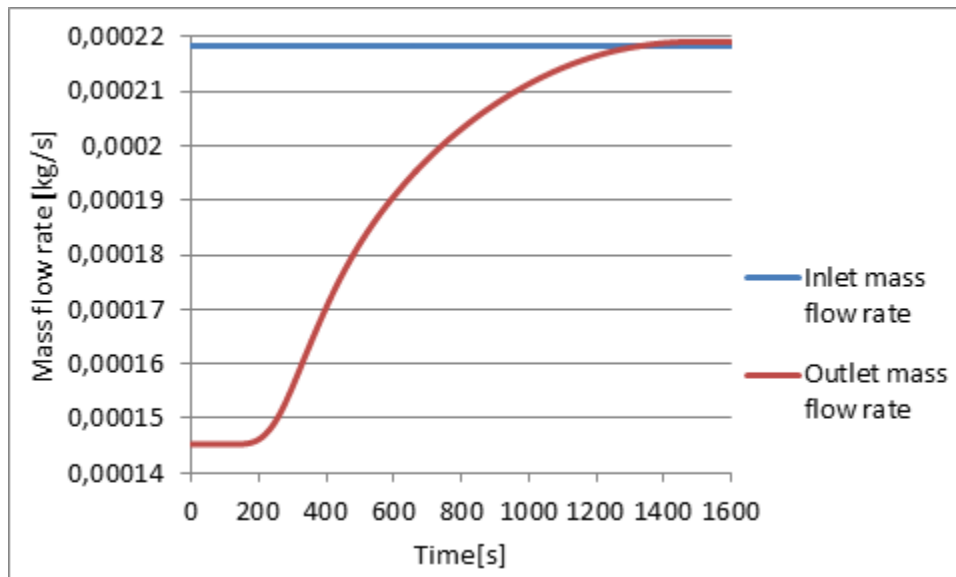


Figure 34: Inlet and outlet mass flow rates

The inlet and outlet mass flow rates are plotted in Figure 34. As there is no adsorption mass should be conserved, however, this seems not to be the case. The total inserted mass is 0.3456 kg while the mass going out is 0.3081. Hence, 11 % of the inserted mass “disappears”. It still remains to find the root of this problem. The system is to be completely analyzed as this might give results supporting or discarding the presumption that the problem lies within the numerical solver method used.

### **Released heat due to adsorption**

The heat of adsorption is the energy that is released when the gas molecules change from gas phase to adsorbed phase, typically in the range of 1 kJ/mol to 10 kJ/mol for hydrogen adsorption [5]

As for now, no mass is adsorbed, only heat released due to adsorption. Discarding the deviations found, the heat is estimated as in the previous section:

The energy required to heat the hydrogen gas from 80 K to 120 K is:



$$Q_2 = \sum_{t=0}^{1300} \dot{m}_{H_2out} Cp(T(t) - 80) + \Delta Q_{stored}$$

$$= 38306 \text{ [J]}$$

This suggests that the heat released due to adsorption should be in the range of

$$Q_3 = Q_2 - Q_1$$

$$= 38306 \text{ J} - 9704 \text{ J}$$

$$= 28602 \text{ J}$$

The data is obtained from the excel sheets exported from the COMSOL plots.

### 5.3. Implementing mass source

Until now the effects of heat transport due to cooling of the tank and adsorption of gas has been investigated. By calculating the energy required for these two processes it has been possible to estimate the heat released due to adsorption. However, for actually adsorbing mass the model needs a defined mass source. From the mass balance in Section 4.1 it is seen that total rate of change of hydrogen content of the element investigated is

$$\frac{\partial}{\partial t} (\rho_b n_{ex} + \varepsilon_t \rho_g)$$

Where total rate of adsorbed hydrogen in the element is

$$\frac{\partial n_{ex}}{\partial t} \rho_b$$

This is the last term to be implemented to complete the transient balances.

#### 5.3.1. System analysis

As mentioned in Section 5.2, to be able to run the simulations the domain pressure was set to 1.6 bar ( $p=6 \times 10^4 \text{ Pa}$ ), which is the same as the inlet pressure. This means that the same initial and boundary conditions imposed for Case 2 are used (given in Table 10). The simulations will be run over a time range of 1600 seconds. The temperature, density, pressure and velocity will be analyzed as in the previous section. To confirm that the evolutions over time are as expected before the adsorption process is analyzed.

**Table 10: Initial and boundary conditions for the Complete System**

Initial Conditions		Boundary Conditions		
T [K]	P [Pa]	$T_{0in}$ [K]	$p_{0in}$ [Pa]	$u_{out}$ [m/s]
120	$6 \times 10^4$	80	$6 \times 10^4$	0.045

## Temperature

Below, a 2D temperature plot of the system after 1600 seconds can be seen. Most of the domain is cooled to 80 K, however there is still a region where the temperature is lower than what would be expected. This means that instabilities are still present in the solver, never the less, as the deviations are small and the complete model will be analyzed as it is at the present conditions. The reasoning for this decision is given in Section 5.5 Modeling restrictions.

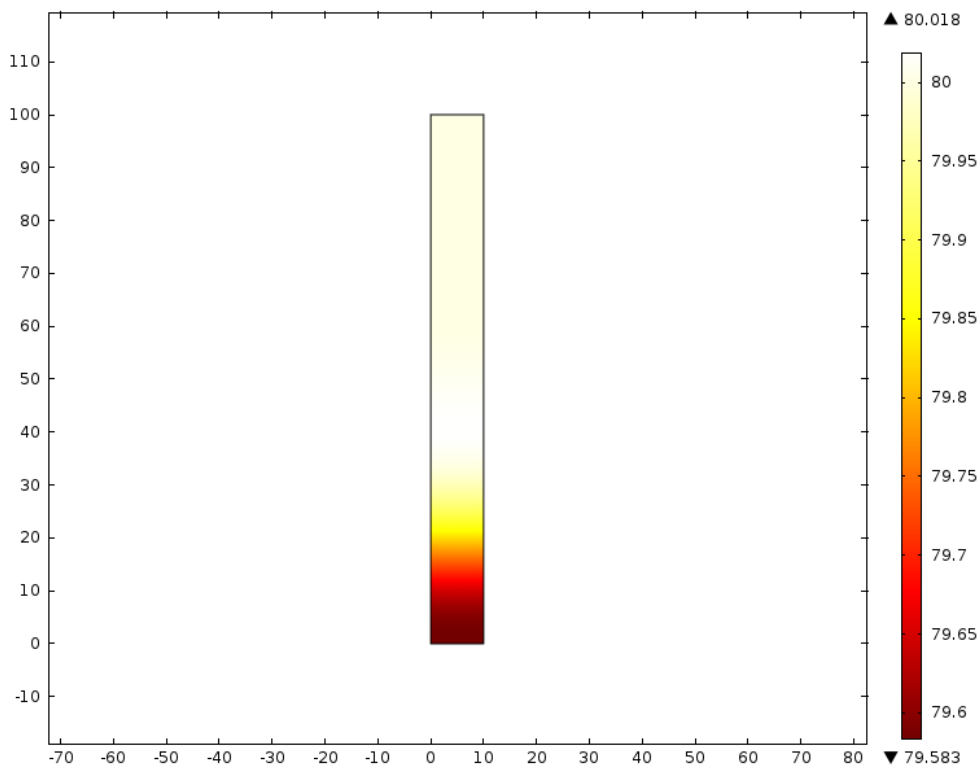
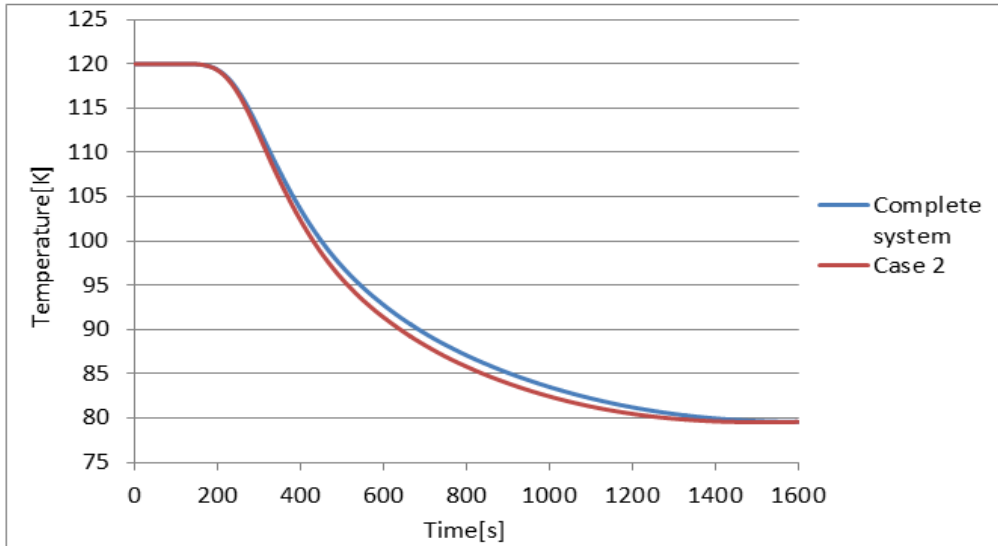


Figure 35: 2D temperature profile at t=1600 seconds

The average outlet temperatures are plotted in Figure 36 to compare the cooling process for the completed system with the one from Case 2. The adsorption process will slow down the cooling process due to the fact that the mass flow rate decreases as hydrogen is adsorbed.



**Figure 36: Average outlet temperatures for the complete system and Case 2**

The density is still seen to follow the temperature as expected and the plots can be found in the Appendix.

**Pressure**

Imposing mass transfer results in a small pressure change as seen below.

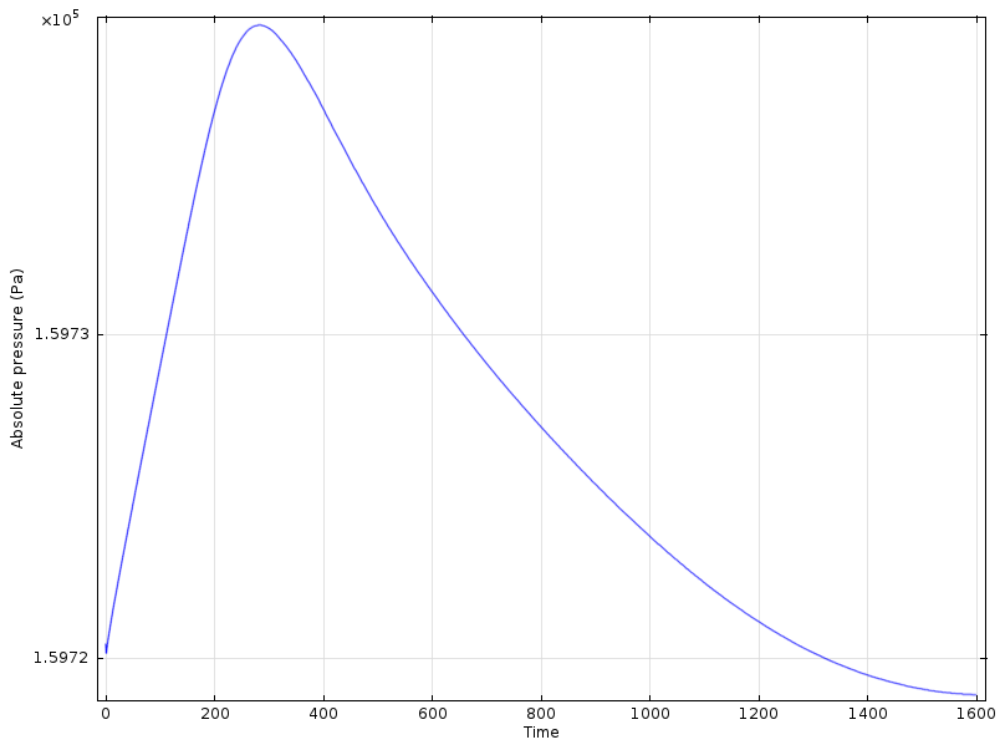


**Figure 37: Pressure change over time.**

Figure 37 gives the pressure vertically through the domain over time. Until now the pressure has remained constant over time across the bed, however as the mass transfer begins the pressure will change.

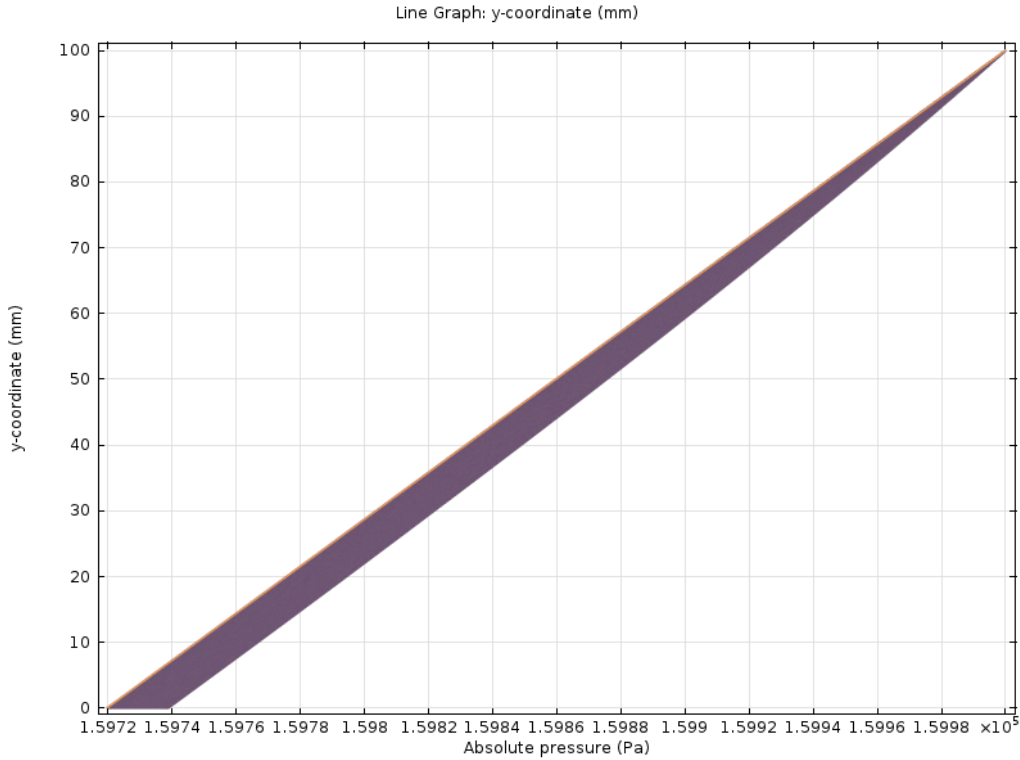


**Figure 38: Pressure drop over the domain for t=0-1600 seconds**

The “thick line” seen in Figure 38 is all the pressure lines for t=0 to t=1600 seconds from the inlet to the outlet of the domain. It is seen that even though not constant, the pressure change does not increase much with time (0.0002bar). The largest pressure drop seen is equal to the pressure drop found for Case 2 and the smallest is:

$$\begin{aligned} \Delta p_{min} &= 1.6 * 10^5 [Pa] - 1.5974 * 10^5 [Pa] \\ &= 260 \text{ Pa (0.1627\%)} \end{aligned}$$

This means that the pressure drop will be in the range from 0.1627 % to 0.175 %.

This behavior is expected and has been commented on in literature. Senthil Kumar et al. [2] showed that the pressure drop across a bed of highly porous material is often negligible. They computed the pressure drop for a non-adsorbing hydrogen gas flow through three different bed designs at 20 bar and 80K. For the axial bed design, which is similar to what is used in this study; the pressure drop was found to be 0.014 bar (1417.33 Pa), this is 0.07 % of the inlet pressure and was found to be negligible. The pressure drop in the present study is larger, however it still seems reasonable.

### **Velocity**

The outlet velocity is set to be constant, however as the hydrogen is adsorbed the velocity will decrease throughout the domain as seen from Figure 39.

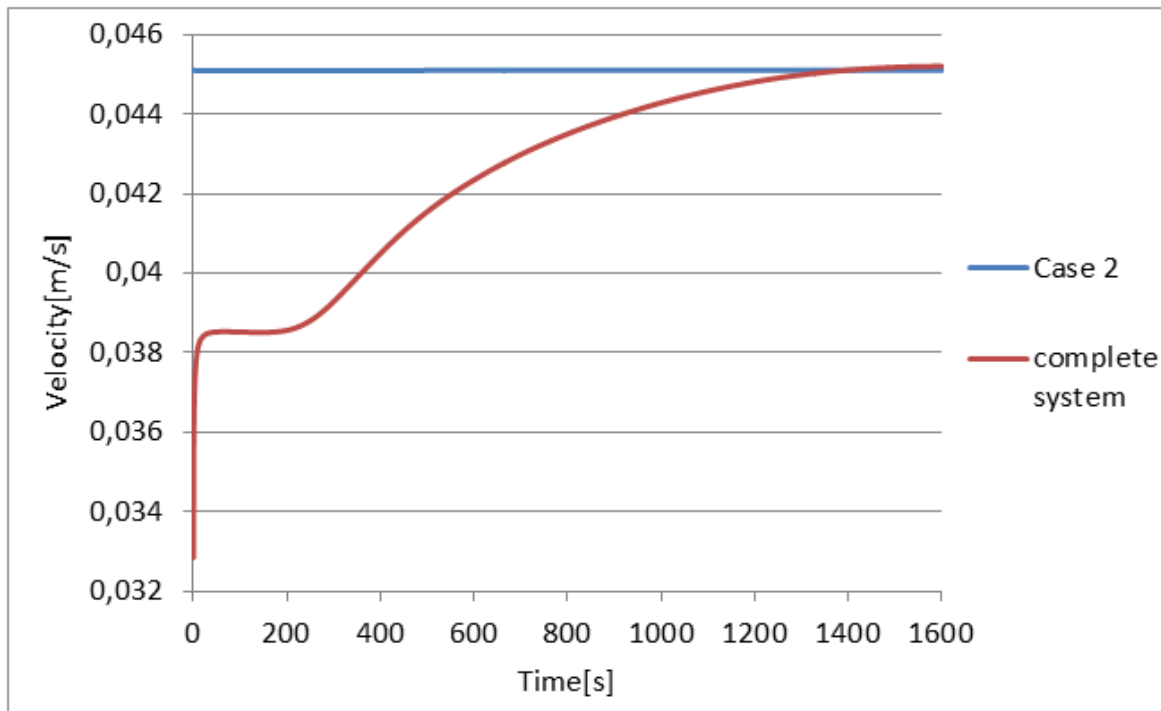


**Figure 39: Average inlet velocity for the complete system and Case 2**

Figure 39 shows the velocity changes over time for Case 2 and for the present completed system. In Case 2 no mass was adsorbed and the velocity changes over time were seen to be negligible. However, this was not expected and believed to be a result of the solver configurations used during the simulations. As the system is completed the velocity magnitude has decreased. If the pressure and velocity boundary conditions are switched it is easier seen that as time passes the outlet velocity will decrease, this has been done in Section 5.4., and hence will not be showed here.

The results seen from the temperature, pressure and velocities suggest that the system behaves as expected, considering the discrepancies discovered for the Simple model and Case 2. While being aware of these, the adsorption process can be analyzed.

### 5.3.2. Adsorption

As the adsorption starts the bed loading is zero. The bed loading is how much of the available adsorption capacity is used on a given location along the bed. Before the whole tank has reached equilibrium at 80 K, there will be three regions existing in the bed at the same time, one saturated, one active and one inactive region. This process can be seen from the figures below. As the gas starts to flow the adsorption begins and the bed loading starts to increase at a given location. After a period of time the bed loading at the uppermost region will reach its adsorption capacity, the region is saturated and no more hydrogen can be adsorbed at this location. In the middle region the temperature is between the feed gas temperature and the initial bed temperature, this means that it is active and cooling and adsorption will take place simultaneously. The bottom region has not yet been cooled down

and the hydrogen merely passes through. This process will continue to propagate throughout the bed until the maximum adsorption capacity of the bed is reached.

Figure 40 gives the adsorbed hydrogen,  $n_{ex}\rho_b V_b$ , at different times. The x-axis gives the length of the domain where 100 mm represents the inlet and 0 mm the outlet. The bed saturates at a value of 0.0198 kg. At the curve representing  $t=1200$  seconds a sudden increase in adsorption capacity is seen, however when looking at the temperature plot in Figure 41 the corresponding time curve has a dip below 80 K and as the temperature decreases more hydrogen is adsorbed. As mentioned in the previous sections this is not a physical phenomenon but solely a result of a numerical instability.

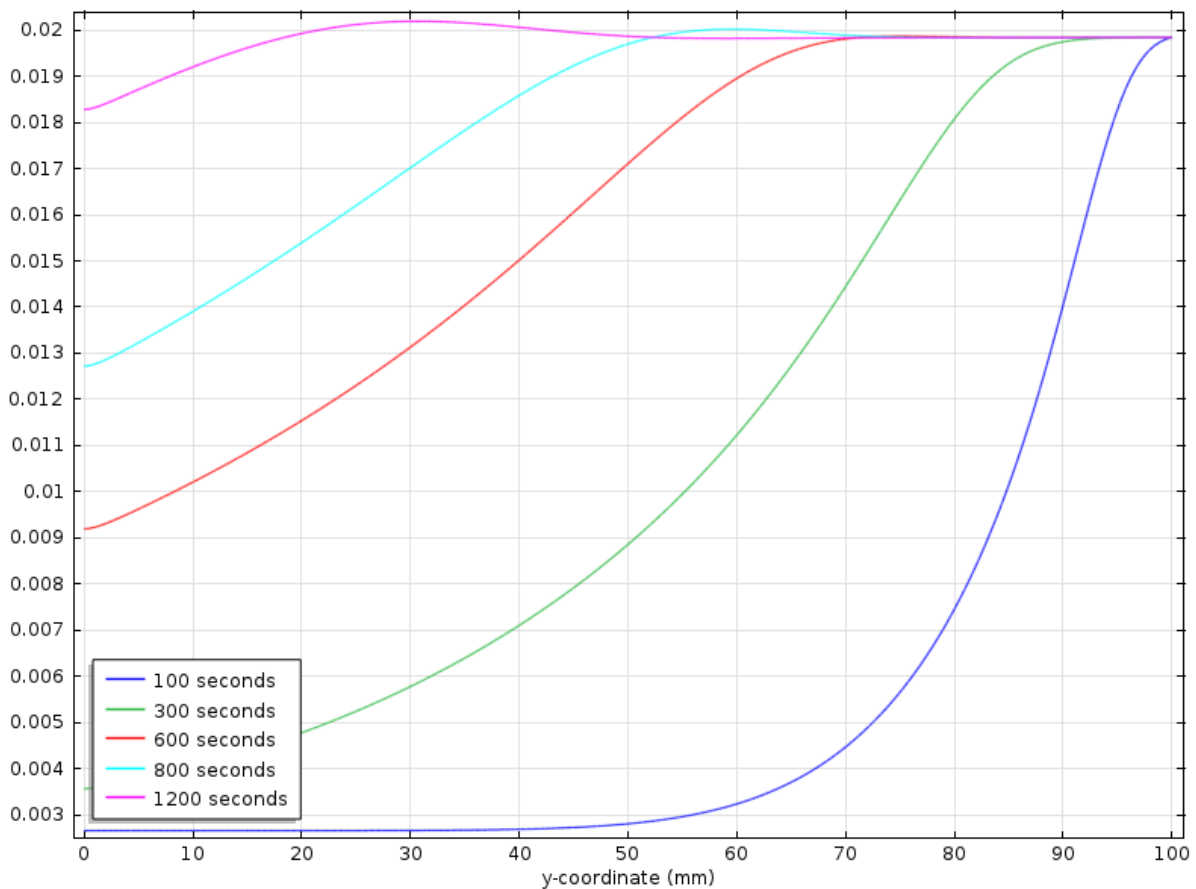


**Figure 40: Adsorbed gas over time in the bed**

Figure 41 shows the temperature evolution over time in the bed. The three regions mentioned above are clearly present and it can be seen that the uppermost half of the domain is saturated after 800 seconds. However 1600 seconds is not enough to fully saturate the entire bed and temperature gradients are seen close to the outlet.

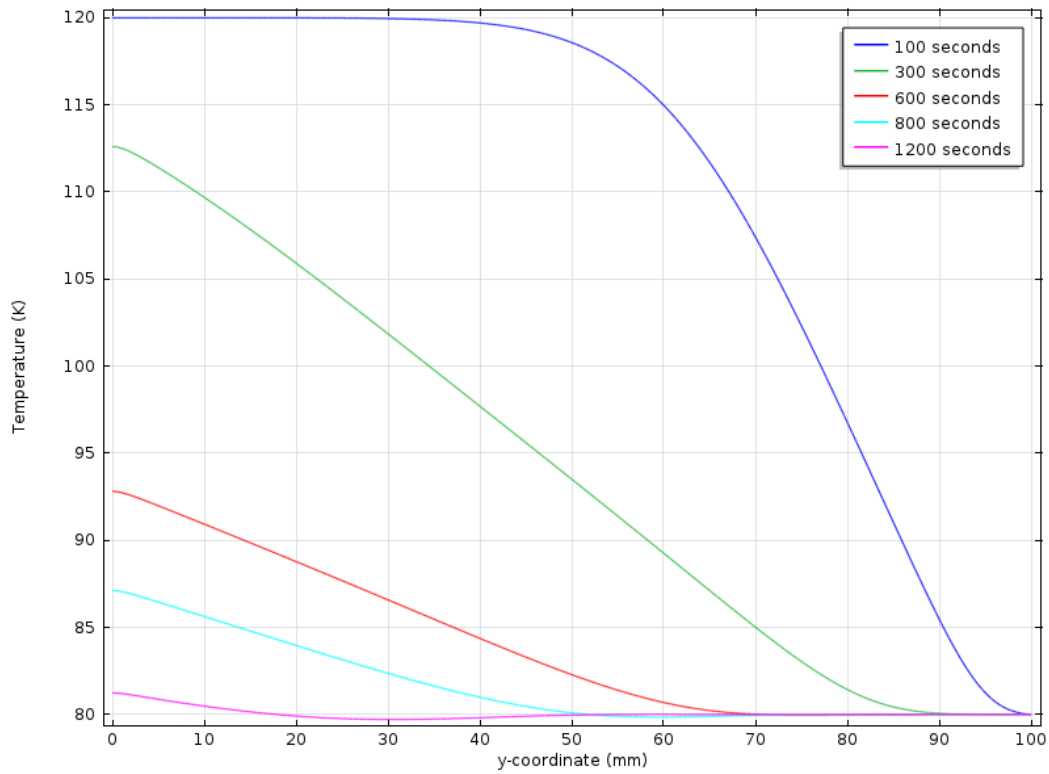


Figure 41: Temperature over time in the bed

### Amount of hydrogen adsorbed

Figure 42 shows the average total load of adsorbed hydrogen,  $n_{ex}\rho_b V_b$ , and the total load of hydrogen,  $n_{ex}\rho_b V_b + \epsilon_t \rho_g V_b$  in the tank over time.

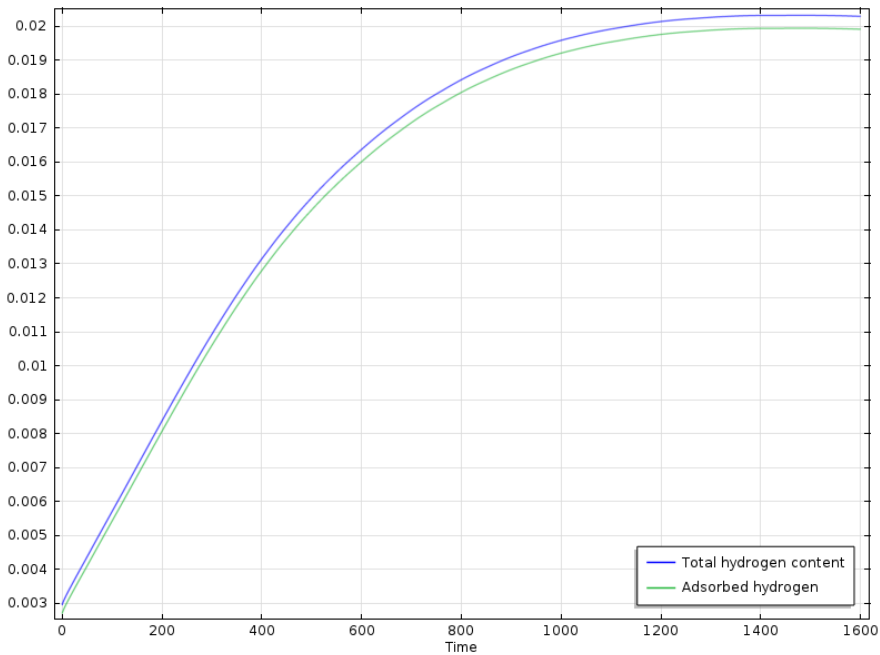


Figure 42: Total and adsorbed hydrogen in the bed over time

The heat released due to adsorption can be calculated from the equation:

$$Q_3 = m_{ads} \Delta H_a \quad (5.9)$$

where

$$m_{ads} = m_{MOF} (C_{80K} - C_{120K})_{H_2} \quad (5.10)$$

The adsorbed mass was found to be:

$$\begin{aligned} m_{ads} &= 0.01995 \text{ kg} - 0.0027 \text{ kg} \\ &= \underline{0.01725} \text{ kg} \end{aligned}$$

$$\begin{aligned} Q_3 &= 0.01725 * 2e6 \left[ \frac{\text{J}}{\text{kg}} \right] \\ &= \underline{34500} \text{ [J]} \end{aligned}$$

This is 17 % higher than the result predicted in Section 5.3. The adsorption values are obtained by exporting data from COMSOL. However, as there seem to be inconsistencies in expected behavior and the actual results, the hydrogen load is calculated manually from the implemented Langmuir equations (4.1 - 4.4) for comparison.

At p=1.6 bar, the Langmuir equation gives

$$\begin{aligned} m_{ads} &= 0.64 \text{ [kg}_{MOF}] (0.0636 - 0.0405) \left[ \frac{\text{kg}_{H_2}}{\text{kg}_{MOF}} \right] \\ &= \underline{0.014784} \text{ kg adsorbed hydrogen} \end{aligned}$$

$$Q_3 = \underline{29568} \text{ [J]}$$

The predicted heat due to adsorption from the model developed in the present study is 14.3 % greater than the one predicted directly from the implemented Langmuir equations. Clearly, this proves that there is a weakness in the developed model as the values from the simulations should be consistent with the ones from the equations.

As the inlet velocity is slower for the completed system, less hydrogen than what was fed into the domain for Case 2 will be inserted. The mass inserted for Case 2 and the completed system are 0.349752 kg and 0.330287 kg, respectively. However, the energy required to cool the domain to 80 K for the completed system is greater. As it cannot be calculated properly, it was estimated as in the precious sections;

$$\begin{aligned} Q_4 &= \sum_{t=0}^{1300} \dot{m}_{H_2_{out}} Cp(T(t) - 80) \\ &= \underline{40575} \text{ J} \end{aligned}$$



The higher value is due to the additional hydrogen gas stored in the void space (see Section 2) of the MOF when the mass transfer is accounted for in the completed model, so:

$$Q_4 = Q_2 + Q_{gas} \quad (5.11)$$

Now that the heat due to adsorption has been calculated the total system energy balance can be checked. Ideally, this should be

$$Q_3 = Q_2 - Q_1 - Q_{gas} \quad (5.12)$$

Where  $Q_1$  and  $Q_2$  would be found in the sections for the Simple Model and Case 2, respectively, and  $Q_{gas}$  would be found from:

$$Q_{gas} = m_{H_2gas} Cp\Delta T \quad (5.13)$$

Where:

$$m_{H_2gas} = m_{in} - m_{out} - m_{ads}$$

However, as the mass was not seemed to be completely conserved, it is not possible to predict the mass of gas stored in the domain, and an estimation will be used:

$$Q_3 = Q_4 - Q_1 \quad (5.14)$$

$$\begin{aligned} Q_3 &= 40575 \text{ J} - 9704 \text{ J} \\ &= \underline{30871 \text{ J}} \end{aligned}$$

This deviates by 10.5 % from the calculated heat of adsorption from Equation 5.9. As the mass was not conserved and as the simulation would predict a greater amount of adsorbed hydrogen than what was calculated directly from the equations, the obtained values are solely indicatives of the magnitudes and not reliable results. The deviations are thus to be expected. Table 11 summarizes the inconsistencies in calculating the heat of adsorption.

**Table 11: Summary of predicted heat of adsorption**

Approach	Heat of adsorption[J]	Deviation from Langmuir equation[%]
Langmuir equation	29568	-
Simulation	34500	14.3
$Q_3 = Q_2 - Q_1$	28602	3.3
$Q_3 = Q_4 - Q_1$	30871	4.2

## 5.4. Discussion

To validate the model developed in this study a comparison to the results obtained in [2] will be carried out and discussed. As inconsistencies in mass conservation have been detected, a comparison to published result will be indicative in finding the weakest links where the model fails to predict the adsorption process actually occurring.

V. Senthil Kumar et al. [2] reduced the mass and heat transfer equations presented in Section 4.1 to a 1-D isobaric system before solving for velocity and temperature in COMSOL. The model developed in the present study is not isobaric, however in the system analysis in Section 4.3.1 it was shown that the pressure drop is negligible, and hence, it seems reasonable to compare the results obtained from the two simulations. The porous material used in [2] is MOF-5 with the listed properties:

- Particle density:  $\rho_p = 601.64 \left[ \frac{kg}{m^3} \right]$
- Bed density:  $\rho_{bed} = 385.05 \left[ \frac{kg}{m^3} \right]$
- Bed porosity:  $\varepsilon_{bed} = 0.36$
- Fe-btc volume fraction:  $\theta = 0.64$
- Specific heat capacity:  $C_{p_{Fe-btc}} = 396 \left[ \frac{J}{kgK} \right]$
- Particle thermal conductivity:  $k = 0.32 \left[ \frac{W}{mK} \right]$
- Permeability:  $\kappa_{br} = 1.1e-8$

To facilitate the comparison, the volume of the domain of the present model was increased to match the one from [2]. Here after, the model developed by Kumar et al. will be referred to as Model 1 and the model developed in the present study will be referred to as Model 2.

**Table 12: Model properties**

	$V_b$	$m_s$	H <sub>2</sub> wt%	H <sub>2</sub> load	A
Model 1	0.2347 m <sup>3</sup>	90.37	5.53	5 kg	0.2347m <sup>2</sup>
Model 2	0.2347 m <sup>3</sup>	90.37			0.2347m <sup>2</sup>

**Table 13: Initial and boundary conditions imposed in Model 1 and Model 2**

	Initial values	Inlet conditions	Outlet conditions
Model 1	<ul style="list-style-type: none"> <li>• T=140 K</li> <li>• p=20 bar</li> </ul>	<ul style="list-style-type: none"> <li>• u=0.0823 m/s</li> <li>• T=80 K</li> <li>• <math>\dot{m}=0.120</math> kg/s</li> </ul>	<ul style="list-style-type: none"> <li>• <math>\frac{\partial T}{\partial x}=0</math></li> </ul>
Model 2	<ul style="list-style-type: none"> <li>• T=140 K</li> <li>• p=19 bar</li> </ul>	<ul style="list-style-type: none"> <li>• u=0.0823</li> <li>• T=80K</li> </ul>	<ul style="list-style-type: none"> <li>• p=19 bar</li> </ul>

The volume, mass of adsorbent, hydrogen load and area are listed in Table 12, while the initial and boundary conditions are listed in Table 13 below.

There are some differences in the imposed outlet boundary conditions as Model 2 has a defined pressure while the temperature gradient is set to zero for Model 1, also a fixed inlet mass flow rate is set in Model 1, while this is not possible to implement in Model 2, and will solely depend on the inlet density, velocity and area from Equation 5.2. However this should be consistent if Model 2 proves to work properly at high pressures.

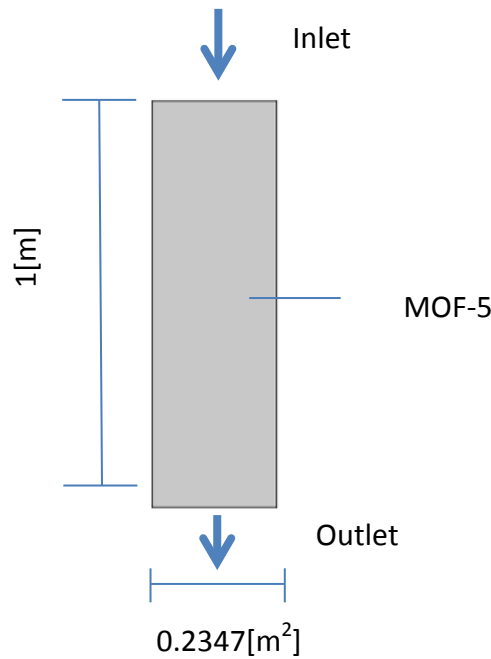


Figure 43: Tank to be compared to [2]

To validate the comparison of the 1-D model with the model developed in the present study the pressure drop over the domain was calculated to prove it is negligible. The values are taken from Figure 44 which gives the pressure drop over the domain at all times.

$$\Delta P_{max} = \frac{67,223}{2000000} 100 = 0.00336\%$$

$$\Delta P_{min} = \frac{51.345}{2000000} 100 = 0.00257\%$$

The results confirm that the pressure drop is negligible, and the two models can be compared.

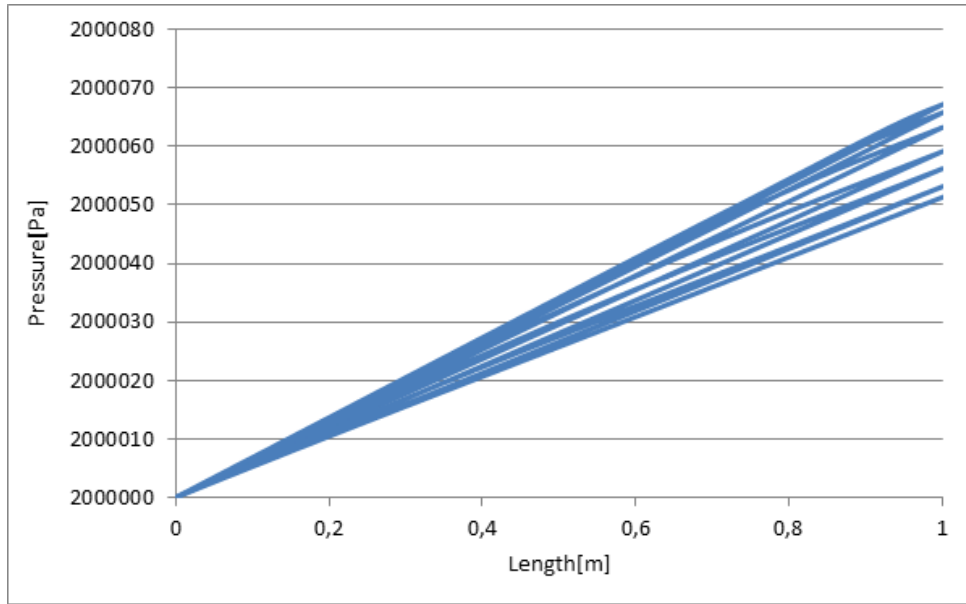


Figure 44: Pressure drop over the domain from present study for t=1-1000 seconds

**Temperature**

In [2] the whole bed is initially at 140 K, as the feed gas enters the domain cooling and adsorption takes place simultaneously. However, for the model developed in this study, instabilities results in a small region just below the inlet where the temperature has a value of 143.47 K at t=0. This can be seen from the 2D plot below. This temperature increase is not a physical phenomenon, but solely a result of numerical fluctuations in the solver discussed in Section 5.2.

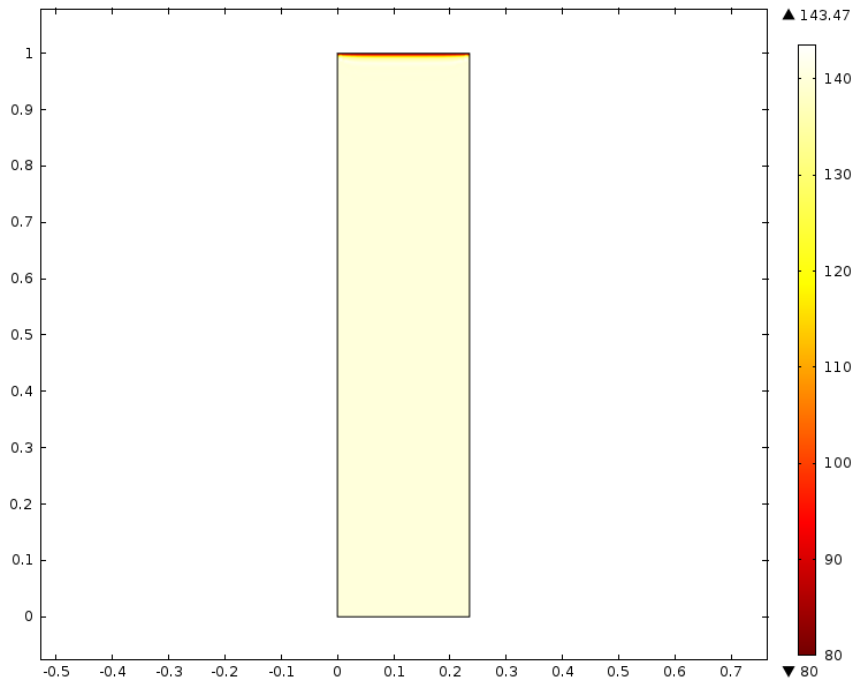


Figure 45: 2D temperature plot of the bed at t=0

Figure 46 shows the temperature evolution in the bed simulated by Model 1. At  $t=0.5$  minutes the region 0-A is saturated at 80 K, A-B is the adsorption zone where the temperature is between the feed gas temperature and the initial temperature, while region B-1 is at the initial temperature and not active so the gas merely passes through.

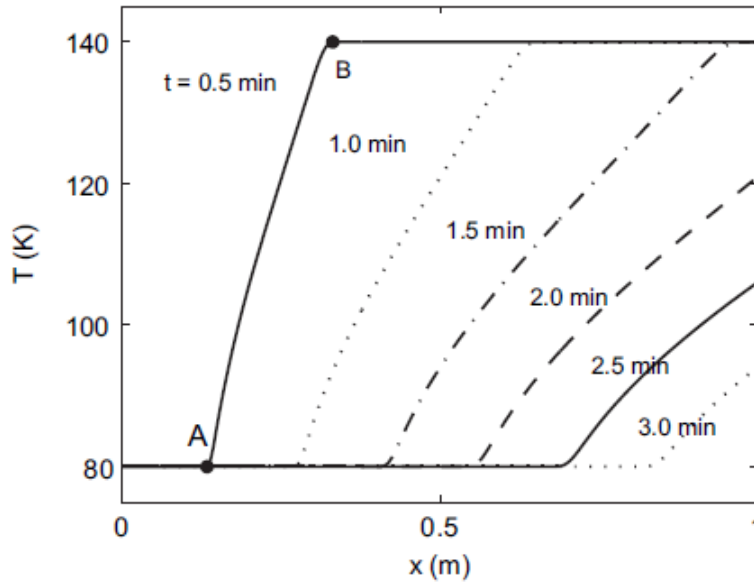


Figure 46: Temperature evolution in the axial flow bed [2]

The same regions are seen in the plot from Model 2 below, however the saturated region at  $t=0.5$  is smaller constituting of 4 % of the total domain, to 13.5 % predicted by Model 2. The cooling process is slower for the present system than what was simulated in [2] and two minutes are required to cool down 13.5 % of the domain for Model 2.

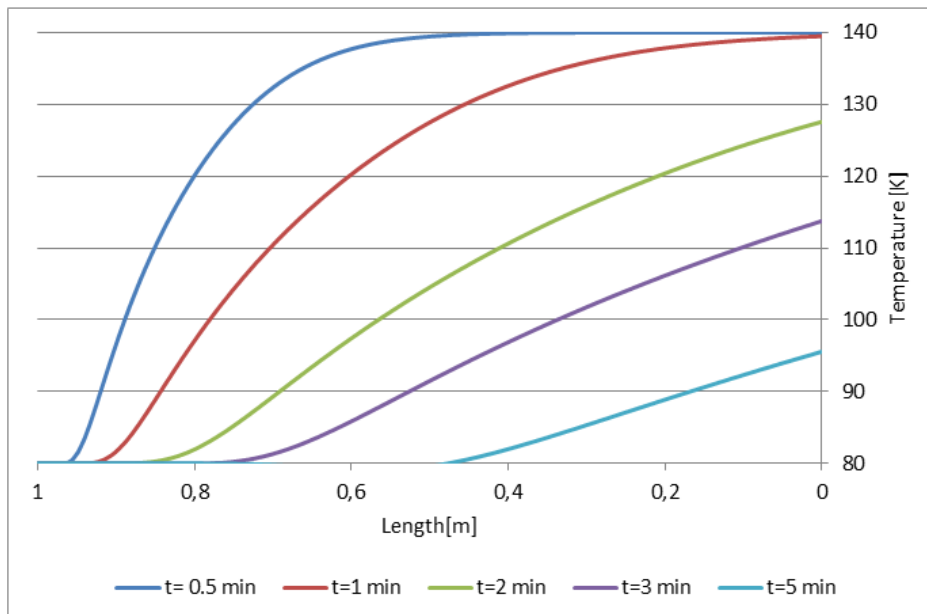


Figure 47: Temperature evolution in the bed for Model 2

**Table 14: Comparison of outlet temperatures**

Time [min]	Outlet Temperature [K]		Decrease in outlet Temperature [%]	
	Model 1	Model 2	Model 1	Model 2
0.5	140	140	-	-
1	140	140	-	-
2	120	127.6	14.28	8.86
3	94.4	113.75	32.57	18.75
5		95.56		31.74

In Table 14 the outlet temperature values for each time interval is listed with the corresponding percentage fall in temperature from the first time interval at t=0.5 minutes to the respective times . It is seen that the outlet temperature decreases faster for Model 1 than Model 2. The inlet velocity is set to be equal, so to explain this deviation a closer look needs to be taken at the mass flow as the results might suggest that more hydrogen is adsorbed in Model 2 as the adsorption process will decrease the mass flow rate. This will be verified in the coming sections.

For a more detailed comparison the temperature was divided into 3 intervals and the slopes for the two models compared.

1. 80-100 K
2. 100-120 K
3. 120-140 K

An overall good agreement in the slopes is seen, especially for Region 2. However, for Region 3 larger deviations are seen as the gas approaches the outlet. The internal decrease in slopes from each time interval in the two models is seen to be consistent for both studies. Hence, it can be concluded that even though the time range of the cooling process in Model 2 deviates from Model 1, the tendency is similar.

## Density

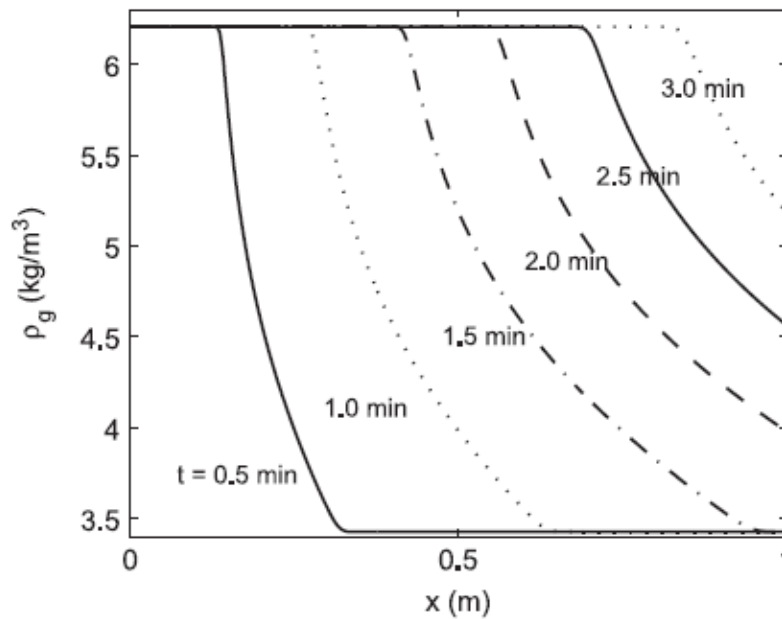
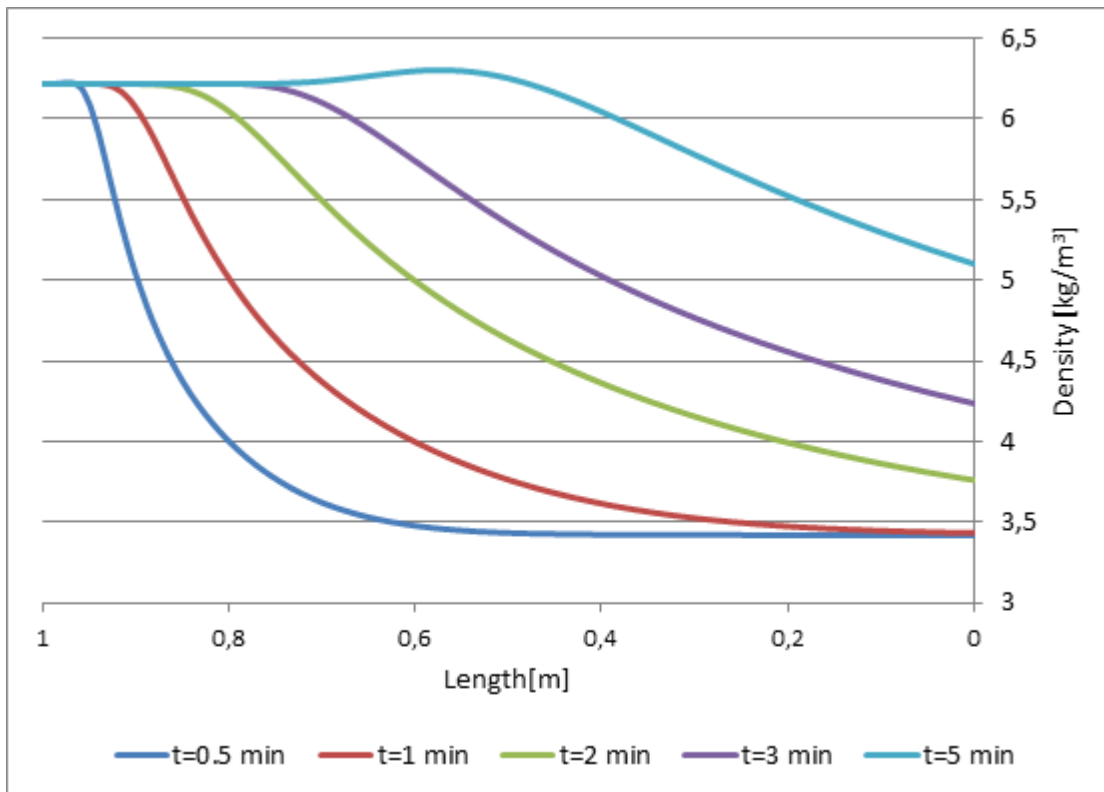


Figure 48: Density evolution in the bed [2]

As the density is inversely proportional to the temperature the deviations between Model 1 and 2 are consistent with the ones found for the temperature. The deviations in the two tables are due to inaccuracies when measuring the values from the Model 1 figures, and are not interpreted to be a result of errors in the models. Also, for  $T = 80 \text{ K}$  Model 2 has a higher density, the inlet density is  $6.208 \text{ kg/m}^3$  and  $6.217 \text{ kg/m}^3$  at  $80 \text{ K}$  for Model 1 and Model 2, respectively.

Table 15: Decrease in outlet density for Model 1 and Model 2

Time [min]	Outlet Density [ $\text{kg/m}^3$ ]		Decrease in outlet Density [%]	
	Model 1	Model 2	Model 1	Model 2
0.5	3.42	3.42	-	-
1	3.42	3.42	-	-
2	4	3.76	14.5	9
3	5.21	4.23	34.36	19.15
5		5.1		33



**Figure 49: Density evolution in the bed predicted by Model 2**

The sudden increase in density at t=5 minutes is a result of the fluctuations in the numerical solver. This will affect the mass flow rate, but not have an impact on the results when comparing for the evolution over the three first minutes.



## Velocity

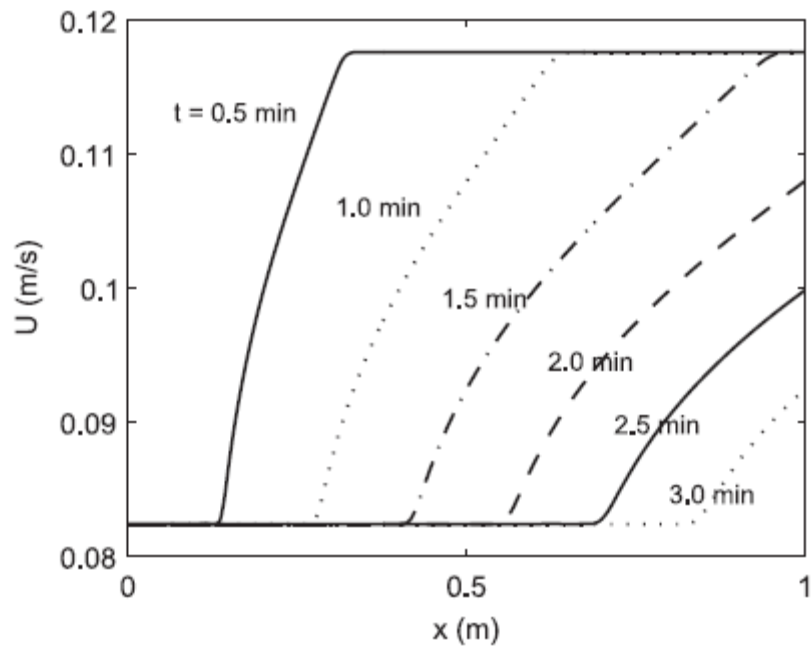


Figure 50: Superficial gas velocity evolution in the bed [2]

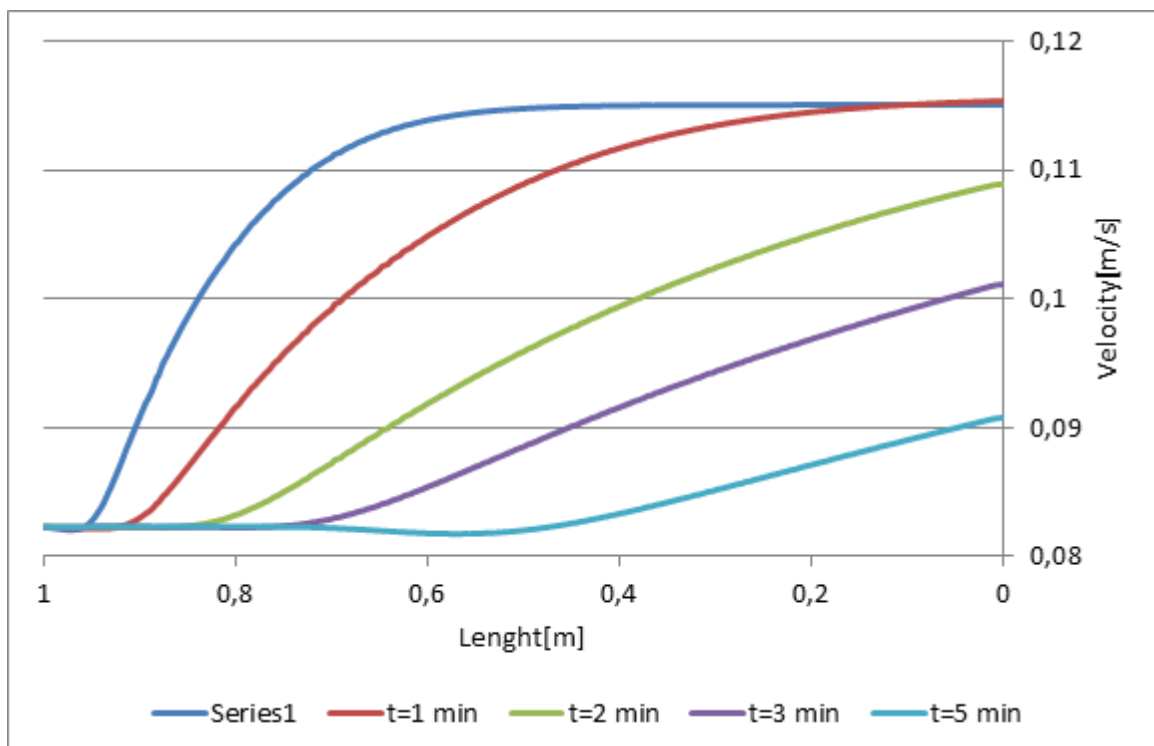


Figure 51: Velocity evolution predicted by Model 2

It is seen that the velocity in Model 1 increases more rapidly through out the domain than what is seen from Model 2. In Sections 5.1 and 5.2, it was found that Model 2 does not

account properly for the transient mass balance. The velocities did not start to increase as the temperature decreased before the adsorption was initiated. This means that the velocity changes seen were solely due to adsorption of mass, and thus are smaller than expected.

**Table 16: Comparison of outlet velocities**

Time [min]	Outlet velocity [m/s]		Decrease in outlet velocity [%]	
	Model 1	Model 2	Model 1	Model 2
0.5	0.117	0.115	-	-
1	0.117	0.1153	0	- 0.26
2	0.108	0.109	7.7	5.2
3	0.092	0.101	21.3	12.2
5		0.091		20.9

Table 16 gives the outlet velocity at each time interval as well as the decrease in outlet velocity from  $t=0.5$  minutes to the respective times. The inlet velocity is the same for the two models; however the velocity increases more rapidly through the tank for Model 1 and two extra minutes are required for Model 2 to decrease 21 % in outlet velocity. Also it is seen that after 1 minute the outlet velocity for Model 2 is 0.26% higher than for 0.5 minutes, this is most likely due to numerical fluctuations. This difference corresponds well with results found from the temperature analysis where it was seen that two minutes was required to cool the domain for Model 2 to the same amount that was cooled in half a minute by Model 1. As done in the previous sections, the velocities from the figures are divided into restricted regions:

1. 0.0823m/s – 0.09 m/s
2. 0.09m/s – 0.1 m/s
3. 0.1m/s – 0.11 m/s
4. 0.11 m/s – 0.1172 m/s

It is found that the slopes for Model 1 and 2 are quite similar for Region 1 close to the inlet. However a diverging trend is seen as the hydrogen gas approaches the outlet with increasing deviations between the slopes for the two models. As mentioned in the temperature analysis, the reason for a slower velocity suggests that more hydrogen is adsorbed in Model 2.

## Mass flow rate

**Table 17: Predicted mass flow rate for the two models**

Time [min]	Outlet flow rate [g/s]		Increase in outlet mass flow rate [%]	
	Model 1	Model 2	Model 1	Model 2
0.5	94.34	92.39	-	-
1	94.34	93	0	0.66
2	100.87	96.18	6.47	3.94
3	112.61	100.59	16.22	8.15
5		108.73		15.03

Table 17 gives the outlet mass flow rate predicted by Model 1 and Model 2, as well as the percentage increase in mass flow rate from  $t=0.5$  minutes to the respective times.

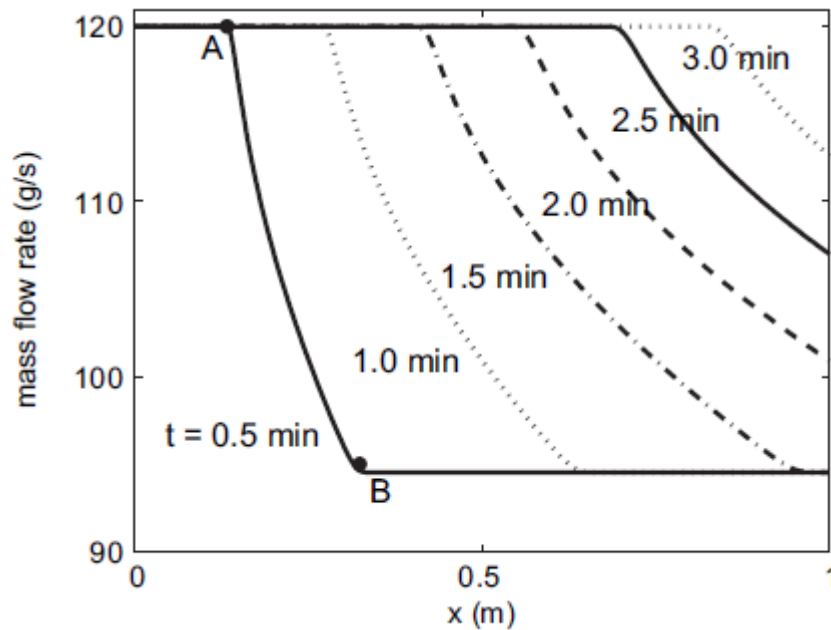


**Figure 52: Mass flow evolution in the bed [2]**

For Model 1 the outlet mass flow rate does not change during the first minute and a half; however a slight increase is seen for Model 2. In accordance with the velocity evolution the increase in outlet mass flow rate is slower for Model 2 than what Kumar et al. simulated in Model 1. It is seen that two additional minutes are required to reach an increase of mass flow rate close to 16 %; this was the same time needed to reach a decrease of 21 % in velocity and hence suggests that the two models correspond well in evolution even though the time intervals deviates.

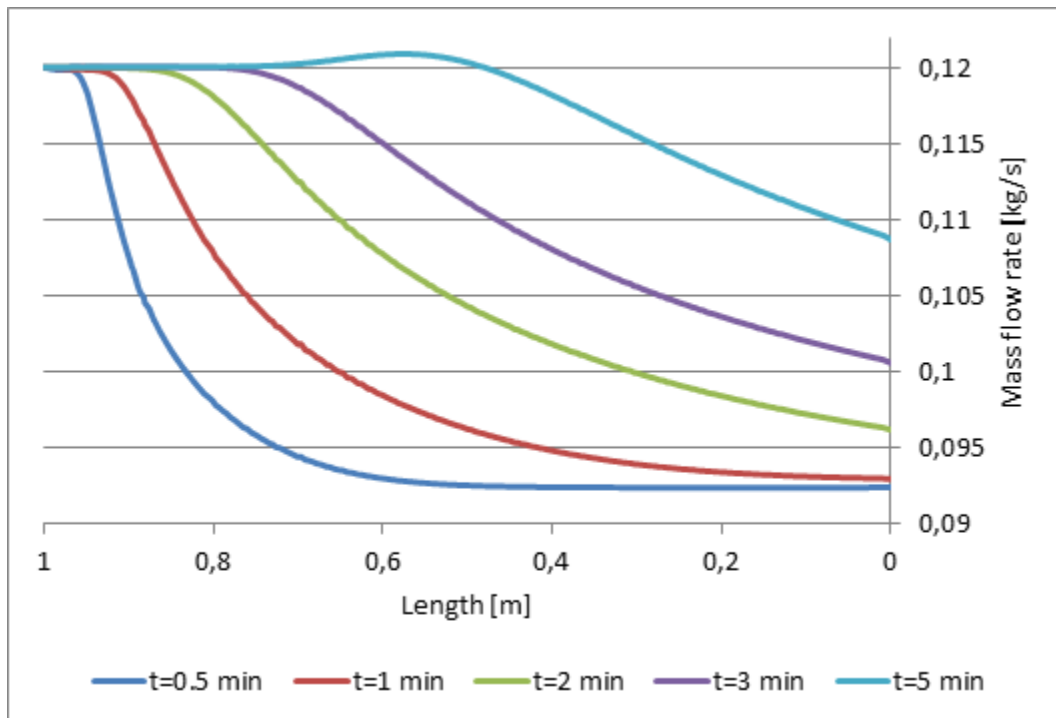


Figure 53: Mass flow rate evolution predicted by Model 2

When dividing the outlet mass flow rate into regions;

1. 92.4-100 g/s
2. 100- 110 g/s
3. 110-120 g/s

it was found that for interval 2 and 3 the slopes of the curves corresponds well, however for the first interval larger deviations is seen. As before it is seen that the slopes of the curves of Model 1 are steeper than the ones from Model 2 and this deviation increases as the gas approaches the outlet.

The fact that the mass flow rate is lower for Model 2 than Model 1 supports the assumption that more adsorption might occur.

## Hydrogen load

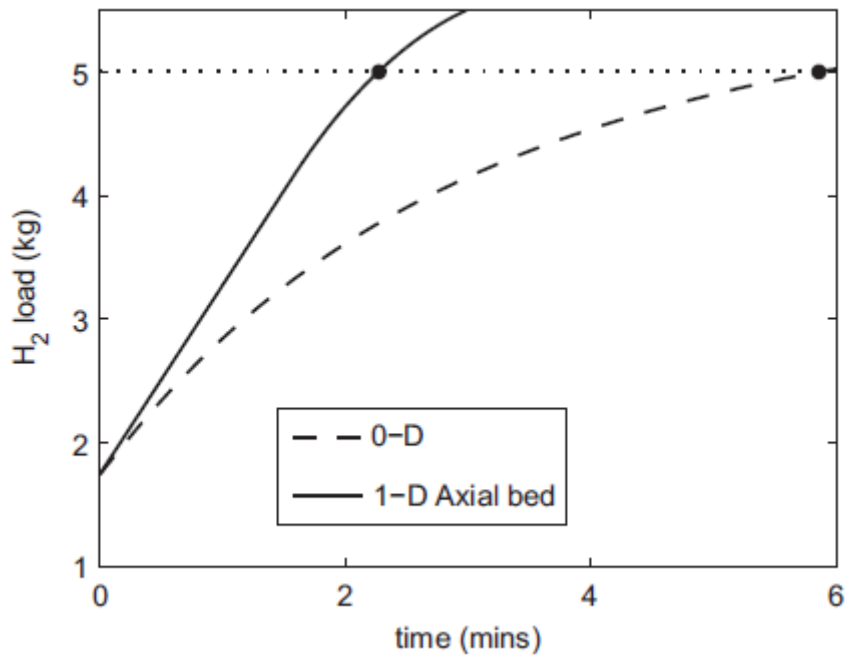


Figure 54 : Hydrogen capacity evolution predicted by the 0-D model and the 1-D axial isobaric model during the isobaric refueling period [2]

In the study carried out by Kumar et al., the isobaric refueling time was found to be 2.26 minutes. In Figure 54, two curves are seen, the dashed line represents the isobaric refueling period for a 0-D model compared to Model 1 in [2], however the 0-D model is not taken into account in this study.

The Langmuir equations (4.1 - 4.4) give:

$$n_{ex,80K} = 0.0636 \text{ kg}_{H_2}/\text{kg}_{MOF}$$

=5.75 kg hydrogen can be adsorbed at 80 K.

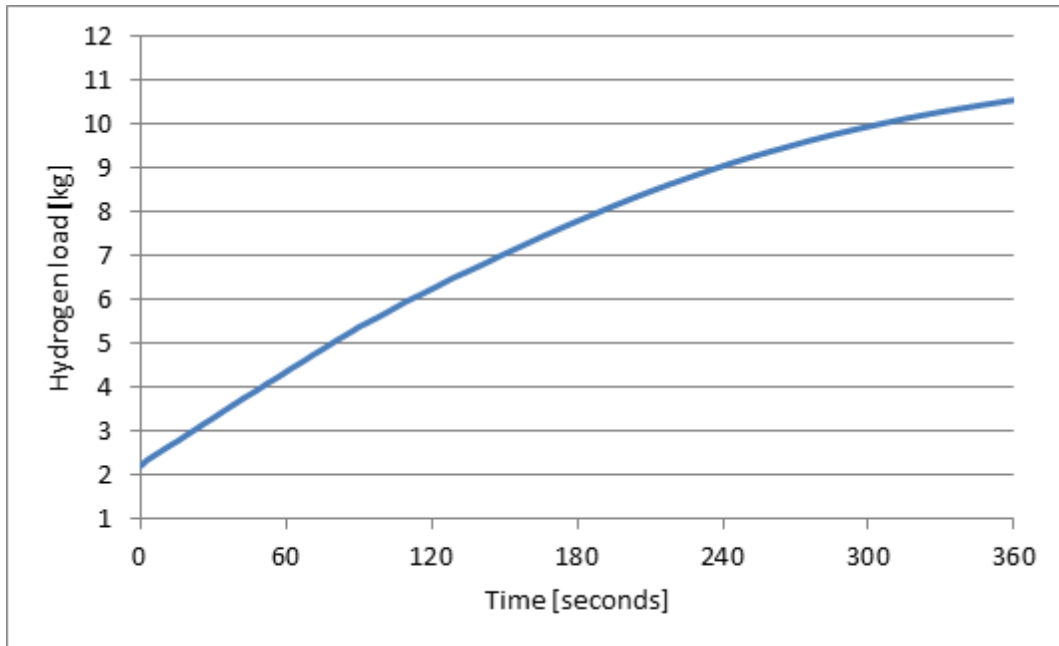


Figure 55: Hydrogen load predicted by Model 2

The hydrogen load in the tank predicted by Model 2 is calculated using;  $n_{ex}\rho_b V_b + \varepsilon_t \rho_g V_b$  and gives both the adsorbed mass and gas in the tank.

Table 18: Comparison of Hydrogen load predicted by Model 1 and Model 2

Time [min]	Hydrogen Load [kg]		Increase in Hydrogen load [%]	
	Model 1	Model 2	Model 1	Model 2
0	1.75	2.205	-	-
0.5	2.5	3,296	30	33
1	3.31	4.348	47.13	49.29
2	4.69	6.237	62.69	64.65
3	5.5	7.79	68.18	71.7

Table 18 gives the hydrogen load for the two models over time and the corresponding percentage increase from  $t=0.5$  minutes to the respective times. As suspected from the previous sections it is seen that the adsorption process is slower for Model 1 than Model 2. After 1.32 minutes the tank is filled with 5 kg hydrogen, while for Model 1 the refueling time is calculated to be 2.26 minutes. This explains why the mass flow rate, velocities and temperature for Model 2 have flatter slopes throughout the domain as more hydrogen is adsorbed at each time step. Table 19 gives the total alternation seen in the different properties compared. Overall it can be concluded that Model 2 needs two additional minutes to reach the percentage amendment seen in Model 1.

**Table 19: Summary of change in properties over time predicted by Model 1 and Model 2**

Property	Time [min]	Change [%]	
		Model 1	Model 2
Temperature [K]	1	0	0
	2	14.28	8.86
	3	32.57	18.75
	5	-	31.74
Density [kg/m <sup>3</sup> ]	1	0	0
	2	14.5	9
	3	34.36	19.15
	5	-	33
Velocity [m/s]	1	0	-0.26
	2	7.7	5.2
	3	21.3	12.2
	5		20.9
Mass flow rate [g/s]	1	0	0.66
	2	6.47	3.94
	3	16.22	8.15
	5	-	15.03

### *Concluding remarks*

When concluding based on the results found, the fact that there might be errors in the tables have to be taken into account. The measured values are conducted manually from the figures predicted by Model 1 and hence, there will be insecurities in the reliability of the values. In addition, as the numerical fluctuations have not been completely eliminated in Model 2, this might have an impact on the results. In addition, there has been detected an inconsistency in the mass conservation. Due to this, emphasis has been put on the trends seen and not the exact values found.

V. Senthil Kumar et al. observed a simulating artifact when running simulations in COMSOL. First, the Lagrange elements method was implied and a small temperature dip upstream of the adsorption front was detected. As they switched to Hermite cubic elements, the artifact vanished (information on the numerical methods can be found in [17]). In the present study not enough time has been devoted to test the different solver settings in COMSOL and for the current imposed conditions, Hermite cubic elements proved not applicable. However this further supports the assumptions that the instabilities detected are purely unphysical and can most probably be eliminated as the correct solver method is found.

From the comparison carried out in this section, it was clearly seen that Model 2 adsorbed hydrogen faster and thus had less steep gradients for every curve compared to Model 1. As

the systems are supposed to be similar by using the same Langmuir constants, initial pressures, temperatures and velocities the found results should also be consistent. The most prominent explanation is believed to lie within the solver configurations. Due to time restrictions, the actual completion of a functional system was prioritized to the retreatment of solving the numerical problems. As the numerical tools in COMSOL are complex, the study of numerical solving methods together with finding the most appropriate method will be time consuming. Furthermore, it will require a fundamental study with a scope drawn away from what is assigned for in the present thesis, namely implement and analyze transient mass and energy balances in COMSOL. The model developed in this study has proved to be functional, however its reliability can be questioned as it is believed that the optimal solver configurations have not yet been found. However the results obtained and analysis conducted will be valuable for further work in eliminating the remaining modeling errors. This will be further commented in Section 6 and Section 7.

### 5.5. Modeling restrictions

Several difficulties were encountered in the process of developing a functional and thermodynamically correct model. COMSOL is a very complex numerical software with a great variety of opportunities for the user and the correct modules and numerical solvers needs to be chosen carefully. The main objective in this study is to describe the transient thermodynamics during the physisorption of hydrogen gas using COMSOL, and a lot of time has been spent on investigating the unexpected results obtained and overcoming the problems with implementing the transient equations.

- The first problem encountered was the great pressure drop during refueling. The depleted fuel tank is at low pressure (1.1 to 4 bar) and higher temperatures (120-140 K) and the gas should be inserted at 20 bar and 80 K. Several tries of defining the domain pressure at low values while enforcing a boundary condition of 20 bar was performed. It was seen that the solver failed to find consistent initial values as the gap between the defined initial and boundary conditions were too great and the solver failed to converge. To impose these great pressure changes the model will have to be built differently.
- Lack of mass conservation. The velocity changes for the Simple model and Case 2 were found to be negligible. However, mass should be conserved and the velocity should change proportionally with density. The unexpected behavior remains unsolved.
- Temperature deviations when increasing the time-range. This problem was investigated in 5.2. It was found that by decreasing the relative tolerance the instability could be reduces even though not fully eliminated. It was decided that as the instability had decreased, no more effort should be put in investigating the problem as completing the model was more desirable, however if was found that Kumar et al.[2] encountered the same problems and managed to overcome them as the solver configurations were adjusted. In the present study changing the solver configurations proved not possible and hence the problem with temperature deviations withstands.



- Implementing the mass source term from the transient mass balance. A lot of time was spent on implementing this term and hence completing the model. It was found that the pressure drop from 1.6 bar at the inlet to 1 bar at the domain generated a great value for  $\frac{\partial n_{ex}}{\partial t}$  at  $t=0$ , impeding the convergence in the solver. Due to this the inlet pressure was set equal to the domain pressure.
- Closing the tank by implementing a thermal insulation at the outlet. The solver would not converge and thus, the system was not analyzed as a closed tank.
- Density evolution at high pressures. The analytical function calculating the density proved to be inaccurate for high pressures, calculating values too low. This inaccuracy was adjusted by disabling the built in function and imposing the piecewise function:

$$\rho_g = \frac{1}{v_{g_0} + v_{g_1}T + v_{g_2}T^2 + v_{g_3}T^3 + v_{g_4}T^4} \quad (5.15)$$

where

$$v_{g_0}=-0.042693, v_{g_1}=0.0028869, v_{g_2}=-5.5122e-6, v_{g_3} =1.6913e-8, v_{g_4} =-1.9513e-11 [2].$$

This is the same function used by Kumar et al. [2], and proved to be more accurate.

- The heat capacity of hydrogen is built in as a function in COMSOL depending on pressure and temperature. However, this value proved to be inaccurate when comparing to NIST web book [16]. Due to this the heat capacity was set to be constant as the model was developed. When comparing Model 1 and Model 2, it was tried to implement the heat capacity as the piecewise function;

$$Cp_g = f_1 \left(\frac{f_2}{T}\right)^2 \frac{\exp\left(\frac{f_2}{T}\right)}{\left[\exp\left(\frac{f_2}{T}\right) - 1\right]^2} + f_3 + f_4 \frac{T}{100} + f_5 \left(\frac{T}{100}\right)^2 + f_6 \frac{100}{T} + f_7 \left(\frac{100}{T}\right)^2 \quad (5.16)$$

Where;  $f_1=4.788937e+03$ ,  $f_2=5.220083e+02$ ,  $f_3=1.496674e+04$ ,  $f_4=-1.204579e+03$ ,  $f_5=8.489895e+01$ ,  $f_6=-5.356621e+03$ ,  $f_7= 2.625154e+03$ . [2]

This is the same function as Kumar et al. [2] used, unfortunately this function proved not possible to implement at the same time as the Equation 5.15. As the density function were set back to the standard analytical function initially used by COMSOL, the values decreased and deviated from the density values obtained in Model 1 and from [16], due to this the heat capacity was set to its standard function and the density function from Equation 5.15 was used. This resulted in a larger and constant heat capacity value for Model 2 than for Model 1.

From a common agreement with the supervisors, it was decided that time should be spent on detecting the errors found in the model even though this would possibly affect the number of simulations that could be run for different initial and boundary conditions. Thus, as the problems were analyzed, and an elimination proved to require a profound study, the completion of the model was prioritized.

## 6. Conclusions

---

The objective of this thesis has been to describe the transient thermodynamics during physisorption of hydrogen gas. A finite volume was to be defined and a commercial numerical software was used in the numerical calculations. In doing this, a literature review was conducted and a model was chosen for implementation into the numerical software.

### Results from literature survey

- The Langmuir model proved to be the most deficient among the three investigated, as it failed to predict the changes in slopes due to the excess adsorption maximum, typically seen with decreasing temperature and/ or increasing pressure. The Ono-Kondo and the Dubinin-Astakhov isotherms showed good agreement with the experimental data over large temperature and pressure ranges. Nevertheless, the Langmuir model was chosen for further implementation into transient mass and energy balances because it was considered vice to implement the most basic adsorption model. This would facilitate necessary modeling adjustments to prevent possible unexpected results.
- It was decided to use the transient mass and energy balances developed by Kumar et al in [2]. As an infinitesimal element within the adsorbent bed is considered, heat leaks and the structural steel masses could be neglected; this was seen as an advantage as it would facilitate the implementation.

### Modeling results

- Energy required to cool the domain was estimated to be 9704 J, which deviated 0.24% from the calculated heat required to cool the MOF.
- Pressure drop across the bed was in the range of 0.1627 % - 0.175% and hence, concluded negligible. This is in good agreement with published results.
- As expected, the density decreased proportionally with temperature. However the inlet velocity did not. This resulted in 11% deviation between mass inserted and mass going out of the system. This was believed to be a result of rounding errors and instabilities in the solver configurations. Unfortunately, this problem remained unsolved.
- Heat due to adsorption heated the domain from 120 K to 123.4 K. This suggested that the implemented Langmuir model worked properly and that heat was released due to adsorption.
- A dip below feed gas temperature was found. This was concluded to be unphysical and solely a result of instabilities in the transient solver. The problem was partly solved by decreasing the relative tolerance in the solver to  $1 \times 10^{-6}$ .
- For implementation of the mass source, the inlet pressure needed to be equal to the domain pressure for the solver to converge. As this was done, the increase in

temperature at  $t=0$  diminished. However, changes in inlet velocity and pressure throughout the domain proved the source term to be active.

- The bed saturated at 0.019 kg hydrogen. The amount of adsorbed hydrogen predicted from the simulations deviated 14.3% from the value calculated by the Langmuir equation. More hydrogen was adsorbed in the simulated model. This was concluded to be a result of mass not being properly conserved as well as instabilities in the solver.

It was decided that no more effort should be spent on investigating the instabilities in the solver as this would be beyond the scopes of this thesis. If to be done, it would possibly be on the expense of completing the simulation model, as it is believed to require an extensive analysis.

- From the comparison with the study performed by Kumar et al. [2], the percentage change in properties would need two additional minutes for the present model to match the values found in the published study. Model 2 reached a 5 kg load in 1.32 minutes, compared to 2.26 minutes for Model 1. It was concluded that the reason for the deviating variable propagations can be found in the solver configurations.

An apparent weakness is found in the model developed in the present study. Never the less, the principal reason for this weakness is believed to have been detected, and if to be overcome, the model is believed to work properly.

## 7. Suggestions for further work

---

- Investigate the different numerical solver parameters and models. Weaknesses have been detected in the model developed in the present work. Due to this it seems important to conduct a detailed numerical analysis for the different solver methods offered in COMSOL Multiphysics.
- Perform an uncertainty analysis. When the numerical instabilities are eliminated, the system will be believed to give reliable results. However, rounding errors will be present, even though lying within the scope of an error estimate. Due to this, it is of great value to evaluate all uncertainty aspects within the assumptions and methods chosen for the completed model.
- Validate a new developed model with experimental data.
- Restrictions in implementing desired initial and boundary conditions have been experienced in the present study. During the refueling process of a depleted tank, great pressure changes will appear as the gas is fed at a pressure typically at 20 bar, while the empty tank has an initial pressure of around 1.1-4 bar. To overcome the large pressure change, a new geometry should be suggested. Alternatively, a valve could be implemented before the inlet. Different modules to simulate the mass transfer should also be tested.
- As the transient equations describing the present system consider an infinitesimal element within the adsorbent bed, the heat leaks into the system are neglected. The heat leak term could be implemented into the energy balance, for instance by implementing the equations developed by Kumar et al. [13]. Also cooling should be inserted at the walls.
- Adsorption models valid over a larger pressure and temperature range should be implemented. The Modified Dubinin-Astakhov and the Ono-Kondo models have both proved to fit well over larger ranges than the Langmuir model, and are thus good candidates.
- When the model proves to give reliable results, different MOFs should be tested and their storage capacity compared.



## 8. References

---

1. Bénard, P. and R. Chahine, *Determination of the Adsorption Isotherms of Hydrogen on Activated Carbons above the Critical Temperature of the Adsorbate over Wide Temperature and Pressure Ranges*. Langmuir, 2001. **17**(6): p. 1950-1955.
2. Kumar, V.S. and S. Kumar, *Generalized model development for a cryo-adsorber and 1-D results for the isobaric refueling period*. International Journal of Hydrogen Energy, 2010. **35**(8): p. 3598-3609.
3. Energy, U.S.D.o. *Hydrogen Storage*. [cited 2012 06.06]; Available from: [http://www1.eere.energy.gov/hydrogenandfuelcells/storage/current\\_technology.html](http://www1.eere.energy.gov/hydrogenandfuelcells/storage/current_technology.html).
4. Schüth, F., *Challenges in hydrogen storage*. The European Physical Journal Special Topics, 2009(176): p. 155-166.
5. Schlichtenmayer, M., B. Streppel, and M. Hirscher, *Hydrogen physisorption in high SSA microporous materials – A comparison between AX-21\_33 and MOF-177 at cryogenic conditions*. International Journal of Hydrogen Energy, 2011. **36**(1): p. 586-591.
6. Aleksić, P., *Experimental investigation of thermal effects in a hydrogen cryo-adsorption storage system*, 2011, Norges teknisk-naturvitenskapelige universitet: Trondheim. p. XII, 171 s.
7. Camilla Foyn Eithun, I.-A.R., *Hydrogen storage: Development of a setup for thermal conductivity measurements of porous materials.*, in EPT2011, NTNU: Trondheim. p. 131.
8. Paggiaro, R.G., *Investigation of Cryogenic Hydrogen Storage on High Surface Area Activated Carbon: Equilibrium and Dynamics*, in Lehrstuhl für Thermodynamik 2008, Technische universität München: München.
9. Richard, M.-A., et al., *Preliminary evaluation of the performance of an adsorption-based hydrogen storage system*. AIChE Journal, 2009. **55**(11): p. 2985-2996.
10. Richard, M.A., P. Bénard, and R. Chahine, *Gas adsorption process in activated carbon over a wide temperature range above the critical point. Part 1: modified Dubinin-Astakhov model*. Adsorption, 2009. **15**(1): p. 43-51.
11. Myers, A.L. and P.A. Monson, *Adsorption in Porous Materials at High Pressure: Theory and Experiment*. Langmuir, 2002. **18**(26): p. 10261-10273.
12. Do, D.D., *Adsorption Analysis: Equilibria and Kinetics*, ed. R.T. Yang. Vol. Vol.2. 1998: Imperial College Press.
13. Senthil Kumar, V., K. Raghunathan, and S. Kumar, *A lumped-parameter model for cryo-adsorber hydrogen storage tank*. International Journal of Hydrogen Energy, 2009. **34**(13): p. 5466-5475.
14. Richard, M.A., P. Bénard, and R. Chahine, *Gas adsorption process in activated carbon over a wide temperature range above the critical point. Part 2: conservation of mass and energy*. Adsorption, 2009. **15**(1): p. 53-63.
15. Zhongyingshi, X.W., *Comparison of Darcy's law, The Brinkman Equation, The Modified N-S Equation and the Pure Diffusion Equation in PEM Fuel Cell Modeling.*, in COMSOL Conference 2007: Boston.
16. NIST web book. Available from: <http://webbook.nist.gov/chemistry/fluid/>.

17. Persephoni Karaolani, G.D.S., K.D Baker. *Parabolic and Hermite Cubic Finite Elements: A Flexible Technique for Deformable Methods*. 1990 [cited 2012 05.05]; Available from:

[www.bmva.org/bmvc/1990/bmvc-90-058.pdf](http://www.bmva.org/bmvc/1990/bmvc-90-058.pdf)

18. Micheal J. Moran, H.N.S., *Fundamentals of Engineering Thermodynamics*. 5th ed2006: John Wiley & Sons, Inc.



**APPENDIX**

---



## APPENDIX A

### Langmuir constants

The parameters used for the Langmuir model, Equations 4.1-4.4:

$$b_0=2.816e-8[\text{Pa}^{-1}]$$

$$B=332.0158[\text{K}]$$

$$q_{m0}=11.7134e-2[\text{kg}_{\text{H}_2}/\text{Kg}_{\text{MOF}}]$$

$$A=131.3231e-6[\text{K}^{-2}]$$

$$\Delta H_a=-4.0[\text{KJ}/\text{mol}] = -2 \times 10^6[\text{J}/\text{kg}]$$

### Governing equations

#### Mass balance

Thermodynamic relations:

$$\frac{\partial \rho_g}{\partial t} = \left( \frac{\partial \rho_g}{\partial T} \right)_P \frac{\partial T}{\partial t} + \left( \frac{\partial \rho_g}{\partial P} \right)_T \frac{\partial P}{\partial t} \quad (4.1)$$

Isothermal compressibility[18]:

$$\kappa = -\frac{1}{v} \left( \frac{\partial v}{\partial P} \right)_T \quad (A.1)$$

$$v_g = \frac{1}{\rho_g} \quad (A.2)$$

$$\kappa_{Tg} = -\frac{1}{v_g} \left( \frac{\partial v_g}{\partial P} \right)_T = \frac{1}{\rho_g} \left( \frac{\partial \rho_g}{\partial P} \right)_T \quad (A.3)$$

Isobaric thermal expansion[18]:

$$\alpha = \frac{1}{v} \left( \frac{\partial v}{\partial T} \right)_P \quad (A.4)$$

$$\alpha_{Pg} = \frac{1}{v_g} \left( \frac{\partial v_g}{\partial T} \right)_P = -\frac{1}{\rho_g} \left( \frac{\partial \rho_g}{\partial T} \right)_P \quad (A.5)$$

Using these relations in (4.19) gives

$$\frac{\partial \rho_g}{\partial t} = -\rho_g \alpha_{P_g} \frac{\partial T}{\partial t} + \rho_g \kappa_{T_g} \frac{\partial P}{\partial t} \quad (4.2)$$

### *Energy balance*

The time derivative of  $H_g(T, P)$  is expanded as

$$\frac{\partial H_g}{\partial t} = \left( \frac{\partial H_g}{\partial T} \right)_P \frac{\partial T}{\partial t} + \left( \frac{\partial H_g}{\partial P} \right)_T \frac{\partial P}{\partial t} \quad (4.3)$$

$$dh = \left( \frac{\partial h}{\partial T} \right)_P dT + \left( \frac{\partial h}{\partial P} \right)_T dp \quad (A.6)$$

Introducing thermodynamic relations:

$$C_p = \left( \frac{\partial h}{\partial T} \right)_P \quad (A.7)$$

$$dh = C_p dT + \left( \frac{\partial h}{\partial P} \right)_T dp \quad (A.8)$$

$$dh = T ds + v dP \quad (A.9)$$

$$ds = \left( \frac{\partial s}{\partial T} \right)_P dT - \left( \frac{\partial v}{\partial T} \right)_T dp \quad (A.10)$$

Substituting (A.10) into (A.9) and setting equal (A.8) gives

$$T \left( \frac{\partial s}{\partial T} \right)_P dT - T \left( \frac{\partial v}{\partial T} \right)_T dp + v dP = C_p dT + \left( \frac{\partial h}{\partial P} \right)_T dp \quad (A.11)$$

$$\left( \left( \frac{\partial h}{\partial P} \right)_T + T \left( \frac{\partial v}{\partial T} \right)_T - v \right) dP = \left( T \left( \frac{\partial s}{\partial T} \right)_P - C_p \right) dT \quad (A.12)$$

When  $dT = 0$

$$\left(\frac{\partial h}{\partial P}\right)_T = v - T \left(\frac{\partial v}{\partial T}\right)_T \quad (\text{A.13})$$

Substituting this into (A.8)

$$dh = C_p dT + \left[ v - T \left(\frac{\partial v}{\partial T}\right)_T \right] dP \quad (\text{A.14})$$

From (A.4) it can be written

$$dh = C_p dT + v[1 - \alpha T] dP \quad (\text{A.15})$$

Introducing this to gas enthalpy

$$\frac{\partial H_g}{\partial t} = C_{p_g} \frac{\partial T}{\partial t} + v_g(1 - \alpha_{p_g} T) \frac{\partial P}{\partial t} \quad (\text{A.16})$$

$$\vec{\nabla} H_g = C_{p_g} \vec{\nabla} T + v_g(1 - \alpha_{p_g} T) \vec{\nabla} P \quad (\text{A.17})$$

$$\frac{\partial H_s}{\partial t} = C_{p_s} \frac{\partial T}{\partial t} + v_s \frac{\partial P}{\partial t} \quad (\text{A.18})$$

Where

$$v_s = \rho_s(1 - \varepsilon_t) \quad (\text{A.19})$$



# APPENDIX B

## Velocity distribution

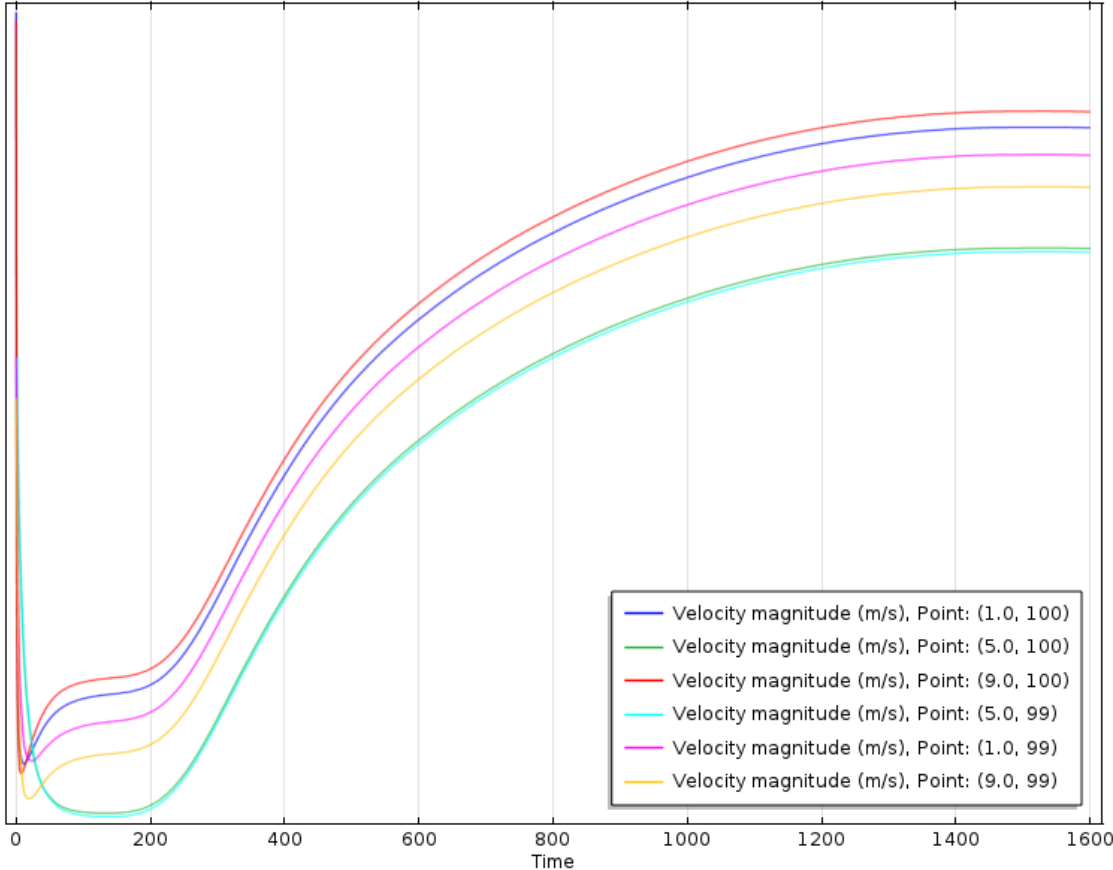


Figure B.1: Inlet velocity at “Cut Points”

Figure B.1 shows the inlet velocities at (1,100), (5,100), (9,100), (1, 99), (5, 99) and (9, 99) in (x,y) notation. The Magnitudes on the y-axis are from 0.0451 to 0.04511, and hence the velocity changes are negligible and equal to the ones predicted from the Line Average plots.

### Density distribution

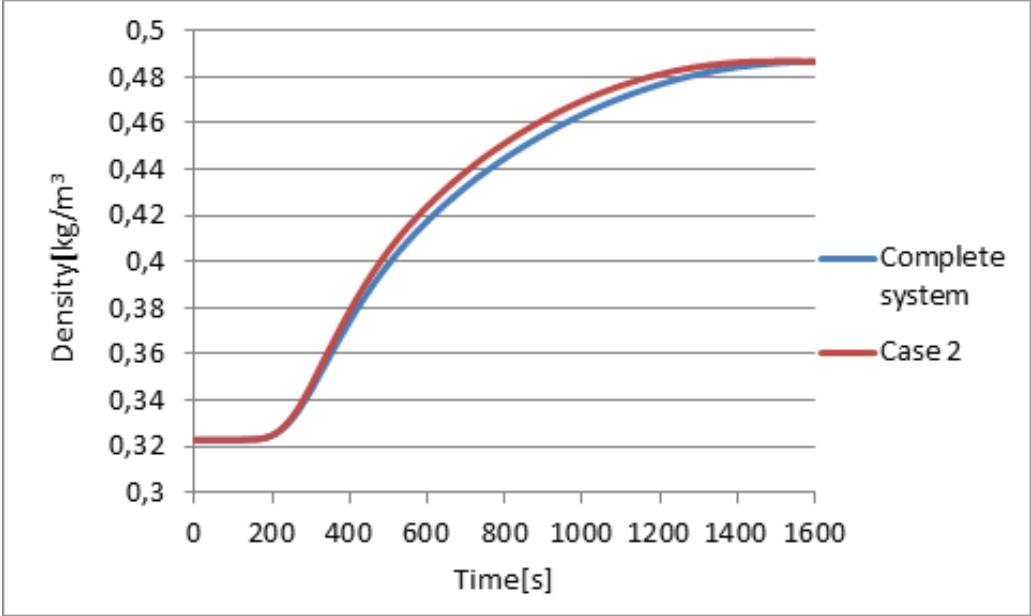


Figure B.2: Average outlet density for Complete system and Case 2